MICROPOROUS INORGANIC MEMBRANES FOR HIGH TEMPERATURE ALKANE DEHYDROGENATION AND PRODUCTS SEPARATION

By
SHAILESH SINGH DANGWAL

Bachelor of Technology in Chemical Engineering
Indian Institute of Technology
Guwahati, India
2012

Master of Science in Chemical Engineering
Oklahoma State University
Stillwater, Oklahoma
2017

Submitted to the Faculty of the
Graduate College of the
Oklahoma State University
in partial fulfillment of
the requirements for
the Degree of
DOCTOR OF PHILOSOPHY
December, 2020

MICROPOROUS INORGANIC MEMBRANES FOR HIGH TEMPERATURE ALKANE DEHYDROGENATION AND PRODUCTS SEPARATION

Dissertation Approved:

Dr. Seok-Jhin Kim

Dissertation Adviser

Dr. Sundar Madihally

Dr. Heather Fahlenkemp

Dr. Allen Apblett

ACKNOWLEDGMENTS

I would like to express my gratitude to my advisor Dr. Seok-Jhin Kim for his enormous help, continuous guidance and constant motivation during my graduate studies. He has been a great mentor who has always inspired and kept me motivated which helped me in finishing my tasks. Under his able guidance, I was involved in the establishment of our lab and learned a lot. The most important thing, which I learned from him, is hard work, honesty towards work and organization skills. Moreover, I would also like to thank my committee members Dr. Sundar Madihally, Dr. Heather Fahlenkemp and Dr. Allen Apblett for agreeing to serve on my thesis committee.

I am grateful to the School of Chemical Engineering at OSU for their financial support throughout this program. I am also thankful to Dr. Jindal Shah and Dr. Mari Andiappan for their suggestions/insights during my Ph.D. study. I would also like to thank Eileen Nelson, Gary Thacker, Shelley Potter and Beth Kelley for their continuous help and support.

I would also like to thank my ex-lab mate Ruochen Liu for his help and support. He has helped me substantially during and even after his stay at OSU. He was always ready to offer his insights and suggestions. I am also grateful to my current lab mates Anil Ronte and Diako Mahmodi for their help inside and outside lab. Anil has always been available to help me in experiments and Diako always came to my rescue for editing my manuscripts. I am also grateful to my friend, colleague and roommate “Sushobhan Pradhan” who helped me a lot in learning the various software like origin, endnote and MATLAB, which helped me in refining plots and results depicted in this work. He has also been an immense help in many personal issues.

Further, I would like to express my heartfelt gratitude to all my friends, namely, Mukesh Singh, Yashwanth Ram, Jui Salunkhe, Masood Ahmed, Rajesh Tolety, Sneha Varaganti, Saurabh Kokad and Neha Pathipati. I have developed life-long friendship with them. Without their love and companionship, this work would not have been possible. It is difficult for me to put into words what their friendship means to me. They all have stood with me through thick and thin. Life became bland after they left OSU. I will always be grateful to all of them for making my life at OSU so much fun.

I will not do the justice if I will not thank Mr. Virender Yadav, my physics teacher from high school. I am forever indebted to him for changing my life completely. Without him, surely I would not have been able to get the prestigious seat at Indian Institute of Technology, my alma mater.

Last but not the least; I would like to thank my parents, Mrs. Jeeta Dangwal and Mr. Virendar Dangwal. I would not have been able to achieve all this, had it not been for their immeasurable sacrifices and support. Their blessing have lasted with me for all my life. I am forever indebted to them and they are the reason for all my accomplishment. I also want to express my thanks to my siblings Beena Rawat, Reena Rawat, Nimmi Bhauriyal and Yogesh Dangwal. They all have contributed emotionally and financially in immense measures all throughout my life. Being a child, pursuing Ph.D. was not even a distant dream; all my family members made it a reality. It is both a debt, which I will never be able to repay, and a decoration, which I will always wear with pride.

DEDICATION

To Mrs. Jeeta Dangwal and Mr. Virendar Dangwal, my parents,

This work is dedicated to you and everyone who dare to dream beyond imagination.

My parents, who fought bravely against all odds,

and inspired me for being resilient and hopeful in tough situations.

Name: SHAILESH SINGH DANGWAL

Date of Degree: DECEMBER, 2020

Title of Study: MICROPOROUS INORGANIC MEMBRANES FOR HIGH TEMPERATURE ALKANE DEHYDROGENATION AND PRODUCTS SEPARATION

Major Field: CHEMICAL ENGINEERING

Abstract: Ethylene, propylene and isobutylene are among the most important intermediates for the production for many chemical products in industry. These chemicals are mostly produced through catalytic dehydrogenation which has thermodynamic limitations in terms of performance. Membrane reactors provide a unique opportunity to overcome these limitation. In this work, MFI zeolite membrane reactor was used to perform ethane, propane, and isobutane dehydrogenation. For ethane, propane, and isobutane dehydrogenation, impact of impact of different operating conditions on reaction performance was studied. In packed bed reactor (PBR), ethane dehydrogenation and propane dehydrogenation reaction performance decreased with increase in reaction side pressure. However, for packed bed membrane reactor (PBMR) reaction performance increased with reaction side pressure. The maximum ethane conversion, ethylene selectivity and ethylene yields obtained were 29%, 97%, and 28%, respectively. Similarly, the highest propane conversion, propylene selectivity and propylene yields obtained were 49%, 97%, and 47%, respectively. For the isobutane dehydrogenation the impact of operating conditions like temperature, sweep gas flow rate, and space velocity was examined. The highest isobutane conversion, isobutylene selectivity and isobutylene yield was 27%, 97% and 26% respectively. Also 1D plug flow reactor (PFR) model was developed for ethane, propane and isobutane dehydrogenation reaction. Model correctly predicted the conversion values and was also used to evaluate the conversion values beyond experimental conditions. However, dehydrogenation reaction in PBMR helped in overcoming thermodynamic limitations and also produced relatively purer products but still there is a need for further purification of these products. For further purification of products in propane dehydrogenation reaction, novel ZIF-8 membrane were synthesized for separating propylene/propane gas mixture. ZIF-8 membrane was synthesized on anodic aluminum oxide (AAO) using secondary growth method. In this study, effect of seeding type, membrane synthesis time, and effect of zinc source was examined. It was found that silicalite seeding, 10 h synthesis time, and $ZnCl_2$ as precursor were the optimized conditions for ZIF-8 membrane synthesis and the reported separation factor for propylene/propane gas mixture was 170 and the corresponding propylene permeance was 0.9×10^{-8} mol m^{-2} s^{-1} Pa^{-1}. Silicalite seeding helped in better attachment of ZIF-8 layer to the support. Though, ZIF-8 membrane exhibited impressive propylene/propane separation performance but still there were inherent defects and pinholes in the ZIF-8 framework because of Zn vacancies. ZnO atomic layer deposition (ALD) was used to cure the defects in the membrane framework. After ALD, ZIF-8 membrane separation performance for propylene/propane gas mixture enhanced from 141 to 270 after two ALD cycles. Further ALD cycles only deposited ZnO on ZIF-8 pores and reduced separation factor for propylene/propane gas mixture. However, propylene and propane gas permeance decreased monotonously with number of ALD cycles.

TABLE OF CONTENTS

Chapter Page

LIST OF TABLES

Table Page

LIST OF FIGURES

Figure Page

Figure Page

Figure Page

CHAPTER I

INTRODUCTION

Summary

This study is divided into three aims. Aim I: Perform alkane dehydrogenation reaction using membrane reactor for overcoming thermodynamics limitation. Aim II: Fabricate novel ZIF-8 membrane for high propylene/propane separation for purifying dehydrogenation reaction products. Aim III: Modify the structure of ZIF-8 membrane using ZnO atomic layer deposition (ALD) to cure pinholes and defects.

The manufacturing of fuels and chemicals has been among the most important chemical processes and has been under scrutiny for technological improvements. Important parameters for improving these processes are catalysis, heat integration, product purification and efficient cleanup [1]. Alkane dehydrogenation reaction generates products like ethylene, propylene and isobutylene that are highly important in chemical industry. Table 1.1 shows the increasing demand of ethylene, propylene, and isobutylene in the recent times.

Table 1.1. Production of ethylene, propylene, and isobutylene year wise in million tons per annum (mtpa)

	2013	2019	2023
Ethylene [2, 3]	142	207.58	263.13
Propylene [4]	85	122	150
Isobutylene [5]	11.59	13.46	16.23

Membrane reactor is one such evolving technology which has several benefits over conventional processes for the production and purification of these chemicals [6]. Combining membrane with catalysis has attracted a lot of attention in recent research [1, 7-11]. Inorganic membrane reactors have already been investigated for number of reactions [3, 12-20]. Alkane dehydrogenation reaction has H_2 and corresponding alkene as products. Membrane reactors help in enhancing dehydrogenation reaction performance in terms of corresponding alkane conversion, product alkene selectivity, and product alkene yield. Apart from enhancing dehydrogenation reaction performance, membrane reactor also helps in separating products (H_2 and alkene) which helps in shifting the reaction equilibrium to the product side and thus helps in improving the product yield [21].

$$Alkane \leftrightarrow Alkene + H_2 \tag{1.1}$$

Dehydrogenation reaction is thermally unfavorable compared to cracking of hydrocarbon because the bond strength C-C (246 KJ/mol) is much lower than C-H bond (363 KJ/mol). However, the catalysts like Pt/Al_2O_3, $Pt\text{-}Sn/Al_2O_3$, and Pd/Al_2O_3 help in ensuring minimal C-C bond rupture. Metal catalyst helps in activating strong C-H bond σ orbital [22]. Thus membrane reactor along with suitable catalyst helps in achieving higher performance [23, 24]. Overall, membrane reactor can perform dehydrogenation reaction and product purification in one single step. The overall purpose of this work is to design efficient ways for conducting dehydrogenation reaction to produce industrially important alkenes and to further purify these

valuable products. In AIM I, we plan to use MFI zeolite membrane for the dehydrogenation of ethane, propane and isobutane. In dehydrogenation reaction, we plan to investigate the impact of different operating parameters such as temperature, pressure, sweep gas flow rate, and space velocity on the dehydrogenation reaction performance. In addition, we plan to develop 1D PFR model for the dehydrogenation reactions in order to validate experimental results and also to predict reaction performance beyond the experimental conditions. Moreover, most valuable products in dehydrogenation reaction are ethane, ethylene, propane and propylene. Dehydrogenation reaction using MFI zeolite membrane helps in a considerable separation of H_2 and corresponding alkene. However, in the retentate, a mixture of unreacted alkane and product alkene still coexists. MFI zeolite membrane has pore size of 0.55 nm, which is higher than the molecular size of ethane, ethylene, propane, and propylene, and thus these gases cannot be separated using the MFI zeolite membrane [25-27]. Therefore, in AIM II, we plan to design the ZIF-8 membrane using novel fabrication techniques for the separation of propylene/propane gas mixture. This membrane can be used to further purify the industrially important dehydrogenation reaction products. In AIM III, we plan to use ZnO atomic layer deposition (ALD) on ZIF-8 membranes to cure the inherent defects in the ZIF-8 framework and to further enhance the separation performance of ZIF-8 membrane for propylene/propane gas mixture. Figure 1.1 depicts the overall schematic used for membrane reactor and the product separation setup. All three aims with details are described as follows.

Aim I: Perform alkane dehydrogenation reaction using membrane reactor for overcoming thermodynamics limitation

We plan to perform dehydrogenation reactions for ethane, propane and isobutane using packed bed membrane reactors (PBMR) and achieve the reaction performance higher than thermodynamic limitations. The purpose is to device new and efficient membrane reactors, which can enhance product yield in the dehydrogenation reactions. We also plan to develop 1D PFR model so that the dehydrogenation reaction performance can be predicted beyond experimental values.

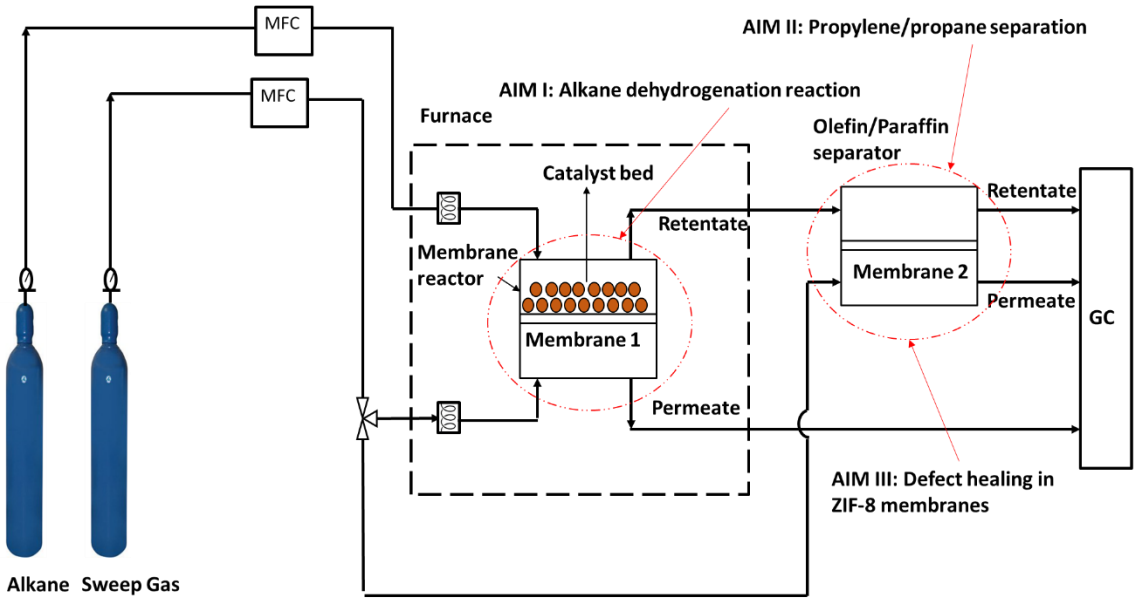

Figure 1.1. Overall schematic of the membrane reactor and product separation setup used in the work

Aim II: Fabricate novel ZIF-8 membrane for high propylene/propane separation for purifying dehydrogenation reaction products

Propylene and propane are among the most important industrial products from the dehydrogenation reactions. In this work, we aim for the purification of propylene/propane gas mixture. Although membrane reactors perform separation, that is mainly for H_2/hydrocarbon separation. Propylene/propane separation is more difficult because of similar physical properties and molecular size. Presently propylene/propane gas separation in industry is carried out via cryogenic distillation, which is very expensive and energy intensive. Membrane separation is a cheap and efficient way to purify these industrially important gases and therefore we plan to perform propylene/propane separation using ZIF-8 membrane under this aim. We plan to design the novel ZIF-8 membranes, which can separate the propylene/propane gas mixtures from dehydrogenation reactions.

Aim III: Modify the structure of ZIF-8 membrane using ZnO atomic layer deposition (ALD) to cure pinholes and defects

ZIF-8 membrane exhibited excellent separation performance for the propylene/propane gas mixture in AIM II (selectivity ~ 170). However, there were still inherent pinholes and defects, which allow the viscous flow of gases across the membranes and thus reduce the separation performance of the membrane. Using ZnO atomic layer deposition (ALD) as a membrane modification technique, we plan to cure these pinholes and defects and tune the pore size in order to enhance ZIF-8 membrane separation performance for the propylene/propane gas mixtures.

CHAPTER II

BACKGROUND AND LITERATURE REVIEW

Summary

We reviewed the literature that dealt with packed bed reactor (PBR) and packed bed membrane reactor (PBMR) for ethane, propane and isobutane dehydrogenation reactions. This chapter discussed different membranes used in dehydrogenation reaction and their corresponding performances. A comprehensive literature review about propylene/propane gas separation using different membranes is also provided.

2.1 Zeolite membrane and zeolite membrane reactors

Zeolites are microporous aluminosilicate minerals made up of tetrahedral units. In the tetrahedral unit, one atom is either Si or Al, which is surrounded by four oxygen atoms. These tetrahedral units are linked to each other by common oxygen atom which gives cavities its structure with definite size and shape [28]. For completely siliceous materials, the framework is electrically neutral. There are more than 170 types of zeolite structures that have been identified so far. Supported polycrystalline zeolite membranes are suitable for the energy efficient separation of gas and liquid mixtures [29]. Macroporous and mesoporous ceramic, stainless steel, glass plates and tubes are some common membrane supports mostly in the form of disc and tubes [30-32]. Many types of zeolites membranes have been tested for many molecular separations

[33-35]. The pore sizes of 8-member ring LTA, 10-member ring MFI, and 12-member ring FAU are about 0.41, 0.56 and 0.74 nm, respectively. These are most extensively studied structures because their pore sizes are suitable for separating a large number of industrially important chemicals for industry.

Zeolites membranes are commonly synthesized by hydrothermal treatment of the substrate surface in liquid phase aluminosilicate precursor, which can be either in the form of clear solution or sol or gel. The crystallization of zeolites and eventual crystal structure are sensitive to the precursor composition, the use of structure directing agents (SDA), the specific route of precursor preparation, the synthesis temperature, and duration. Undesirable impurity crystal phases might also be present in zeolite films and can affect the morphology, impurity, and chemical stability [36].

The process for the synthesis of polycrystalline zeolite membranes on porous substrate is shown in Figure 2.1. In an insitu crystallization process, zeolite nuclei form on the surface either by heterogeneous nucleation or by deposition of the nuclei generated in the bulk solution. While in the seeded secondary growth method, the zeolite seed layer is pre coated using separately synthesized zeolite suspensions. The discrete layer of nuclei or seed crystals subsequently evolves in a continuous film by crystal growth in a synthesis solution. Final zeolite membrane consists of inter-grown crystals with minimized intercrystalline spaces. These intercrystalline spaces are considered as microdefects because they are larger than the zeolite pores and decrease molecular separation performance [26].

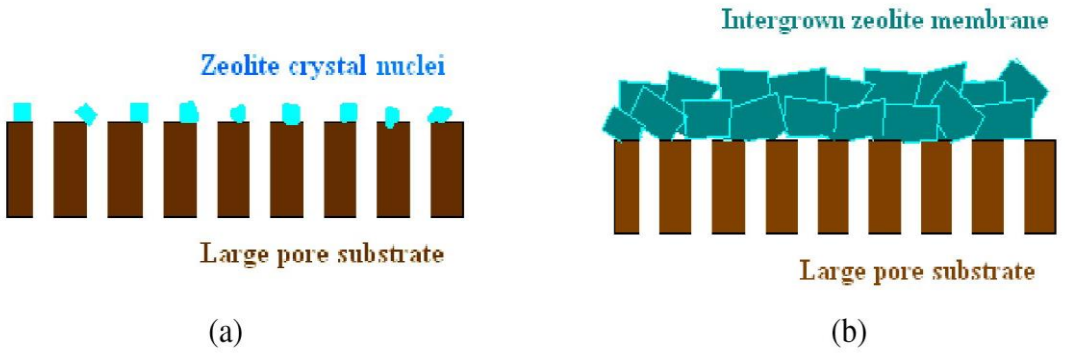

Figure 2.1. Schematic description of zeolite membrane formation on a porous substrate (a) nucleation on surface, and (b) crystal growth into continuous polycrystalline membrane [37]

Alkane dehydrogenation reaction is highly energy intensive and it requires high temperature for operation [38, 39]. Moreover, the performance of alkane dehydrogenation reaction is limited due to the thermodynamic constraints. In order to successfully enhance the performance of dehydrogenation reaction, we need membranes, which are stable at high temperature and have good separation performance for the H_2/alkane gas mixture. Zeolite membranes have known to be extremely stable for the high temperature operation and have shown good performance for H_2/alkane mixture separation [40-44]. Other than the membrane stability, economic viability of membrane reactor is also an important aspect which needs to be looked at for their industrial implementation. Moparthi et al. conducted the feasibility study of silica and palladium membranes for dehydrogenation reactions. A comparative study of membrane and conventional reactor was performed using simulation methodology. Dehydrogenation of ethylbenzene and propane using silica and palladium membrane reactors were considered for the comparison. Impact of membrane area per reaction zone volume, temperature, reaction and permeation zone pressure, membrane thickness, and sweep gas flow rate on economics was investigated. It was found that membrane reactor operation was yielding 60-70% more profit than conventional reactor using simulation [45]. This shows that membrane reactor

holds a brighter future for the industrial implementation. There has been substantial work done for the dehydrogenation of lower alkane as summarized in the following sections.

2.1.1 Ethane dehydrogenation

Ethylene is an important chemical engineering ingredient and is used in polymerization, oxidation, and alkylation [46]. Such diverse usage of the ethylene provides the driving force for studying the ethane dehydrogenation reaction (EDH). The increasing importance of H_2 as a fuel also adds to the demand for designing efficient ways for EDH reaction. Because the EDH reaction is endothermic, the reaction is only favored at high temperatures for obtaining high ethane conversion, high reaction activity, and high ethylene selectivity [47-49].

$$C_2H_6 \leftrightarrow C_2H_4 + H_2, \qquad \Delta H^{\ominus}_{298.15K} = 136.94\ kJ/mol \tag{2.1}$$

Various studies have been performed for EDH reaction in both packed bed reactors (PBR) and packed bed membrane reactors (PBMR). For example, Galvita et al.[47] conducted EDH reaction in PBR mode for Pt/Mg(Al)O and Pt-Sn/Mg(Al)O catalyst. The reported ethane conversions were 9.8%, and 4.3% respectively, less than the equilibrium limit of 16% at 600 ^{o}C. Gobina et al. [3, 50-52] conducted EDH membrane reactor (MR) experiments for Pd–Ag membrane with Pt/Al_2O_3 as a catalyst showing ethane conversion of 18% against an equilibrium limitation of 3.5%. Szegner. et al. [53] used composite alumina PBMR with $Pt\text{-}Sn/Al_2O_3$ for EDH, and ethane conversions were 16% and 8% in PBMR and PBR mode, respectively, at 550 ^{o}C.

However, there have been very few reports about studying the effect of reaction pressure on the performance of EDH reaction. As EDH is a volume expansion reaction, ethane conversion is expected to decrease with an increase in pressure in PBR, but in PBMR, the effect of reaction pressure on reaction performance yields different impact on the reaction results. For example, there have been a few studies

performed on the impact of pressure in a PBMR operating at the high temperature. Brunetti et al.[54, 55] performed water gas shift (WGS) in combination of CuO/CeO_2 catalyst and a silica MR. The temperature and pressure were varied in a range of 220–290 ^oC and up to 600 kPa respectively, resulting in the optimum CO conversion of 95%, which was 8% higher than PBR. Lee et al.[56] not only studied the effect of pressure on reaction equilibrium but also the permeability for catalytic dry reforming of methane for a MR. The MR showed better performance than a PBR but with increasing reaction pressure, the enhancement in H_2 and CO yields in the MR reached a maximum value and then declined. Barbieri et al.[57] studied performance of the MR in a WGS reaction. In the MR mathematical modelling, the impact of the feed flow rate, feed pressure and temperature on the catalyst performance was studied, which confirmed the CO conversion enhancement and reduction of MR volumes. Alexander et al. [58] stated that WGS catalytic membrane reactor combined with a Pd-membrane showed enhancement in the efficiency of the WGS reaction when operated at elevated temperatures and pressures. In this work, we tried to see the impact of reaction pressure on the performance of ethane dehydrogenation reaction.

2.1.2 Propane dehydrogenation

Propylene is an important intermediate chemical for the production of petrochemicals such as polypropylene and acrylonitrile. After ethylene it is the second most important product in the chemical industry [59]. The propane dehydrogenation reaction (PDH) is a key step in propylene (C_3H_6) production, which, as stated before, is an important raw material for the production of polypropylene [60-65]. Propylene and other light olefins are mainly produced by light oil fractions through steam cracking and fluid catalytic cracking [66, 67]. Fixed bed reactors, fluidized bed reactors and membrane reactors are the common reactors used for the propane dehydrogenation reaction [15, 68-71]. Pt or Pt-Sn catalysts are widely used for the alkane dehydrogenation reactions [72-75].

$$C_3H_8 \leftrightarrow C_3H_6 + H_2 \qquad \Delta H^{\ominus}_{298.15K} = 129.4\ kJ/mol \qquad (2.2)$$

There has already been considerable work done on PDH reaction in membrane reactors. Chang et al.[76] performed PDH reaction in an isothermal high temperature tube MR containing a Pd-coated γ-Al_2O_3 membrane and a Pt/K/Sn/Al_2O_3 packed catalyst. With Pd membrane propane conversion was 2 times higher than equilibrium values and 6 times higher than conventional reactor conversion. Ricca et al. [59] studied selective PDH reaction with Pd-based membrane. Selective removal of hydrogen from reaction side helped in substantial reduction of operating reaction temperature and also decreased the coke formation. Peters et al.[77] investigated PDH reaction using a Pd-based membrane. It was observed that coke formation was significant under the operating conditions (450-500 ^oC) and under low H_2 to propylene ratio. In sequential membrane reactor process, the effect of steam content on catalyst and membrane activity and stability was investigated. It was found that the presence of steam is good for catalyst stability but amount of H_2 produced is independent on steam content between 7% to 20%. A stable membrane performance is obtained at 200 ^oC at hydrogen recovery factor (HRF) varying from 38% to 50%. Wu et al.[78] used a Pd/Ag composite hollow fiber membrane reactor (MR) by depositing submicron sized Pt (0.5 wt.%)/ γ-alumina catalysts for PDH reaction. At 450 ^oC, the propane conversion of 42% was reported in the hollow fiber MR at the initial stage of the reaction but diminished to 6% after 40 min of operation due to the deactivation of the catalyst. Yildirim et al.[79] studied the performance of dense Pd-Ag, silica and Pd-dispersed membrane systems on PDH reaction respectively. Pd-Ag showed very high H_2 selectivity and thus showed a better performance giving a fourfold conversion increase on the equilibrium at a relatively low temperature of 400°C. Sheintuch et al. [80] presented a kinetic model for propane dehydrogenation on a Pt,Sn/Mg(Al)O which accounted for the product distribution due to main and side reactions, for deactivation rates and for diffusion resistance. Parameters were estimated from steady state experiments at varying pressure and from the temperature programmed experiments and were compared with previous published models with similar catalysts. These model suggested that pressure should be kept below 5 bar and steam around 10% in feed while pellet size mainly affects selectivity and its effect of conversion is very small. Didenko et al. [81] used PDH reaction to show that the effect of Pd membrane thickness, temperature, space velocity and sweep gas flow rate on process behavior are interrelated. It was concluded that in order to maintain the balance of the rates when

one condition was changed, a detailed optimization of the temperature, feedstock, and sweep gas flow rate consumption was required. Schäfer et al.[82] studied the PDH reaction in a high temperature packed bed catalytic MR with a H_2 selective silica membrane and a commercial Pt-Sn/Al_2O_3 catalyst. Due to removal of H_2 in the MR, high propane conversion was achieved in comparison to an analogous fixed bed traditional reactor (TR). The H_2 removal in the MR increased coking of the catalyst, and the performance of the MR and TR became similar after 200–300 min. Ziaka et al.[83] investigated PDH reaction in MR with a sol gel alumina membrane and a commercial 5% Pt/γ-Al_2O_3 catalyst. Reported propane conversion was 22% in the MR and 11% in the TR at 550°C, respectively, which can be attributed to the separation and removal of the H_2 and propylene in MR. Collins et al.[84] performed the PDH reaction in microporous silica based MRs and packed bed TRs with a Pt loaded aluminosilicate catalyst. Silica MR showed propylene yield 1.48 times higher than the TR yield with the same flow rate at 550 °C. The catalyst deactivation rates in MRs were generally higher than TRs. Liu et al.[85] investigated bimetallic PtSn/γ-Al_2O_3 catalysts promoted by doping indium(In) for PDH reaction. Results showed that the In addition improved catalytic performance and stability of PtSn/γ-Al_2O_3 catalyst. The presence of In not only maintained the catalytic activity and propylene selectivity but also suppressed the hydrogenolysis reaction during PDH. Propane conversion and propylene selectivity of 41% and 96% are obtained after 53h of operation.

However, there have been multiple studies for the propane dehydrogenation in conventional and membrane reactor but until now, there has not been a reported study for the effect of reaction pressure on the performance of propane dehydrogenation reaction in a membrane reactor. In this work, we used MFI zeolite membrane reactor to investigate the impact of pressure and the other operating conditions such as temperature, space velocity, and sweep gas flow rate on the performance of the propane dehydrogenation reaction.

2.1.3 Isobutane dehydrogenation

Isobutylene is used in the production of synthetic rubber, plastics, and various chemical and petro-chemical products such as methyl tert-butyl ether, alkylate gasoline, and butyl rubber [86]. The widespread method used to synthesize isobutylene is catalytic dehydrogenation of isobutane [87]. A dehydrogenation reaction requires relatively higher operating temperature for achieving high yield in a conventional reactor. Rigorous operating conditions result in inevitable catalyst deactivation because of coke formation [88-93]. However, in packed bed membrane reactors, with the addition of H_2 selective membrane, higher reaction performance than a conventional reactor can be achieved at the same operating conditions because it allows the reaction equilibrium to move towards the forward reaction.

$$i-C_4H_{10} \leftrightarrow i-C_4H_8 + H_2, \qquad \Delta H^{\Theta}_{298.15K} = 117.75 kJ/mol \tag{2.3}$$

In recent years, isobutane dehydrogenation (IBDH) has received plenty of attention as an industrial process due to versatile use of isobutylene [94-98]. Takeshi et al.[17] used a palladium MR to conduct IBDH reaction with Pt-Al_2O_3 and Cr_2O_3-Al_2O_3 catalyst. Pt-Al_2O_3 catalyst exhibited lower isobutylene yield in comparison to the Cr_2O_3-Al_2O_3 catalyst, but in both the cases isobutylene yield was higher than the thermodynamic limit. Johan et al.[99] studied IBDH in a DD3R zeolite MR at 439 ^oC and 489 ^oC. Isobutane was used as the incoming feed stream with nitrogen as sweep gas. At 500 ^oC, the DD3R zeolite membrane exhibited an exceptional H_2/isobutane permselectivity of 520 as well as a moderate H_2 permeance of ~4.5 $\times 10^{-8}$ mol m^{-2} s^{-1} Pa^{-1}. The isobutylene yield in MR was 41%, where the equilibrium yield was 28% at 489 ^oC. The increased performance can be attributed to the removal of almost 85% of H_2 from the reaction side at lower space velocity. Removing H_2, increased the coke formation, suppressed hydrogenolysis reaction, and decreased the catalyst activity [100-102]. Ciavarella et al.[20] researched IBDH reaction in a PBMR, integrated with a bimetallic Pt-In-zeolite fixed catalyst bed with a microporous MFI zeolite tubular membrane. The effect of sweep gas flow rate on membrane performance was investigated in both countercurrent and concurrent mode. The isobutylene yield of PBMR was four times larger than that of the PBR. Weiqiang

et al.[103] studied IBDH both experimentally and by modelling for a PBMR and PBR using a Pt/alumina catalyst. Comparative tests showed that a PBMR had higher isobutylene yield and higher selectivity. The simulations results were in good agreement with experimental results but slightly over predicted values. Casanave et al.[19] studied IBDH in a zeolite PBMR in combination with the Pt-In catalyst. Increased isobutylene yield was achieved in a PBMR by separation of H_2 from the reaction side. Both counter and concurrent methods were operated and it was found that H_2 selectivity and reaction performance was higher in countercurrent mode.

Van dyk et al.[104] investigated both Pd and MFI catalytic membrane reactors (CMRs). Both CMRs included Pt catalyst with the membranes for IBDH and showed higher isobutylene yield than PBR. Although both membranes showed different separation properties, the two CMRs showed a similar isobutylene yield of 24%. This can be attributed to the fact that the whole process was kinetically limited and thus any increase in separation properties could not increase isobutylene yield. Loannides et al.[18] studied IBDH using a commercial chromia-alumina catalyst for both PBR and PBMR using a dense silica membrane. The impact of temperature and feed composition on reactor performance was studied. A decrease in catalyst activity was observed in the initial 2-3 h and this reduction of catalyst activity escalated with the temperature but was reduced by H_2 addition in the feed. H_2 permeance for the membrane was found to be 8.1×10^{-7} mol m^{-2} s^{-1} Pa^{-1} and the H_2/hydrocarbon permselectivity was around 80-300. At all operating conditions, a PBMR showed better isobutylene yield and selectivity than a PBR. Farsi et al.[87] studied modeling for IBDH reaction in PBRs that operated in radial flow. It was simulated heterogeneously based upon the laws of energy and mass conservation. In the model, IBDH was treated as the main reaction and propane dehydrogenation, coke formation, and hydrogenolysis were considered as side reactions. The isobutylene yield and conversion of isobutane at optimum conditions were 91% and 40%, respectively. Kobayashi et al.[86] studied the impact of iron oxide on IBDH reaction over a Pt/Fe_2O_3-Al_2O_3 catalyst and found that catalyst activity, selectivity, and stability were greatly improved after a small amount of Fe_2O_3 was

incorporated to the catalyst. Analysis of the adsorbed carbon monoxide by FT-IR revealed that the electron density of the Pt was enhanced by the formation of bimetallic particles.

In this work, we used MFI-type zeolite membranes in order to investigate the impact of operating conditions on the IBDH reaction at 500-650 ºC. Moreover for zeolite PBMR, a one dimensional (1D) model of a plug flow reactor (PFR) was built and utilized to check for accuracy as well as to study the effect of operating conditions upon the performance of IBDH PBMR beyond experimental conditions.

2.2 ZIF-8 membranes

Products from membrane reactors like propylene and ethylene, along with unreacted reactants like ethane and propane are valuable and are sought after in industry. However, the separation of olefin/paraffin mixture is a difficult task because of the similar physical properties and similar molecular size [105-107]. Currently olefin/paraffin separation is performed in industry using cryogenic distillation involving more than 200 stages and it is very energy intensive due to low relative volatilities [108]. Currently 120 TBTU (Tera British thermal units) is consumed for the olefin/paraffin separation using cryogenic distillation. Therefore even small improvements in separation performance can substantially save energy and thus cost in petrochemical industry [109-111]. Membrane separation processes have been recognized as an attractive alternative as they have the potential to be energy efficient, ecofriendly and cost effective [112]. Several types of membranes have been studied such as polymeric [107, 113], carbon molecular sieve [114-116], and zeolite membranes [117]. However, these membranes are not currently suitable for practical applications because of the drawbacks associated with their separation factor, permeability, and durability [118, 119]. Therefore, there is a clear need for developing new membranes to enhance the propylene and propane separation performance.

Various strategies have been developed to grow ZIF-8 film on porous substrates. Pan et al. [120] found that ZIF-8 membranes synthesized in a solution containing water can induce better intergrowth of

grains due to easier deprotonation of the imidazole ligands in water than in methanol. Kwon et al. [121] prepared a thin ZIF-8 membrane through in situ synthesis, which produced well intergrown ZIF-8 membranes with significantly enhanced microstructure, resulting in the high propylene/propane selectivity. Shah et al. [122] investigated the role of sodium formate in the synthesis of ZIF-8 membranes to enhance ligand deprotonation in organic solutions. Pan et al. [123] measured the effects of activation procedure after ZIF-8 membrane synthesis. The optimal activation process included solvent exchange to remove residual water by using methanol and room temperature drying at a low evaporating rate.

Recently, zeolitic imidazolate frameworks (ZIFs) have been recognized as novel candidates for efficient olefin and paraffin separation. ZIFs are a subclass of metal organic frameworks (MOFs), possessing zeolite topologies originated from the metal-ligand-metal bond angle of 145°, which is similar to the Si-O-Si bond angle in zeolites [124]. Among the varieties of ZIFs that exist, ZIF-8, composed of zinc ions interconnected with 2-methylimidazole, has been the most promising candidate for propylene/propane separation [125-127]. The effective pore size of ZIF-8 falls in the range of 4.0-4.2 Å, which is larger than the crystallographic diameter of 3.4 Å owing to the flopping motion of the ligands. This allows the membrane to separate propylene (~4 Å) from propane (~4.3 Å) based on the size exclusion mechanism [128, 129]. Zhang et al. [129] reported that the diffusivity of propylene was approximately 100 times higher than that of propane by estimating diffusivity in a ZIF-8 crystal. These studies demonstrate the great potential of ZIF-8 membrane to be used for propylene/propane separation based upon their diffusivity differences.

Various strategies have been developed to grow ZIF-8 film on porous α-alumina substrates. Pan et al. [130] found that ZIF-8 membranes synthesized in a solution containing water can induce better intergrowth of grains due to easier deprotonation of the imidazole ligands in water than that containing methanol. Although significant progress was obtained on the propylene/propane separation with ZIF-8 membrane grown on porous α-alumina substrates, the preparation of substrate required rigorous conditions including hydraulic pressing at 10 tons and sintering temperature of ~1100 ^{o}C with high energy consumption and low reproducibility [128]. In addition, the relatively limited propylene permeance of as low as 0.2 $\times 10^{-8}$ mol m^{-}

^{2} s^{-1} Pa^{-1} were reported when the α-alumina disk was used as an substrate [119, 131]. Another promising choice for membrane support is an anodic aluminium oxide (AAO) substrate with straight nanochannels and narrow pore size distributions. This has been studied for the separation of larger molecules and used for the fabrication of porous materials [132]. Various MOFs have been successfully fabricated on AAO such as MOF-5 [133], HKUST-1[134], Sr/Eu(II)-imidazolate [135], MIL-53 [136], etc. The relatively thinner AAO substrate with the straight pore channels inside are expected for a better ZIF-8 crystallization and resulted in higher gas permeance. There were very few studies which reported about ZIF membranes on AAO.

Since the ZIF-8 particle sizes were demonstrated to induce changes in surface area, stabilities, and gas adsorptions, the species of zinc sources was investigated in order to generate the appropriate ZIF-8 crystal size for propylene/propane separations [137]. For example, the effects of zinc salts on the ZIF-8 membrane synthesis were studied by Kwon et al. [128]. When $ZnCl_2$ was employed as the zinc source, the synthesized ZIF-8 membrane showed separation factor of around 38 and the propylene permeance of around 2.7 $\times 10^{-8}$ mol m^{-2} s^{-1} Pa^{-1}. However, when the zinc source was changed to zinc nitrate, the ZIF-8 membrane became non selective for propylene/propane gas mixture [128].

It should be noted that ZIFs and zeolites have similar crystallization process [138-140], which is feasible for the ZIF-8 film growth on a zeolite seeded substrate. Since the silicalite-type zeolite nanocrystals can be anchored on the AAO substrate through hydrogen bonding, it can be also used as the seeding layer to enhance the interactions between ZIF-8 membrane and AAO substrate compared to traditional ZIF-8 nanocrystal seed layer. In this work, the effort has been made to find the optimal membrane synthesis time, the optimal seeding type material and the appropriate zinc source (linker) for efficient propylene/propane separation.

CHAPTER III

ZEOLITE MEMBRANE REACTORS

Summary

Using MFI zeolite membranes, alkane dehydrogenation reactions were performed. Packed bed membrane reactors (PBMR) were able to achieve higher performance than packed bed reactor (PBR) and thermodynamic limitations. The highest conversion obtained was 24%, 49%, and 27% for ethane, propane and isobutane dehydrogenation reaction in PBMR mode, respectively (12%, 22%, and, 11% in PBR mode, respectively). A 1D PFR model was also developed in the MATLAB and the results were validated with experimental values. The model was used to successfully predict conversion values for dehydrogenation reactions.

In this chapter, MFI zeolite membrane fabrication procedure using secondary growth method is explained. The experimental setup and the operating conditions used in the dehydrogenation reaction of ethane, propane, and isobutane is also summarized. H_2/Alkane separation performance as a function of temperature is evaluated in order to study the feasibility of MFI zeolite membrane for corresponding alkane dehydrogenation reaction. 1D PFR model development is explained for dehydrogenation reaction. In addition, experiment and modelling result for alkane dehydrogenation are discussed in details. 1D PFR model

is first validated with experimental results and then the model is used to predict dehydrogenation reaction performance beyond experimental conditions.

3.1 Ethane dehydrogenation (EDH) reaction using MFI zeolite membrane reactor

3.1.1 Experimental section

MFI zeolite membrane was used to conduct the dehydrogenation reaction for ethane, propane and isobutane in this work. The MFI zeolite membrane was synthesized on a seeded α-alumina disk by the secondary growth method. Macroporous α-alumina disks (Coorstek) of 1 in. diameter, 1 mm thickness, and 25% porosity were used as supports for MFI zeolite membrane preparation. Details of polishing α-alumina disks prior to membrane growth are identical to those described previously [141, 142]. To prepare a seeded α-alumina disk, the MFI seeds were dip coated on the α-alumina supports and dried, using same procedures described elsewhere [142, 143]. The synthesis solution was prepared as follows: tetrapropylammonium hydroxide (TPAOH, 1 M, Sigma–Aldrich) was mixed in the deionized water. After 30 min of stirring, tetraethyl orthosilicate (TEOS, 98%, Acros) was added dropwise to the solution under constant stirring. The molar composition of the gel was TEOS: 0.095 TPAOH: 35.42 H_2O. After the precursor was stirred for 3 h, it was transferred into the Teflon lined stainless steel autoclave (Parr). The polished α-alumina disk was placed vertically at the bottom of the vessel and completely immersed in the synthesis solution. The synthesis experiments were performed at 150 ^oC for 17 h. After the hydrothermal reaction, membrane was washed thoroughly with deionized water, dried, and calcined in air at 550 ^oC for 6 h to remove the template. The membranes were dried at 70 ^oC in an oven overnight.

The membranes were used for gas separation experiments and membrane reactor experiments. The membrane was tested for the permeation of equimolar H_2/Alkane and H_2/Alkene gas mixtures at room

temperature and in a temperature range of RT to 600 °C. The membrane permeance for gas as component i is defined as

$$P_{m,i} = \frac{Q_i}{A_m \cdot \Delta P_i}, \qquad (i = H_2, C_2H_6, C_2H_4, C_3H_8, C_3H_6 etc) \tag{3.1}$$

where Q_i (mol/s) is the amount of gas permeated over a time period of t (s); A_m (m^2) is the active membrane area which is 2.01 cm^2 excluding the area sealed by the graphite gasket; and ΔP_i (Pa) is the transmembrane pressure, $\Delta P_i = (P_i)_f - (P_i)_p$, where $(P_i)_f$ and $(P_i)_p$ are the partial pressures of i in the feed and permeate sides, respectively. Permselectivity for a gas mixture A/B ($a^o_{A/B}$) is defined as the ratio of pure gas permeance:

$$\alpha^o_{A/B} = \frac{P_{m,A}}{P_{m,B}} \tag{3.2}$$

Separation factor for a binary gas mixture A/B separation factor ($\alpha_{A/B}$) is given by

$$\alpha_{A/B} = \frac{(y_A / y_B)_{permeate}}{(y_A / y_B)_{feed}} \tag{3.3}$$

where y_A and y_B are mole fractions of gases A and B, respectively.

The membrane reactor system used for the dehydrogenation of ethane, propane and isobutane is schematically shown in Figure 3.1. The disc membrane was mounted in a stainless steel cell sealed by soft graphite gaskets (Mercer Gasket & Shim). A total amount of 550 mg of Pt/Al_2O_3 catalyst was spread evenly over the membrane surface to form a uniform catalyst bed. A thin pad of carbon cloth and quartz wool was placed on top of the catalyst layer to fix the catalyst bed and to allow feed gas to diffuse freely. The permeate side was swept by Ar flow at atmospheric pressure and its flow rate was maintained at 20 cm^3/min for all experiments, except for those which focus on the effect of F_{Ar}. Flow rates of ethane and Ar were controlled by mass flow controllers (MFC, Aalborg).

The flow rate of the exit stream from the reactor was frequently checked by soap bubble tests. Preheating coils were employed for both feed and sweep gases to ensure that they reached set temperature before entering the reactor. The retentate and permeate gases were analyzed by an online GC (Shimadzu GC2014) equipped with a molecular sieve 13X column for the thermal conductivity detector (TCD) and an alumina plot column for the flammable ionization detector (FID). A heating and cooling rate of 0.5 ^{o}C/min was used. The corresponding alkene product, unreacted alkane, H_2, and the byproducts (methane, xylene, and benzene) from side reactions, such as thermal cracking and catalytic cracking, were analyzed to observe the influence of operating conditions on reaction conversion and selectivity. Minor byproducts such as higher alkanes and higher olefins (propylene and butylene) and aromatics (benzene, xylene, and toluene) were found to be far less than 1% and excluded from further consideration. The alkane conversion was calculated based on the total alkane feed flow rates entering as feed and exiting the reactor in both the permeate and retentate streams:

$$\chi_{Alkane} = 1 - \frac{F_{Alkane}^{out}}{F_{Alkane}^{in}} \tag{3.4}$$

The selectivity for gas component *i* is defined as:

$$S_i = \frac{F_i^{out} - F_i^{in}}{F_{Alkane}^{in} - F_{Alkane}^{out}} \qquad (i = C_2H_4, CH_4, C_3H_6, C_4H_8 etc) \tag{3.5}$$

The yield for gas component *i* is calculated by:

$$Y_i = \frac{\chi_{Alkane} \times S_i}{100} \qquad (i = C_2H_4, CH_4, C_3H_6, C_4H_8 etc) \tag{3.6}$$

The weight hourly space velocity (WHSV) is defined by:

$$WHSV = \frac{\upsilon_{feed}^{Alkane} \times \rho_{Alkane}}{m_{cat}} \tag{3.7}$$

The H_2 recovery R_{H2} for PBMR system is defined as

$$R_{H_2} = \frac{\text{Amount of } H_2 \text{ in permeate}}{\text{Total amount of } H_2 \text{ generated by reaction}} \tag{3.8}$$

The permeate side H_2 concentration is defined as follows

$$y_{H2,P} = \frac{J_{H_2}}{J_{H_2} + J_{C_2H_6} + J_{C_2H_4} + J_{C_3H_8} + J_{C_3H_6}} \tag{3.9}$$

Where J_{H2}, J_{C2H6} , J_{C2H4}, J_{C3H8}, and J_{C3H6} are respectively the H_2, C_2H_6, C_2H_4, C_3H_8, and C_3H_6 fluxes across the membrane.

where υ_{feed}^{Alakne} is the volumetric rate of alkane in the feed stream at standard temperature and pressure (STP), and m_{cat} is the mass of catalyst. The catalyst used in the PBMR and PBR experiments was 1% Pt/Al_2O_3 (Sigma Aldrich) denoted here as 'Pt/Al_2O_3' catalyst. When the membrane mounted cell was used in PBR mode, the entering sweeping gas was removed and the exit of the reaction side was connected to the original sweeping inlet. The gas stream from the reaction side thus passed through the permeate chamber to exit from permeate side. The operating conditions for experiment and modelling for ethane dehydrogenation reactions are summarized in Table 3.1.

Equation 3.10 shows the permeance of gas i as a function of temperature. For the membrane reactor modelling, permeance as a function of temperature is required to perform calculations. Data from equimolar binary gas separation experiments was regressed to fit into equation 3.10. H_2/alkane and H_2/alkene binary gas separation data from RT to 600 °C at 1 atm was fit into equation 3.10 and corresponding parameters like $P_{m,i}^{o}$ and $E_{a,i}$ for gases were calculated by regressing the permeation data.

$$P_{m,i} = P^{o}{}_{m,i} \exp\left(-\frac{E_{a,i}}{RT}\right) \qquad (i = C_2H_6, C_2H_4, C_3H_8, C_3H_6, H_2) \tag{3.10}$$

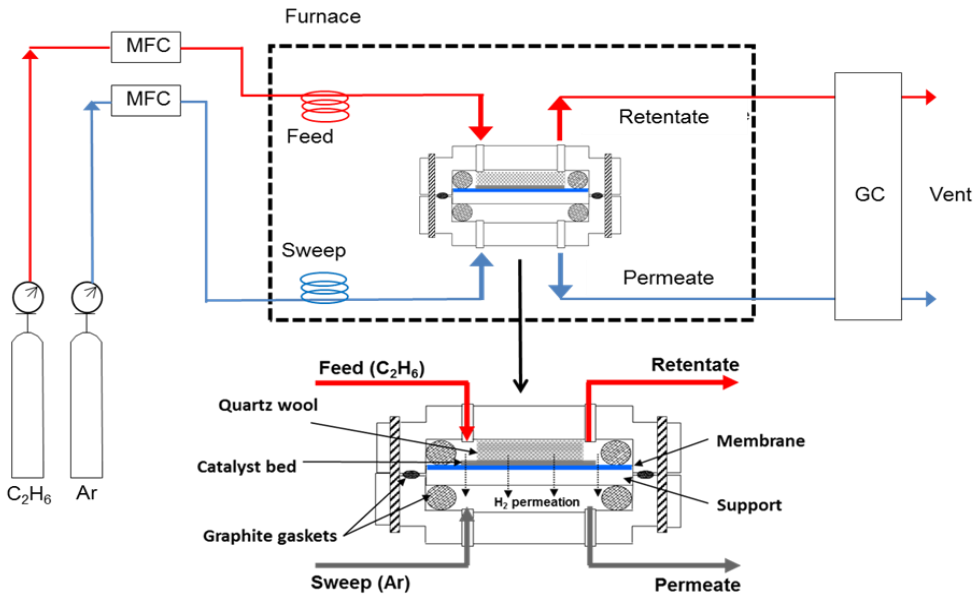

Figure 3.1. Schematic diagram showing membrane reactor system used for dehydrogenation reaction

Table 3.1. EDH membrane reactor conditions

	Experimental	Calculation
Reaction temperature, °C	500-600	500-800
Weight hourly space velocity (WHSV), h^{-1}	0.74	0.15-2.81
C_2H_6 feed flow rate, F_{C2H6}, cm^3 (STP)/min	3	1-19
Ar sweeping flow rate, F_{Ar}, cm^3 (STP)/min	20	3-30
1% Pt/Al_2O_3 catalyst loading (m_{cat}), g	0.55	0.55
Reaction pressure at retentate exit, atm	1.0-5.0	1.0-8.0
Permeate pressure, atm	1.0	1.0

3.1.2 Modelling section

The EDH reaction is endothermic as shown in

$$C_2H_6 \leftrightarrow C_2H_4 + H_2\,,\ \Delta H^{\ominus}_{298.15K} = 136.94\ kJ/mol \tag{3.11}$$

The following rate expression was used for modelling and taken from reference [50, 53].

$$Rate = k\left(P_{ethane} - \frac{P_{ethylene} \times P_{hydrogen}}{K_{Eq}}\right) \tag{3.12}$$

where k is the kinetic rate constant, $P_{hydrogen}$, $P_{ethylene}$ and P_{ethane} are partial pressures of H_2, ethylene and ethane in the reaction side, and K_{eq} is the equilibrium constant.

The expression for kinetic rate constant and equilibrium constants have been studied in the literature [144, 145].

$$k = k_0 \exp\left(\frac{-E}{RT}\right) \tag{3.13}$$

$$K_{eq} = 7.28\times10^{6} \exp\left(\frac{-17000}{T+273}\right) \tag{3.14}$$

where the rate constant (k_0) and activation energy (E) for the system are 4.23×10^{-3} mol m^{-2} s^{-1} Pa^{-1} and 20.6 kcal mol^{-1} and R is the gas constant [53, 143, 146-148].

For reactor modeling, multiple assumptions were used: ideal gas behavior, negligible mass transfer resistance in the macroporous substrate and the catalyst layer (~ 760 μm), isothermal steady state operation, and negligible side reactions. The average particle sizes of Pt/Al_2O_3 catalysts was ~22 nm [149]. The 1D PFR model was used, which considers both reaction (feed) side and permeate side under the plug flow conditions.

For a differential section of the reactor, the 1D PFR model was considered and mass balance equation is given by the following equations:

$$dF_i = F_i\big|_{A+dA} - F_i\big|_A = dn_i - dQ_i \tag{3.15}$$

$$dn_i = \nu_i r_A dA \tag{3.16}$$

$$dQ_i = P_{m,i}(\Delta P_i)_A dA \tag{3.17}$$

where F_i (mol/s) is the feed flow rate, A (m^2) is the membrane area, ΔP_i (Pa) is pressure difference for species i across the membrane, $P_{m,i}$ (mol m^{-2} s^{-1} Pa^{-1}) is the permeance of component i, v_i is stoichiometric coefficient of component i, n_i is the rate of material generation by reaction (mol/s), and Q_i (mol/s) is the gas flow rate through the membrane. Numerical methods were used to solve the differential equations after dividing membrane into small sections (total 150) of equal area.

3.1.3 Results and discussion

Figure 3.2 presents the SEM images for surface and cross sections of the MFI zeolite membranes, which shows well intergrown polycrystalline films having thickness of ~7 μm. At room temperature, the membrane showed preferential adsorption of C_2H_6 and C_2H_4 in comparison to H_2. One possible explanation can be "adsorption diffusion" mechanism which means adsorption effect dominates over diffusion, thus C_2H_6 and C_2H_4 showed higher permeance than H_2 at room temperature. As the temperature is increased, the surface coverage of the adsorbing components (C_2H_6 and C_2H_4) decreased and opened up pore space for the nonadsorbing gas (H_2) to enter and pass through the membrane [37]. Therefore, H_2 diffusion became more predominant than the adsorption of C_2H_6 and C_2H_4. $P^o_{m,i}$ and $E_{a,i}$ in equation 3.10 are shown in Table 3.2 for H_2 and ethane at different temperatures.

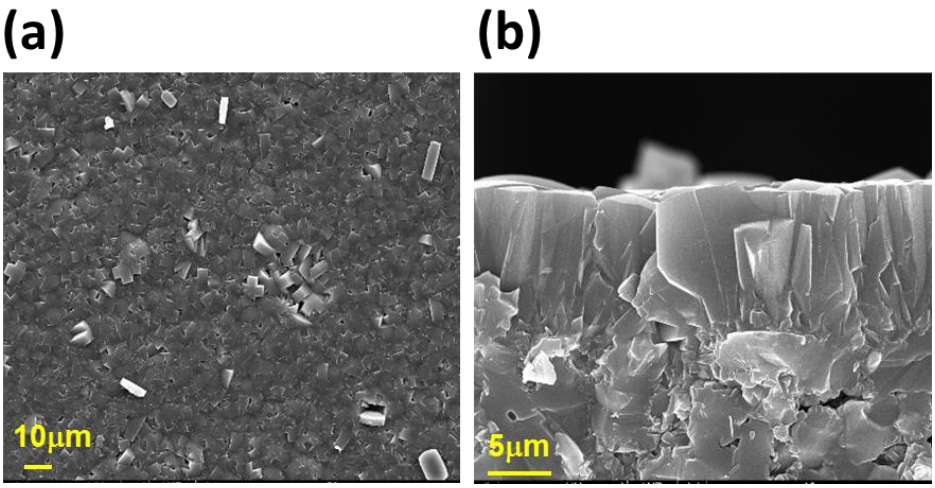

Figure 3.2. SEM images of the secondary grown zeolite MFI membrane (a) surface and (b) cross section

Table 3.2. $P^{0}_{m,i}$ and $E_{a,i}$ for equation 3.10 and $\alpha_{H2/i}$ at different temperatures

	500 °C		550 °C		600 °C	
	H_2	C_2H_6	H_2	C_2H_6	H_2	C_2H_6
P^{o}_{m}, 10^{-8}, mol m^{-2} s^{-1} Pa^{-1}	12.9	2.60	13.4	3.10	13.8	3.30
$E_{a,i}$, kJ/mol	0.96	3.49	1.02	3.76	1.09	3.92
$\alpha_{H2/i}$	-	3.06	-	3.18	-	3.31

The MFI-type zeolite PBMR was used to investigate the impact of reaction pressure on ethane dehydrogenation reaction at 1-5 atm. Experiments were conducted in the temperature range of 500-600 °C with pure ethane as a feed, WHSV of 0.74 h^{-1} and Ar sweeping flow rate (F_{Ar}) of 20 cm^3/min and as shown in Figure 3.3, the PBMR surpassed the equilibrium limit at all operating pressures. As the pressure was increased, more H_2 permeated across the membrane, which allowed reaction to move more in the direction

of the product side and helped in enhancing the ethane conversion. However, ethane conversion levelled off at ~5 atm, which can be attributed to the limiting reaction rate at that temperature. For PBR, it was found that ethane conversion decreased with increasing pressure because it is a volume expansion reaction. The ethane conversion increased from 24% to 29% for a pressure increase from 1 to 5 atm. With experimental results, the 1D PFR model was successfully validated. It should be noted that the PBMR model predicted slightly higher values than experimental values. This is probably because the modeling does not take into account the decrease in actual permeance values (H_2, C_2H_4, and C_2H_6) which results from coke deposition on the membrane surface over time. PBR model also underestimated ethane conversion values probably because only EDH reaction is considered in the model even though there are substantial amounts of by products (methane, propylene, and isobutylene) from multiple side reactions.

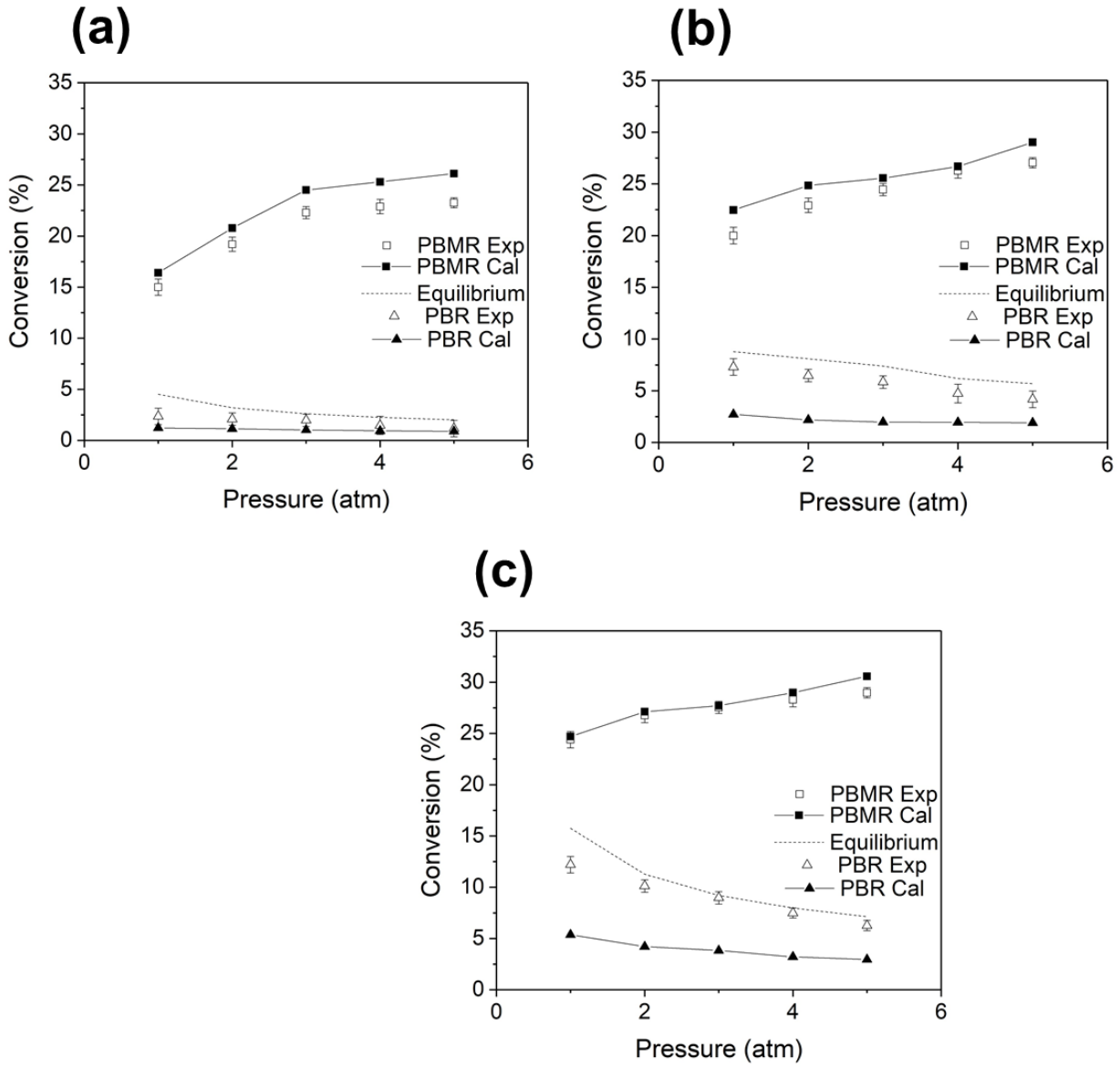

Figure 3.3. Effect of reaction pressure on ethane conversion for (a) 500 °C, (b) 550 °C, and (c) 600 °C in PBMR and PBR (WHSV = 0.74 h^{-1}; F_{Ar} = 20 cm^3/min; and p_{perm} = 1 atm)

The effect of reaction pressure on ethylene selectivity and ethylene yield was also investigated. Figure 3.4 shows that the increase of reaction pressure enhanced both selectivity and yield of ethylene in PBMR. With increase in reaction pressure, more ethylene was formed, therefore increasing the ethylene

selectivity and thus ethylene yield. In PBR operation, an increase in pressure decreased the amount of product formed because it is a volume expansion reaction, which causes a decrease in ethylene selectivity and ethylene yield.

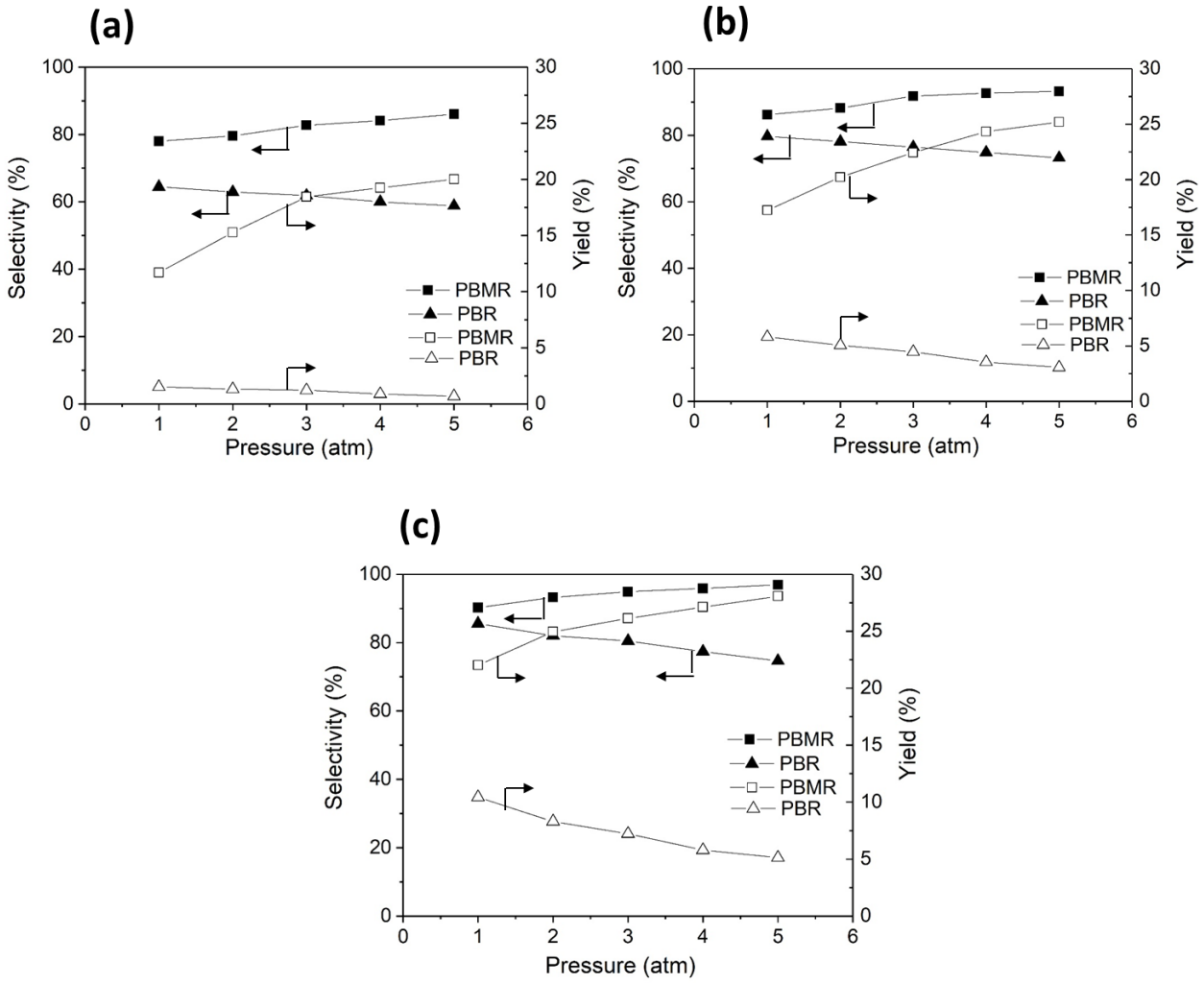

Figure 3.4. Effect of reaction pressure on ethylene selectivity and ethylene yield for (a) 500 ºC, (b) 550 ºC, and (c) 600 ºC in PBMR and PBR (WHSV = 0.74 h^{-1}; F_{Ar} = 20 cm^3/min; and p_{perm} = 1 atm)

The effect of reaction pressure on R_{H2} and $y_{H2,p}$ in PMR and PBMR was also investigated as shown in Figure 3.5. The enhancement of reaction pressure increased the driving force for the H_2 transfer though

the membrane, which led to greater R_{H2}. While R_{H2} increased with feed pressure, $y_{H2,p}$ showed a decreasing trend with increasing reaction pressure. This observation implies the possibility that the increase of reaction pressure also enhanced the permeation of other gases (e.g., ethane and ethylene). The decrease of $y_{H2,p}$ with high reaction pressure but limited $\alpha_{H2/C2H6}$ is due to excessive permeation of unreacted ethane. Due to this, more ethane was present in permeate side than H_2 at elevated pressure, which explains the decrease in $y_{H2,p}$ with enhancement in reaction pressure.

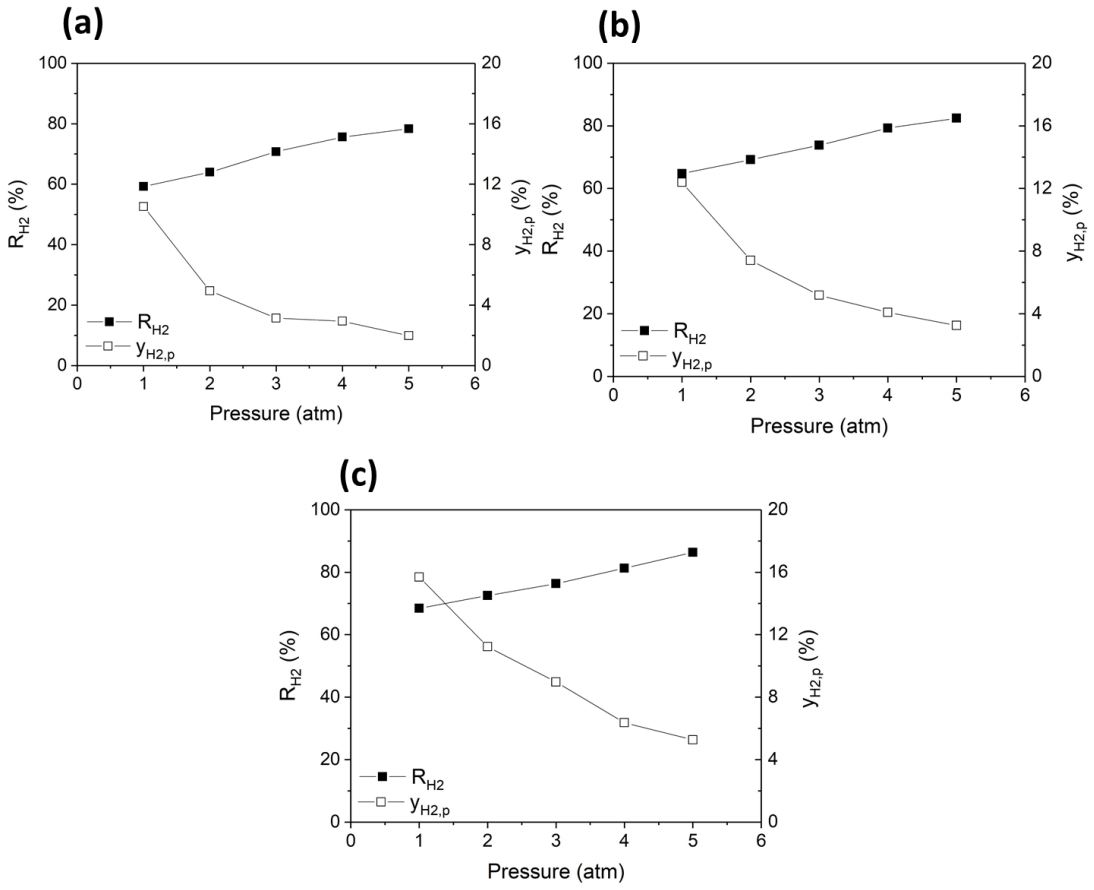

Figure 3.5. Effect of reaction pressure on R_{H2} and $y_{H2,p}$ for (a) 500 °C, (b) 550 °C, and (c) 600 °C in PBMR (WHSV = 0.74 h^{-1}; F_{Ar} = 20 cm^3/min; and p_{perm} = 1 atm)

In all the experiments, a catalyst deactivation was observed, which rapidly decreased the catalyst activity in ~1 h after EDH reaction started. Catalyst deactivation and regeneration are important considerations for alkane dehydrogenation reactions. Some dehydrogenation technologies use H_2 as a feed diluent to reduce coking and elongate the catalyst lifetime between regeneration cycles [150]. H_2 is considered to inhibit the formation of coke because it decreases the content of coke precursors (light hydrocarbons such as ethylene and propylene), which can form the oligomers and carbonaceous compounds [47]. In this work, impact of H_2/C_2H_6 ratio in feed on catalyst deactivation was studied for both PBR and PBMR reaction.

Figure 3.6 a-c shows the influence of $R_{H2/C2H6}$ (H_2 concentration in the feed), on ethylene yield, ethylene selectivity and conversion of ethane. We can see in Figure 3.6d that there was substantial change in ethane conversion values in the first one hour (region A_1). All the values shown in this study were taken after 1 h (region A_2) when steady state was ensured so that there was hardly any change in the outlet composition. It was found that ethane conversion and ethylene selectivity decreased as $R_{H2/C2H6}$ increased. When H_2 was used in the feed, there was more H_2 in the reaction side, which caused the shift of the EDH reaction in the direction of reactant thus lesser conversion. Moreover, when there is more H_2 in the feed, hydrogenolysis reaction also becomes important and selectivity of ethylene also decreased as $R_{H2/C2H6}$ increased. However, ethane conversion and ethylene selectivity values for the PBMR were higher than the PBR as expected.

As shown in Figure 3.6d, both ethane conversion and ethylene selectivity significantly declined with increasing time on stream, especially in the absence of H_2. This is due to catalyst deactivation, which occurs via deposition of carbonaceous matter (generated by undesired side reactions such as propylene cracking) on the active surface of the catalyst [47]. However, the addition of H_2 provided a much more stable time dependence of the catalyst activity and selectivity up to ~6 h of EDH, albeit with an initially lower conversion than with a pure hydrocarbon feed. The PBR and PBMRs showed similar trends of ethane conversion and ethylene selectivity. The initial lower conversion is probably because an increase in H_2

partial pressure not only decreases thermodynamic driving force but also increases competitive adsorption of H_2 with ethane on the catalyst [78, 151-153].

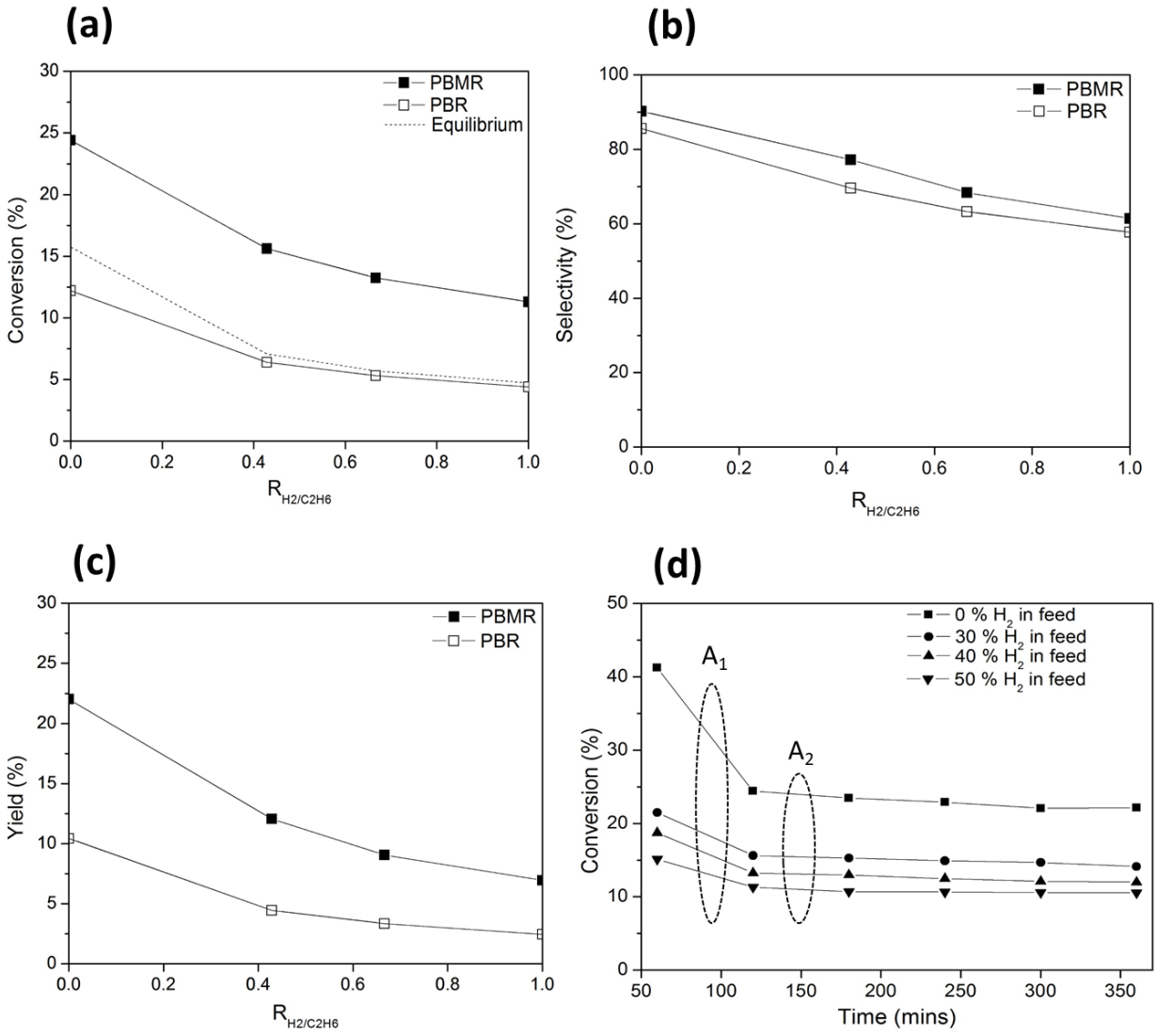

Figure 3.6. Effect of H_2 concentration in feed on (a) ethane conversion, (b) ethylene selectivity, (c) ethylene yield, and (d) ethane conversion versus EDH reaction time for PBMR at WHSV of 0.74 h^{-1}, temperature of 600 °C, p_{feed} = 1 atm, p_{perm}=1 atm, and the feed (H_2+C_2H_6 mixtures) of 10 cm^3/min

Methanation is also an important side reaction in the EDH reaction. The effect of pressure on the methane selectivity was examined for both PBR and PBMR at 500-600 °C. The WHSV and F_{Ar} were fixed at 0.74 h^{-1} and 20 cm^3/min, respectively. As shown in Figure 3.7 methane selectivity was found to be a function of reaction pressure between the PBR and PBMR operations. Methane selectivity decreased with increasing pressure for the PBMR because the increase of reaction pressure transferred more H_2, an important reactant (equation 3.18 and equation 3.19) for the methanation reaction, to the permeate side. Thus because of less H_2 available in the feed side, less methanation occurred [154]. On the other hand, for PBR, the overall reaction is not thermodynamically favored with an increase in reaction pressure, thus methane selectivity also decreased.

$$C_2H_6 \rightarrow 2C^* + 3H_2 \tag{3.18}$$

$$C^* + 4H^* \rightarrow CH_4 \tag{3.19}$$

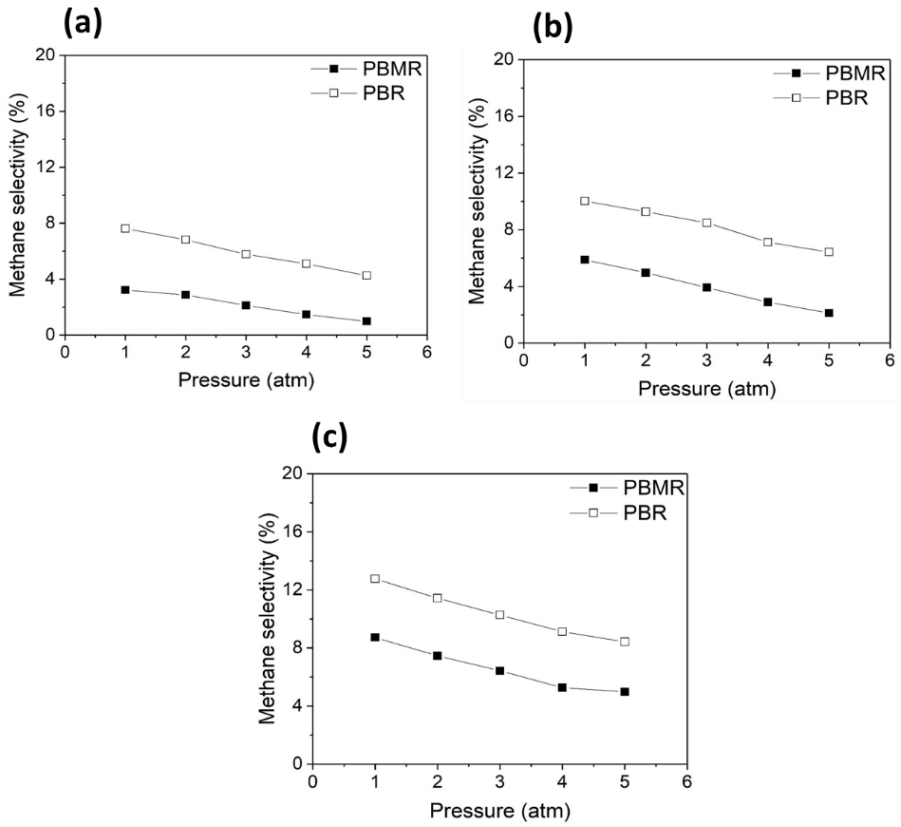

Figure 3.7. Effect of pressure on methane selectivity at (a) 500 °C, (b) 550 °C, and (c) 600 °C for PBR and PBMR (WHSV = 0.74 h^{-1} and F_{Ar} = 20 cm^3/min)

After validating the model with experimental values, the next objective of the modelling was to study the effect of pressure on ethane conversion in EDH reaction and find the most optimized reaction conditions. To investigate the impact of reaction pressure on ethane conversion beyond the experimental values, a 1D plug flow model was used.

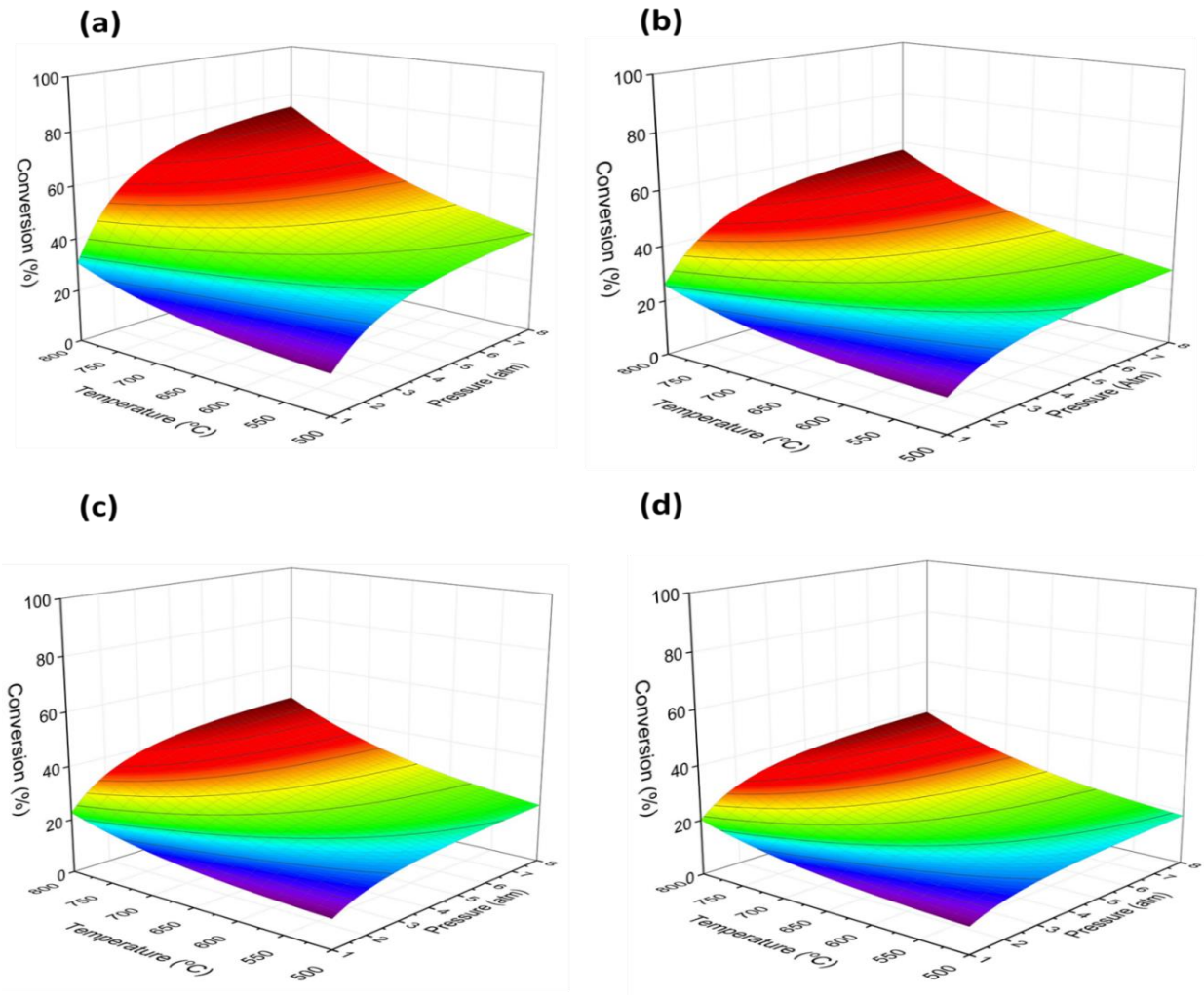

Figure 3.8. Effect of reaction pressure and temperature on ethane conversion for (a) WHSV = 0.74 h^{-1}, (b) WHSV = 1.04 h^{-1}, (c) WHSV = 1.34 h^{-1}, and (d) WHSV = 1.63 h^{-1} for F_{Ar} = 20 cm^3/min

Figure 3.8 depicts the effect of temperature and reaction pressure on ethane conversion in PBMR. The simulation was performed for WHSV= 0.15-2.81 h^{-1} in temperature range of 500-800 ^oC and pressure range of 1-8 atm for F_{Ar} = 20 cm^3/min. It was shown that increasing temperature and pressure enhanced ethane conversion, however, ethane conversion tended to level off above 6 atm. One possible reason is that the rate of product formation became equal to the product permeation rate across the membrane above 6 atm and the whole process became reaction limited. The highest ethane conversion obtained was ~75% at

800 ^{o}C and 6 atm for WHSV = 0.74 h^{-1}. These results indicate that pressure and temperature have a huge impact on ethane conversion and a membrane with moderate performance can possibly be used to achieve high ethane conversion if appropriate operating conditions are chosen.

Figure 3.9 presents the impact of reaction pressure on ethane conversion along the reactor length for PBR and PBMR. Along the reactor length, it was observed that ethane conversion for PBMR increased with enhancing the reaction pressure, which is due to the increase in H_2 permeation across the membrane. However, for PBR, conversion of ethane decreased along the length of the reactor with an increase in the pressure because EDH is a volume expansion reaction and an increase in the reaction pressure shifts the equilibrium towards the reactant side and thus ethane conversion decreases.

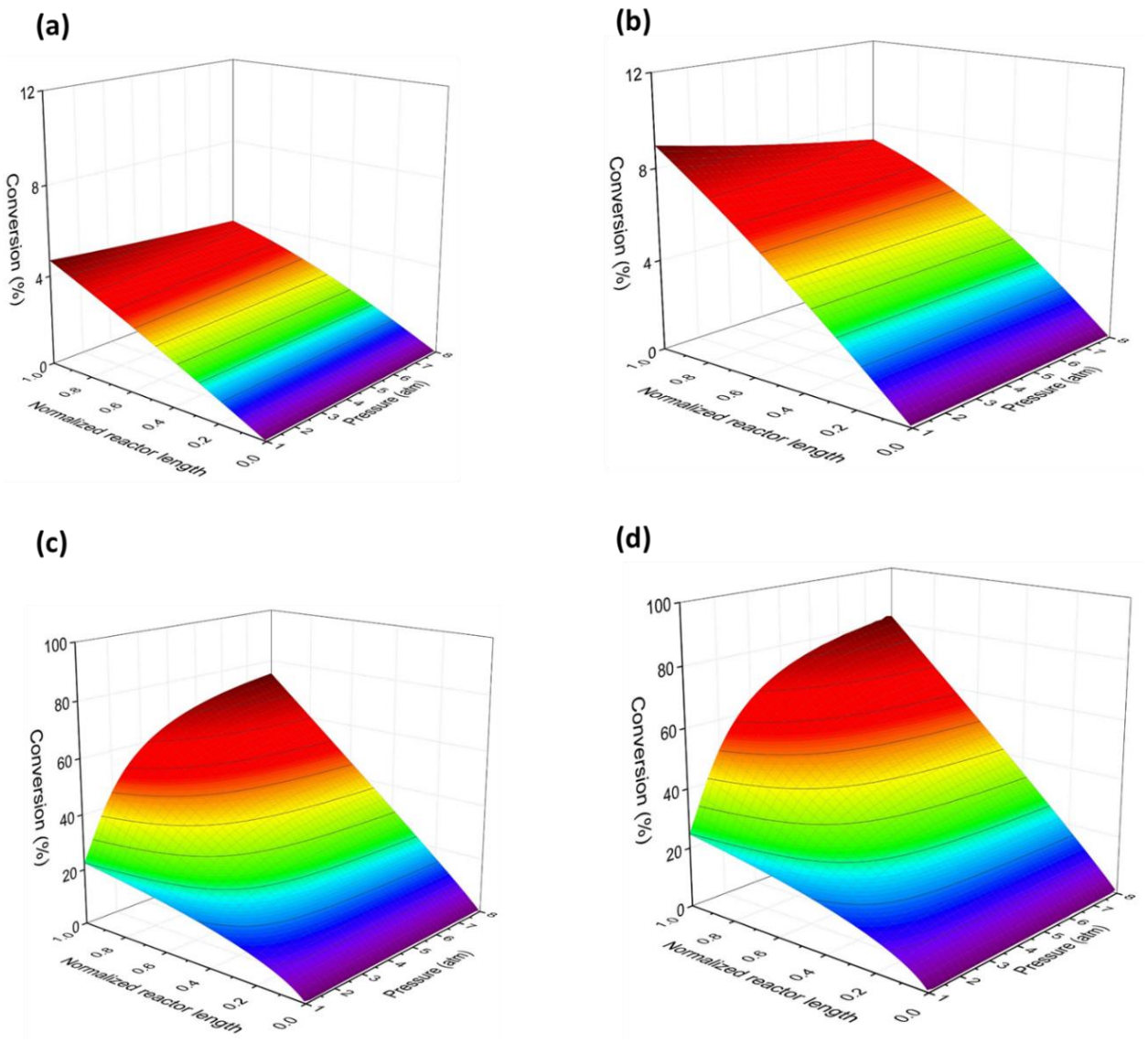

Figure 3.9. Effect of reaction pressure along the normalized reactor length on ethane conversion for (a) PBR at 600 ºC, (b) PBR at 650 ºC, (c) PBMR at 600 ºC, and (d) PBMR at 650 ºC for F_{Ar} = 20 cm^3/min and WHSV = 0.45 h^{-1}

Figure 3.10 depicts the impact of reaction pressure and membrane area. Membrane area is shown as A/A_0 where A is area of membrane area used in calculations and A_0 is the area of membrane used in experiment (2.0 cm^2). Membrane area had a significant impact on ethane conversion, which was as high as

93% at pressure of 3.0 atm and A/A_0 of 1.5. The model calculations were performed at F_{Ar} of 20 cm^3/min and WHSV of 0.45 h^{-1}.

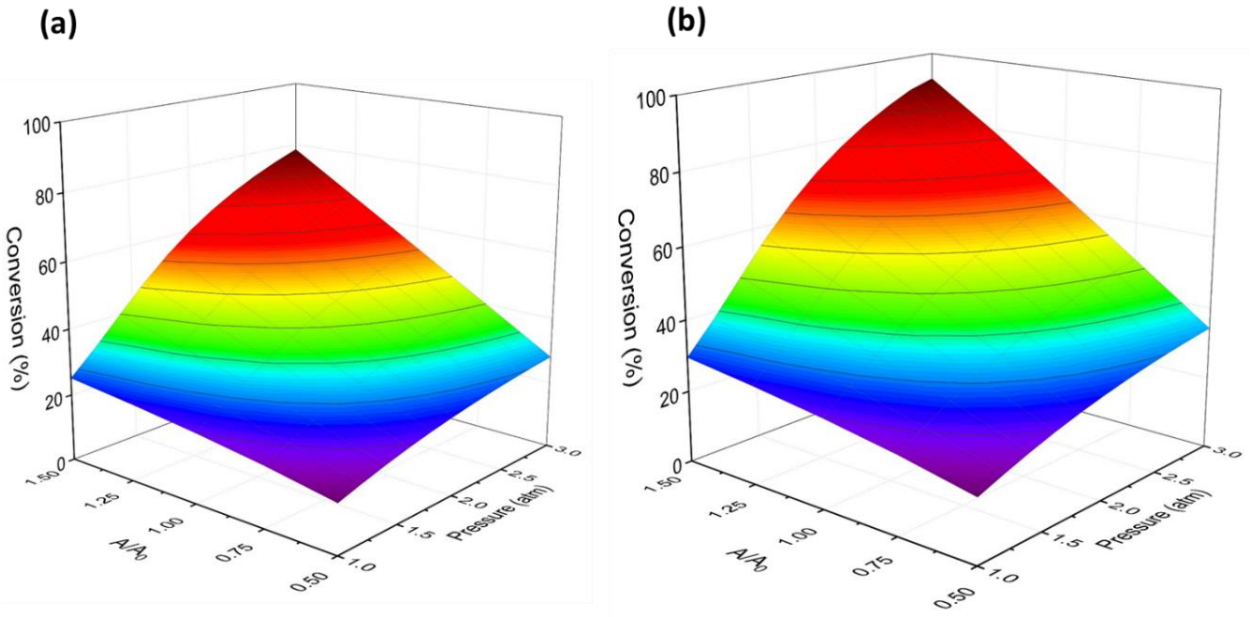

Figure 3.10. Effect of reaction pressure along the normalized area on ethane conversion for PBMR at (a) 550 ^oC and (b) 650 ^oC for F_{Ar} = 20 cm^3/min and WHSV = 0.45 h^{-1}

3.2 Propane dehydrogenation (PDH) reaction using MFI zeolite membrane reactor

3.2.1 Experimental section

The experimental setup used in the PDH reaction experiments were similar to the one explained in section 3.1.1. In addition, the MFI zeolite membrane was used for evaluating the PDH experimental results shown in this section. The operating conditions used for PDH reaction are summarize in Table 3.3.

Table 3.3. PDH membrane reactor conditions

	Experimental	Calculation
Reaction temperature, °C	500-600	500-800
Weight hourly space velocity (WHSV), h^{-1}	1.1	0.15-2.61
C_3H_8 feed flow rate, F_{C3H8}, cm^3 (STP)/min	5	1-15
Ar sweeping flow rate, F_{Ar}, cm^3 (STP)/min	20	3-30
1% Pt/Al_2O_3 catalyst loading (m_{cat}), g	0.55	0.55
Reaction pressure at retentate exit, atm	1.0-5.0	1.0-8.0
Permeate pressure, atm	1.0	1.0

3.2.2 Modelling section

The main purpose of modeling is to analyze the effects of membrane properties and the reaction conditions on C_3H_8 conversion and optimize the reaction operating conditions. Control experiments were conducted to evaluate the reaction rate parameters for the PDH modeling. Rate expression used for the

modelling is shown in equation 3.20 to 3.22. Rate constant (k) and equilibrium constant (K_{eq}) were evaluated by PDH reaction in the PBR mode. The gas mixture of C_3H_8, C_3H_6, and H_2 was introduced in the feed. At each temperature, control experiments were conducted with varying C_3H_8 flow rate while keeping the flow rate of the other two gases constant. The two compositions used in feed at each temperature were (33.3%, 33.3%, 33.3%) and (50%, 25%, 25%) for propane, propylene and H_2 mixture. Using the composition of effluent gases after steady state was achieved, partial pressures for each gas and the rate of reaction was evaluated for different flow rate at each temperature. Then the two linear equations were solved at each temperature to evaluate k and K_{eq} at that temperature. The rate constant and equilibrium constant evaluated at different temperatures were used to fit equations. 3.21 and 3.22.

$$Rate = k\left(P_{propane} - \frac{P_{propylene} \times P_{hydrogen}}{K_{Eq}} \right) \tag{3.20}$$

$$k = k_0 \exp\left(\frac{-E}{RT} \right) \tag{3.21}$$

$$K_{eq} = A\exp\left(\frac{-B}{T + 273} \right) \tag{3.22}$$

where R is the universal gas constant, K_{eq} (atm) is the equilibrium constant, E (J mol^{-1}) is the activation energy, and k (mol s^{-1} $gcatalyst^{-1}$ Pa^{-1}) is the rate constant.

There are assumptions in the modeling of the reactor: (i) negligible mass transfer resistance in the thin catalyst layer, (ii) pressure independent permeance and ideal gas behavior, (iii) isothermal steady state operation and the macroporous substrate, and (iv) negligible side reactions. Model results were compared with experimental results, validated, and used to calculate PBMR performance beyond the experimental conditions. In this study, a 1D PFR model was developed while considering plug flow conditions in the reactor modeling. In a differential section of the reactor, the following equations were used for the mass balance equation. The equations for a 1D PFR model were utilized:

$$dF_i = F_i\big|_{A+dA} - F_i\big|_A = dn_i - dQ_i \tag{3.23}$$

$$dn_i = \nu_i r_A dm_c \tag{3.24}$$

$$dQ_i = P_{m,i}(\Delta P_i)_A dA \tag{3.25}$$

where n_i is the rate of material generation by reaction (mol s^{-1}), m_c (g) is the catalyst weight, Q_i (mol s^{-1}) is the gas flow rate across the membrane, $P_{m,i}$ (mol m^{-2} s^{-1} Pa^{-1}) is the permeance of component *i*, F_i (mol s^{-1}) is the feed molar flow rate, v_i is the stoichiometric coefficient of species *i* and ΔP_i (Pa) is the pressure difference for component *i* across the membrane. Differential equations were solved by dividing the membrane into 150 equally sized sections of area. By setting $Q_i = 0$, the PFR model is described by equation 3.23.

The PDH reaction parameters in rate expression were evaluated by varying the feed flow rates during the control experiments at 550-650 °C. Figure 3.11 depicts the procedure used in determining the constants k_0, *E*, A, and B in equation 3.21 and 3.22 with each temperature point being used. Equation 3.26 presents the final power law rate equation for the dehydrogenation reaction occurring in Pt/Al_2O_3 catalyst. In these conditions, equation 3.26 was obtained as a combined rate equation only capable of being used to study the specific flow conditions and reactor structure of this study.

$$Rate = 4.01\times10^{-10}\exp\left(\frac{-34824}{RT}\right)\left(P_{propane} - \frac{P_{propylene}\times P_{hydrogen}}{723.49\exp\left(\frac{-8813.7}{T+273}\right)}\right) \tag{3.26}$$

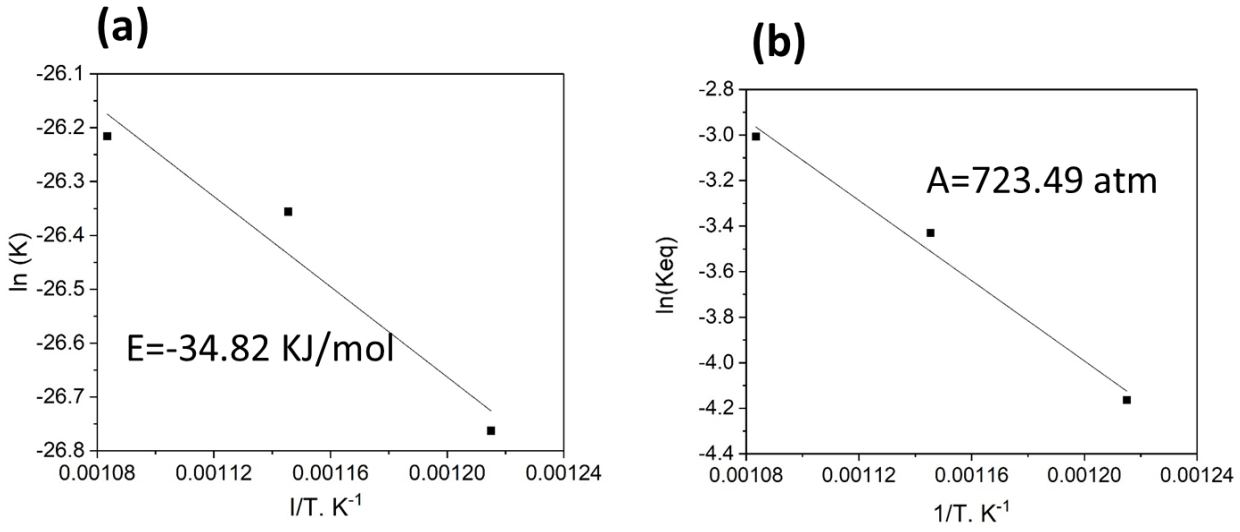

Figure 3.11. PDH reaction rates in PBR mode showing (a) relationship between rate constant and temperature and (b) relationship between equilibrium constant and temperature

3.2.3 Results and discussion

MFI Zeolite membrane was used for studying the impact of reaction side pressure on performance of propane dehydrogenation reaction. Initially membrane was tested for equimolar H_2/C_3H_8 and H_2/C_3H_6 separation from RT to 600 °C to see the feasibility of MFI zeolite membrane at high temperature. At room temperature, membrane was more selective towards C_3H_8 and C_3H_6 and thus the H_2/C_3H_8 and H_2/C_3H_6 separation factors were 0.31 and 0.52 respectively. However, H_2/C_3H_8 and H_2/C_3H_6 separation factors increased with the increase in temperature as can be seen in Figure 3.12. This can be understood by the fact that at room temperature adsorption dominates separation and C_3H_8 and C_3H_6 adsorb more on zeolite surface in comparison to H_2. But as the temperature is increased diffusion dominates separation and H_2 being smaller molecule diffuses faster than C_3H_8 and C_3H_6 and thus H_2 permeance increases faster with the temperature which further causes the increase in H_2/C_3H_8 and H_2/C_3H_6 separation factor, which were reported to be 5.67 and 4.40 at 600 °C, respectively.

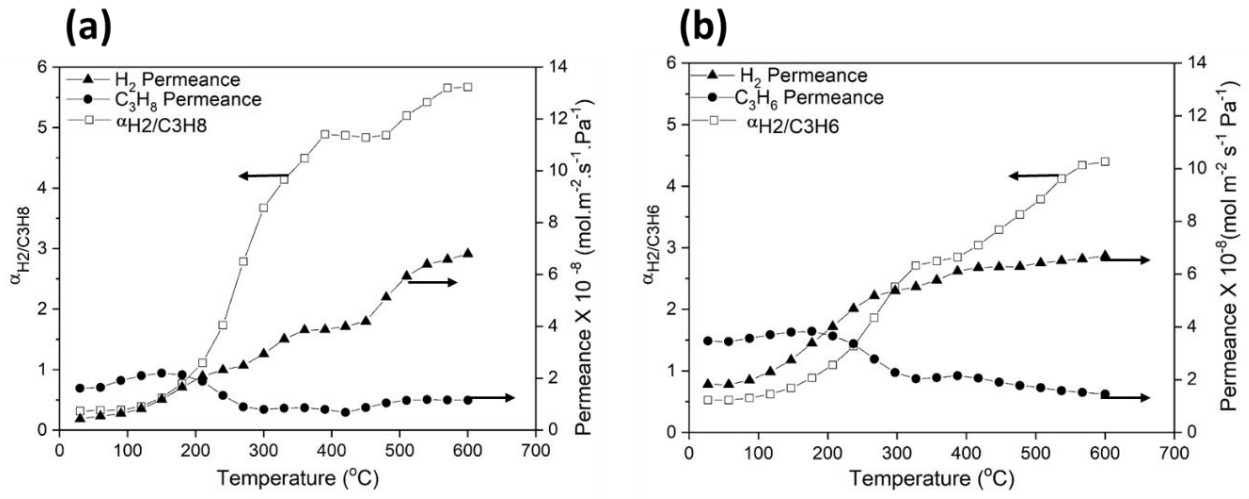

Figure 3.12. Permeation characteristics of (a) H_2/C_3H_8 and (b) H_2/C_3H_6 equimolar mixtures in MFI zeolite membranes as a function of temperature

High separation performance for H_2/C_3H_8 and H_2/C_3H_6 at 600 °C made MFI zeolite membrane an ideal candidate for studying the impact of operating conditions on the propane dehydrogenation reaction. Impact of temperature in PDH reaction was investigated in the range 500-650 °C with pure propane as feed, WHSV of 1.1 h^{-1}, and F_{Ar} of 20 cm^3/min. With increase in temperature the reaction occurs at a faster rate due to its endothermic nature which causes more propylene to form and thus propane conversion, propylene selectivity, and propylene yield increases both for PBR and PBMR. For all conditions, propane conversion, propylene selectivity, and propylene yield were higher in PBMR than the PBR and equilibrium limit. The 1D model also accurately predicted the values and trend for the propane conversion. However, for PBR experimental conversion values were slightly higher than the modelling values. This is because there were many side reactions in the experiment which not only lead to the formation of many side products such as ethylene, ethane, and methane but these side reactions also contributes to the conversion, while in the model only conversion to propylene is considered. For PBMR, the model predicted slightly higher values than experiment possibly because permeance values of C_3H_8, C_3H_6 and H_2 were assumed constant for the model but permeance values for the experiment slightly decreased as reaction proceeded. Also as shown in Figure

3.13(c), Ø (ratio of reaction and permeation rate) decreased with temperature. With increase in temperature both reaction and permeation rate increases, however permeation rate increased faster than reaction rate which led to the reduction in Ø and also shifting of equilibrium to the forward direction which eventually led to the enhancement of propane conversion, propylene selectivity and propylene yield.

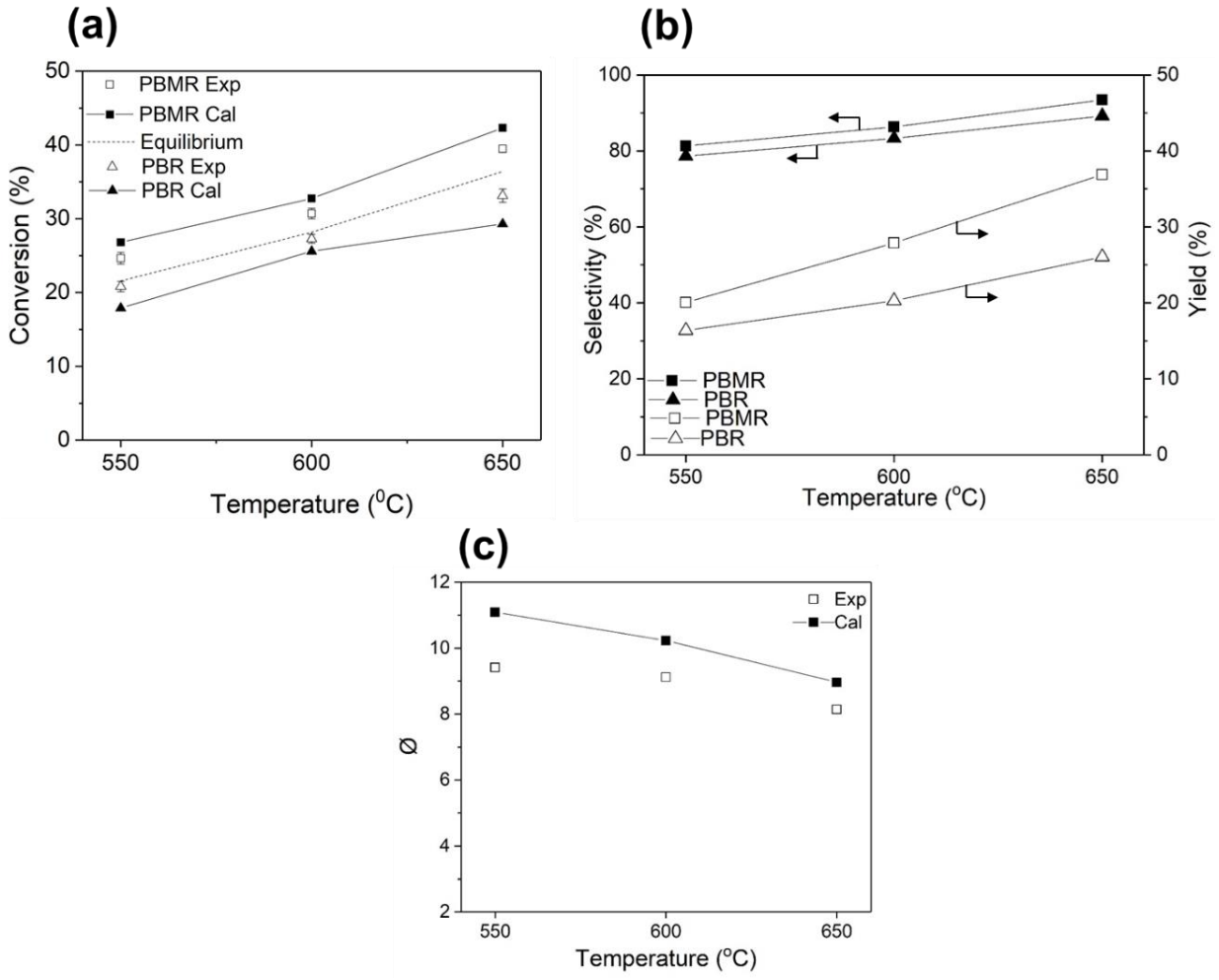

Figure 3.13. Effect of reaction temperature on (a) propane conversion, (b) propylene selectivity and propylene yield, and (c) Ø (WHSV = 1.1 h^{-1}; p_{perm} = 1 atm; and F_{Ar} = 20 cm^3/min)

Figure 3.14 shows the impact of WHSV on PDH reaction for WHSV of 0.82-2.74 h^{-1}, F_{Ar} of 20 cm^3/min, and 600 °C. At lower WHSV propane spends longest time with the catalyst bed, due to this reason

the highest propane conversion of 48% was observed at the lowest WHSV of 0.66 h^{-1}. Due to the same reason, the reactant in the reactor spends less time at higher WHSV, which causes a decrease in propane conversion, propylene selectivity, and propylene yield. Moreover with increase in WHSV, reaction rate decreases and there is no impact on permeation rate which causes the decrease in Ø with the increase in WHSV.

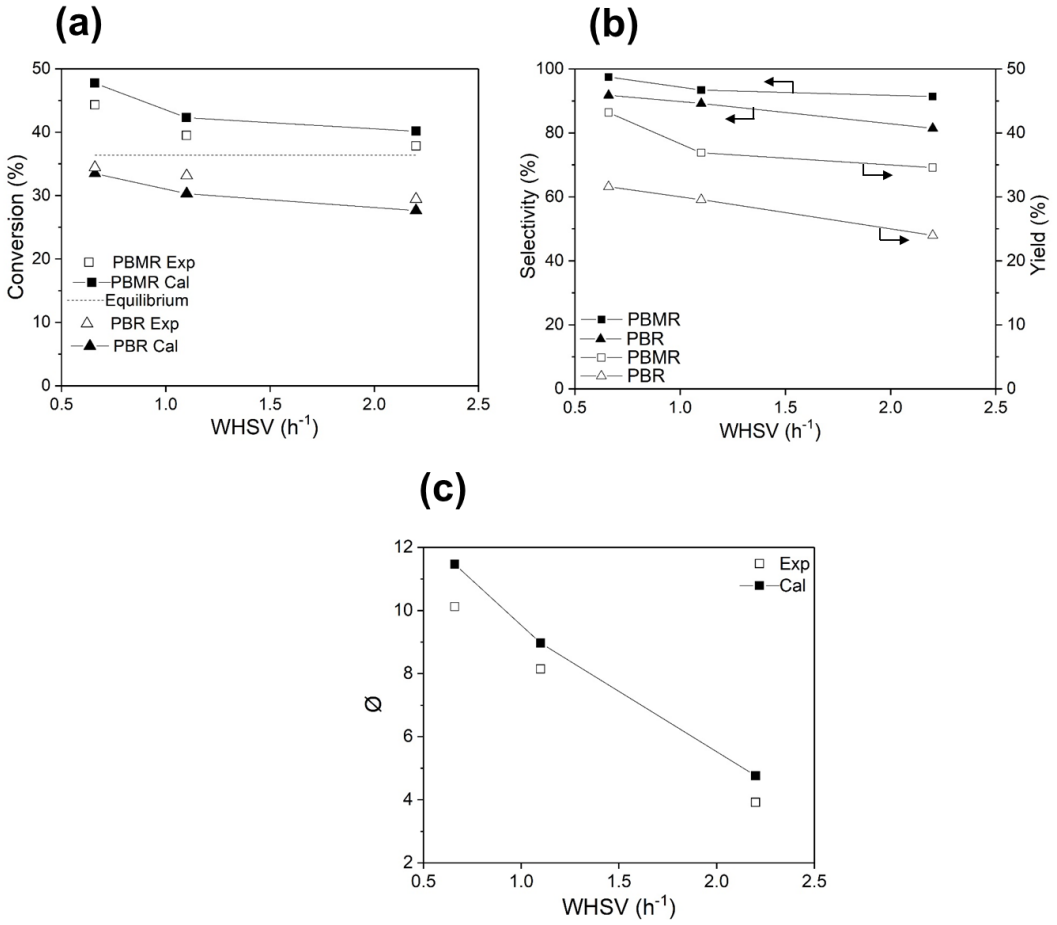

Figure 3.14. Effect of WHSV on (a) propane conversion, (b) propylene selectivity and propylene yield, and (c) Ø (temperature = 600 °C; p_{perm} = 1 atm; *and* F_{Ar} = 20 cm^3/min)

Further, the impact of F_{Ar} on PDH reaction was investigated. As shown in Figure 3.15, propane conversion, propylene selectivity, and propylene yield of the PBMRs increases with increasing F_{Ar}. With

increase in F_{Ar}, partial pressure of H_2 in the permeate was decreased whereas partial pressure in retentate side remained same. This caused enhancement in the driving force for the H_2 permeation across membrane. Thus H_2 is removed more effectively which shifts the reaction equilibrium to the product side and higher reaction performance was obtained. Also with increasing F_{Ar}, permeation rate increases substantially without any change in reaction rate which reduced Ø as can be seen in Figure 3.15c.

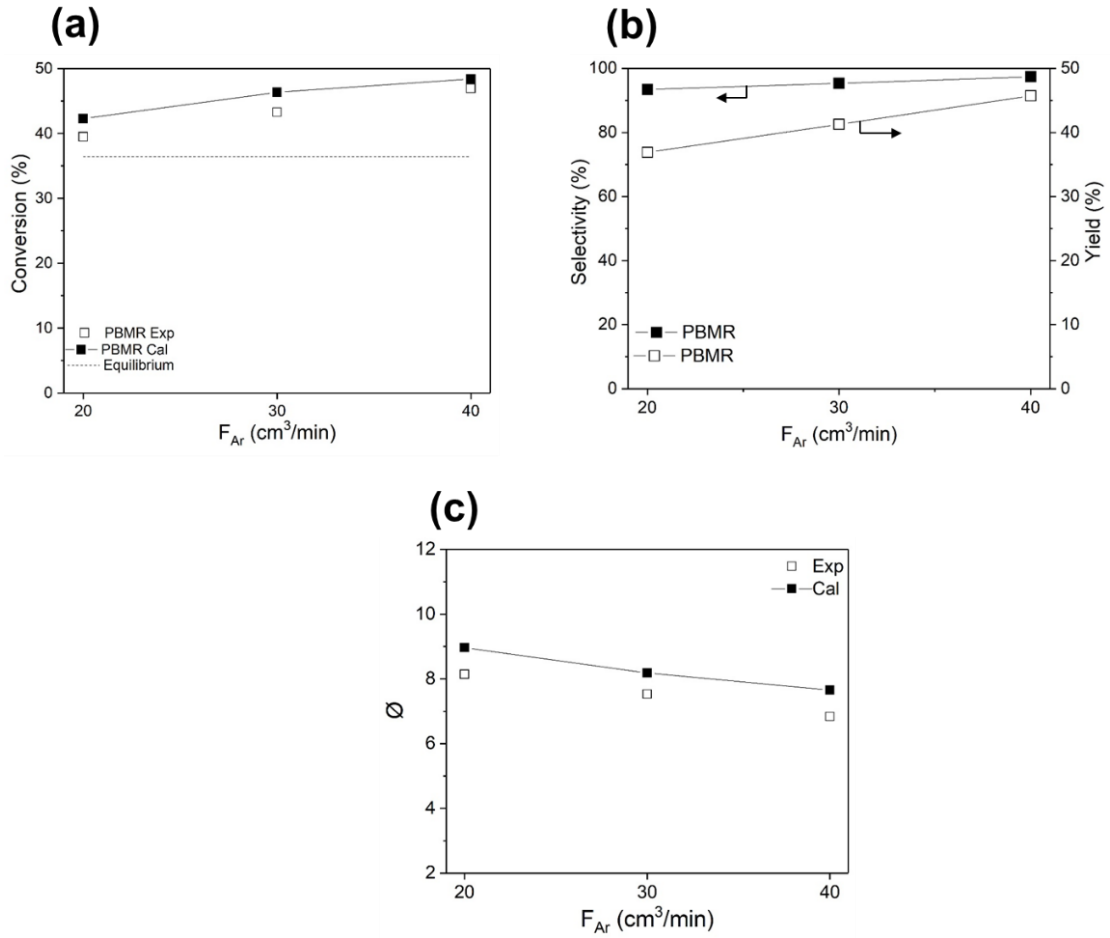

Figure 3.15. Effect of F_{Ar} on (a) propane conversion, (b) propylene selectivity and propylene yield, and (c) Ø (temperature = 600 °C; p_{perm} = 1 atm; and WHSV = 1.1 h^{-1})

Subsequently, impact of pressure was investigated for the range of 1-5 atm on PDH reaction using this MFI zeolite membrane, Experiments were conducted at 500 and 600 °C with pure propane as feed,

WHSV of 1.1 h^{-1} and Ar sweeping flow rate (F_{Ar}) of 20 cm^3/min. As expected packed bed membrane reactor exhibited higher propane conversion than equilibrium limit and packed bed reactor conversion. With increase in pressure, propane conversion decreased for PBR because propane dehydrogenation is a volume expansion reaction and increase in pressure shifts the equilibrium to the reactant side. However, for packed bed membrane reactor increase in pressure increases the propane conversion. With increase in pressure, more H_2 permeates across the membrane, which shifts the reaction equilibrium to product side in case of PBMR. This allows the propane conversion to increase from 39% at 1 atm to 49% at 5 atm for PBMR. The 1D PFR model results were validated with the experimental results as can be seen in Figure 3.16. The model correctly predicted the values and trend for effect of pressure on conversion. However, for PBMR model predicted slightly higher values than experimental values. Model did not consider the decrease in actual permeance values (H_2, C_3H_8, and C_3H_6) which results from coke deposition on the membrane surface over time and this was probably responsible for the higher propane conversion values from model. Moreover, PBR model estimated slightly lower values for the propane conversion values possibly because no side reactions were considered in the model even though there are substantial amounts of by products (methane, ethylene, propylene, and isobutylene) from multiple side reactions. Figure 3.16c shows that with increase in pressure, Ø decreases which can be understood by the substantial enhancement in permeation rate across the membrane due to increase in pressure.

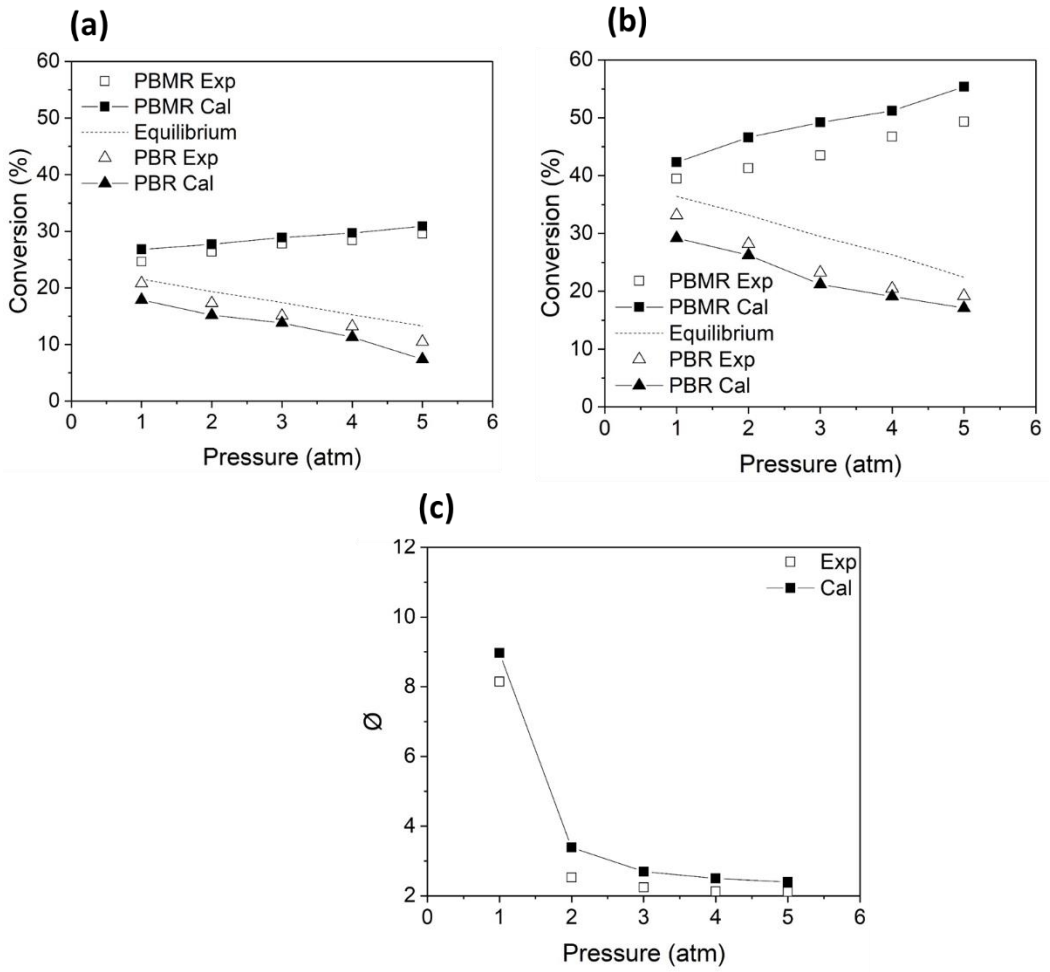

Figure 3.16. Effect of reaction pressure on propane conversion for (a) 500 °C, (c) 600 °C in PBMR and PBR, and (c) Ø (WHSV = 1.1 h^{-1}; F_{Ar} = 20 cm^3/min; and p_{perm} = 1 atm)

Figure 3.17 shows the impact of reaction pressure on propylene selectivity and propylene yield. With the increase in reaction pressure, both propylene selectivity and propylene yield increased in PBMR. With increase in reaction pressure, more propylene was formed with increase in pressure, which caused the increase in propylene selectivity and thus propylene yield. However, in PBR operation, increase in pressure decreased the amount of propylene formed because it is a volume expansion reaction, which reduces in propylene selectivity and propylene yield as can be seen in Figure 3.17.

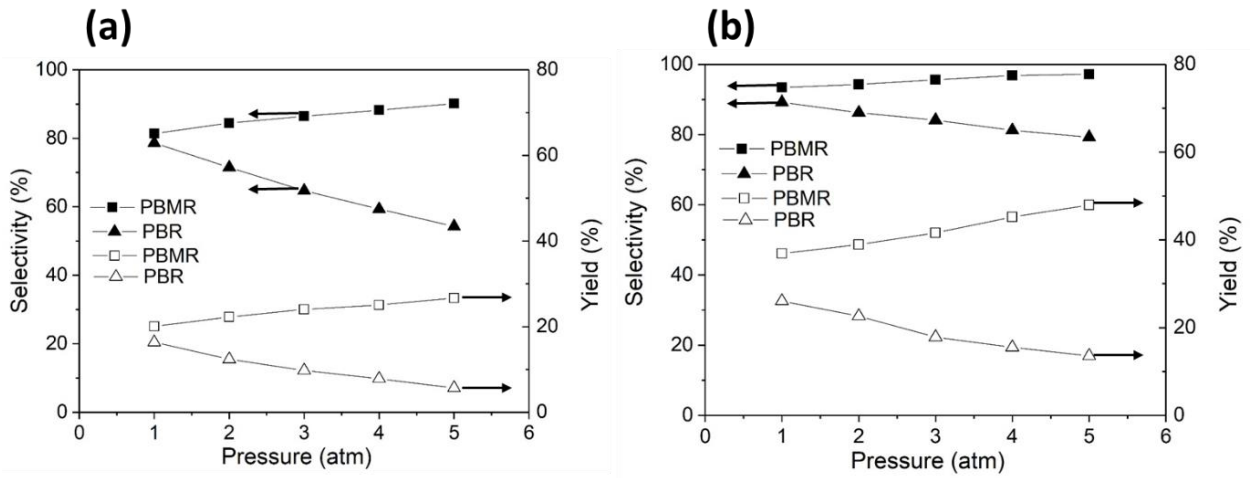

Figure 3.17. Effect of reaction pressure on propylene selectivity and propylene yield for (a) 500 °C and (b) 600 °C in PBMR and PBR (WHSV = 1.1 h^{-1}; F_{Ar} = 20 cm^3/min; and p_{perm} = 1 atm)

Impact of reaction pressure on R_{H2} and $y_{H2,p}$ in PMR and PBMR is shown in Figure 3.18. Driving force for the H_2 permeation though the membrane increases with reaction pressure, which enhances R_{H2}. While R_{H2} increased with feed pressure, $y_{H2,p}$ showed a decreasing trend with increasing reaction pressure. This happens because along with H_2, unreacted propane and propylene also permeates across the membrane. This causes the decrease of $y_{H2,p}$ because there is more unreacted propane in feed side than H_2 and thus in proportional amount it permeates through the membrane. Due to this, more propane was present in permeate side than H_2 at elevated pressure, which explains the decrease in $y_{H2,p}$ with enhancement in reaction side pressure.

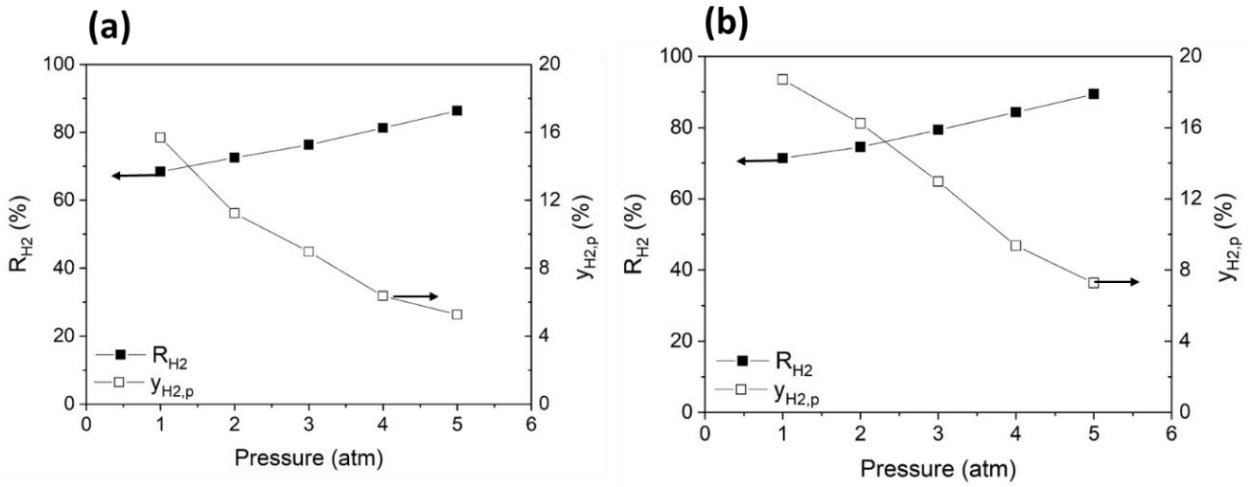

Figure 3.18. Effect of reaction pressure on R_{H2} and $y_{H2,p}$ for (a) 500 °C and (b) 600 °C in PBMR (WHSV = 1.1 h^{-1}; F_{Ar} = 20 cm^3/min; and p_{perm} = 1 atm)

Methane is the most important side product in propane dehydrogenation reaction. The effect of pressure on methane selectivity was investigated for both PBR and PBMR at 500 and 600 °C. WHSV and F_{Ar} were maintained at 1.1 h^{-1} and 20 cm^3/min, respectively. As shown in Figure 3.19, methane selectivity decreased with increasing pressure for the PBMR because with increase of reaction pressure more H_2 was permeated across the membrane, an important reactant (equation 3.27 and equation 3.28) for the methane formation, to the permeate side. Thus because of less H_2 available in feed side, less methanation occurred [154]. However, for PBR, the amount of H_2 available was higher which explains higher methane selectivity for PBR in Figure 3.19.

$$C_3H_8 \rightarrow 3C^* + 4H_2 \tag{3.27}$$

$$C^* + 4H^* \rightarrow CH_4 \tag{3.28}$$

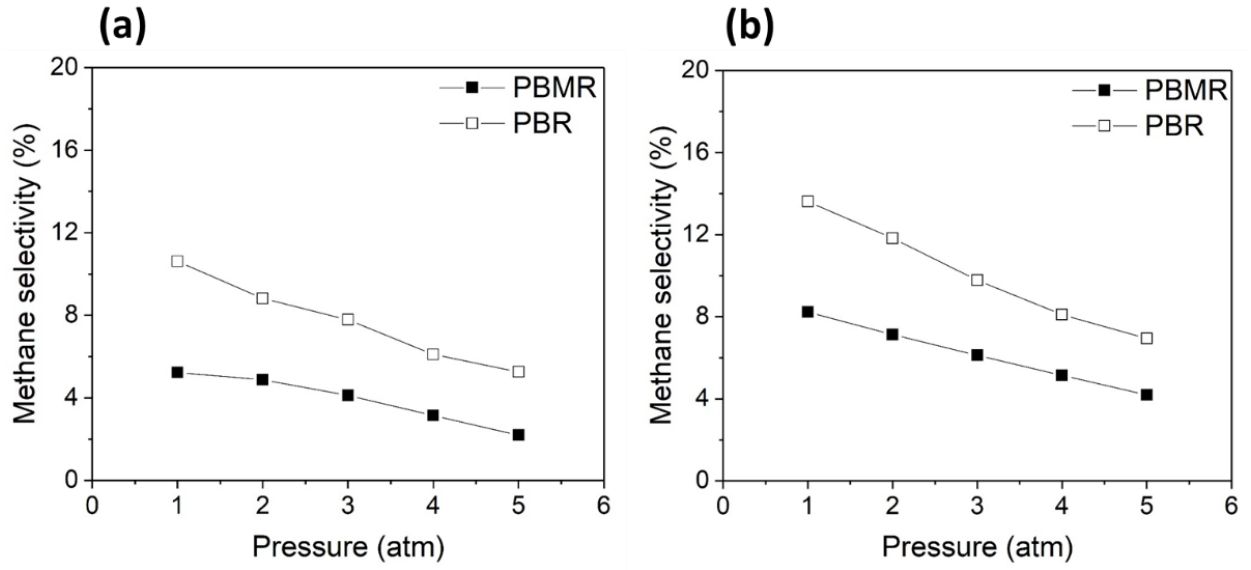

Figure 3.19. Effect of pressure on methane selectivity at (a) 500 °C and (b) 600 °C for PBR and PBMR (WHSV = 1.1 h^{-1} and F_{Ar} = 20 cm^3/min)

Moving forward, 1D PFR model was used to investigate the impact of pressure on the performance of propane dehydrogenation reaction beyond experimental conditions. Figure 3.20 depicts the effect of temperature and reaction pressure on propane conversion in PBMR. The simulation was performed for WHSV= 1.1 and 2.1 h^{-1} in temperature range of 500-800 ^oC and pressure range of 1-6 atm for F_{Ar} = 20 cm^3/min. It was found that increasing temperature and pressure enhanced propane conversion. However, propane conversion tended to level off around 6 atm. One possible reason is that the rate of the product formation became equal to the product permeation rate across the membrane above 6 atm and the entire process became reaction limited. The highest propane conversion obtained was ~96% at 800 ^oC and 6 atm for WHSV = 1.1 h^{-1}. These results indicate that pressure and temperature have significant impact on propane conversion and a membrane with moderate performance can be used to achieve high propane conversion if appropriate operating conditions are chosen.

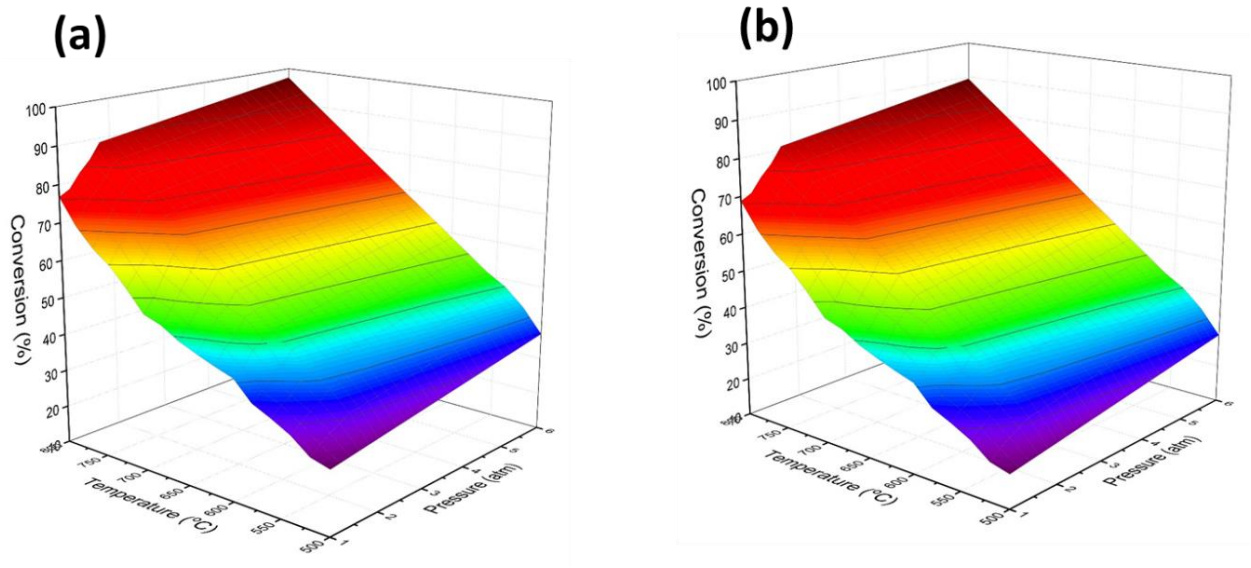

Figure 3.20. Effect of reaction pressure and temperature on propane conversion for (a) WHSV = 1.1 h^{-1} and (b) WHSV = 2.1 h^{-1} for F_{Ar} = 20 cm^3/min

Figure 3.21 presents the impact of reaction pressure on propane conversion along the reactor length for PBR and PBMR. Along the reactor length, it was observed that propane conversion for PBMR increased with enhancing the reaction pressure, which is due to the increase in H_2 permeation across the membrane. However, for PBR, conversion of propane decreased with the length of the reactor with an increase in pressure because PDH is a volume expansion reaction and an increase in reaction pressure shifts equilibrium towards the reactant side and thus propane conversion decreases.

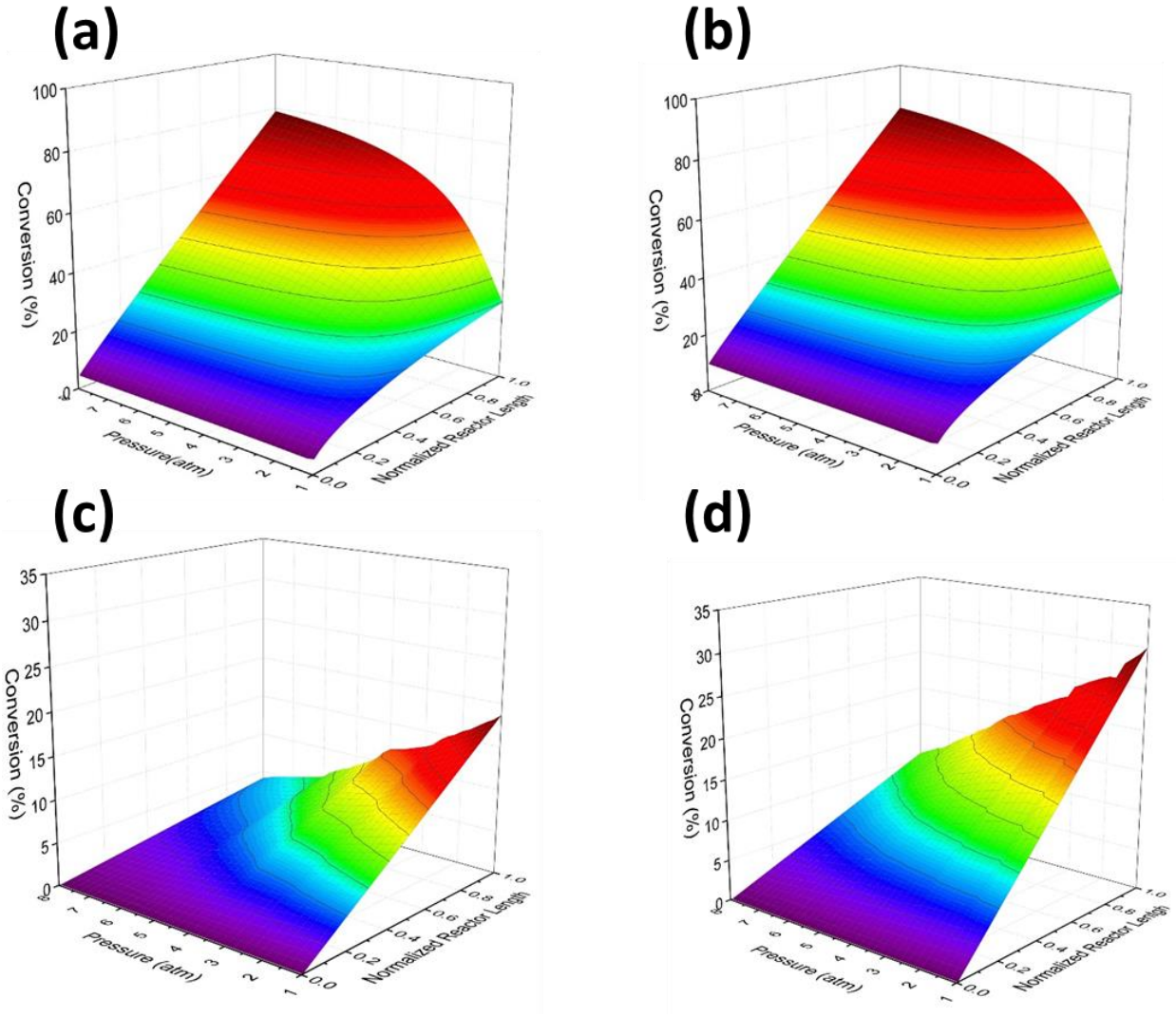

Figure 3.21. Effect of reaction pressure along the normalized reactor length on propane conversion for (a) PBMR at 500 ºC, (b) PBMR at 600 ºC, (c) PBR at 500 ºC, and (d) PBMR at 600 ºC for F_{Ar} = 20 cm^3/min and WHSV = 1.1 h^{-1}

Figure 3.22 shows the impact of reaction pressure and membrane area. Membrane area is shown as A/A_0 where A is area of membrane used in calculations and A_0 is the area of membrane used in experiment (2.0 cm^2). Membrane area had a significant impact on propane conversion, which was as high as 99% at

pressure of 3.0 atm and A/A_0 of 1.5. The model calculations were performed at F_{Ar} of 20 cm^3/min and WHSV of 1.1 h^{-1}.

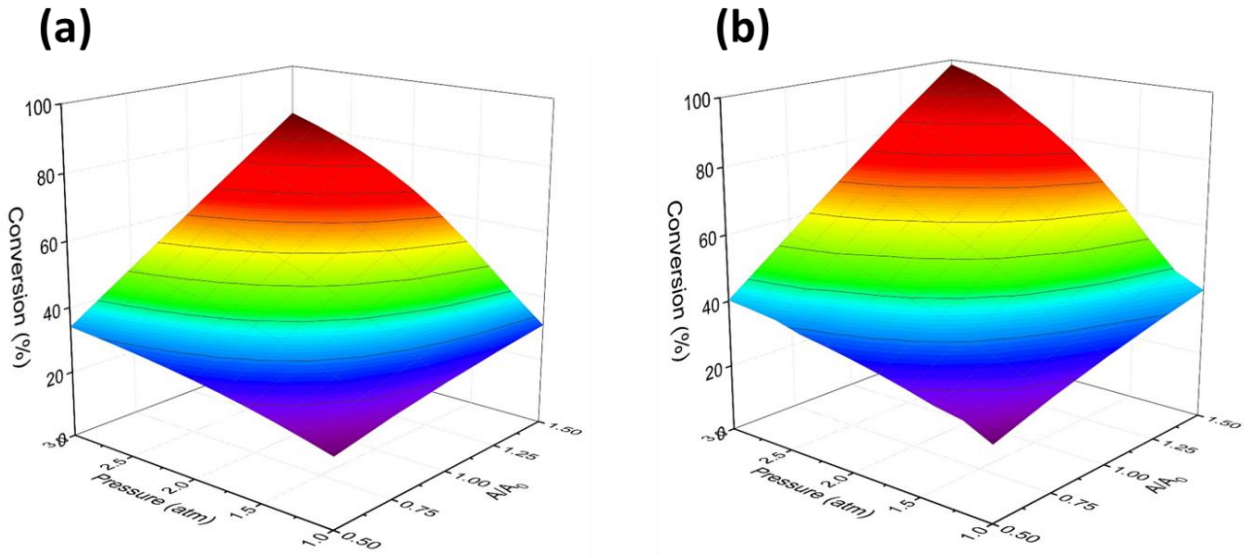

Figure 3.22. Effect of reaction pressure along the normalized area on propane conversion for PBMR at (a) 500 °C and (b) 600 °C for F_{Ar} = 20 cm^3/min and WHSV = 1.1 h^{-1}

3.3 Isobutane dehydrogenation (IBDH) reaction using MFI zeolite membrane reactor

3.3.1 Experimental section

The experimental setup used in the IBDH experiments were similar to the one explained in section 3.1.1. Moreover, the MFI zeolite membrane was used for evaluating the IBDH experimental results shown in this section. The operating conditions used for IBDH reaction are summarize in Table 3.4.

Table 3.4. IBDH membrane reactor condition

	Experimental	Calculation
Reaction temperature, °C	500-650	500-800
Weight hourly space velocity (WHSV), h^{-1}	0.8–2.7	0.3–5.2
Reactor pressure at retentate exit, atm	1.0	1.0 - 7.0
Permeate pressure, atm	1.0	1.0
1% Pt/Al_2O_3 catalyst loading (m_{cat}), g	0.55	0.55
i-C_4H_{10} feed flow rate, $F_{i\text{-}C4H10}$, cm^3 (STP)/min	3-10	1-19
Ar sweeping flow rate, F_{Ar}, cm^3 (STP)/min	0-40	0-40

3.3.2 Modelling section

The main purpose in modeling is to analyze the effects of membrane properties as well as reaction conditions on i-C_4H_{10} conversion and to find the optimized operating conditions for the reaction. Control experiments were conducted to evaluate reaction rate parameters for the IBDH modeling. Rate expression

used for the modelling is shown in equations 3.29 to 3.31. Rate constant (k) and equilibrium constant (K_{eq}) were evaluated by IBDH reaction in the PBR mode. Gas mixture of i-C_4H_{10}, i-C_4H_8, and H_2 was introduced in the feed. At each temperature, control experiments were conducted with varying i-C_4H_{10} flow rate while keeping the flow rate of the other two gases constant. The two compositions used in feed at each temperature were (33.3%, 33.3%, 33.3%) and (50%, 25%, 25%) for isobutane, isobutylene and H_2 mixture. Using the composition of effluent gases after steady state was achieved, partial pressures for each gas and rate of reaction was evaluated for different flow rate at each temperature. Then the two linear equations were solved at each temperature to evaluate k and K_{eq} at that temperature. The rate constant and equilibrium constant evaluated at different temperatures were used to fit equations 3.30 and 3.31.

$$Rate = k\left(P_{isobutane} - \frac{P_{isobutylene} \times P_{hydrogen}}{K_{Eq}} \right) \tag{3.29}$$

$$k = k_0 \exp\left(\frac{-E}{RT} \right) \tag{3.30}$$

$$K_{eq} = A\exp\left(\frac{-B}{T + 273} \right) \tag{3.31}$$

where R being the universal gas constant, K_{eq} (atm) is the equilibrium constant, E (J mol^{-1}) is the activation energy, and k (mol s^{-1} $gcatalyst^{-1}$ Pa^{-1}) is the rate constant.

The assumptions while developing the model for isobutane dehydrogenation reaction were similar to what described in section 3.2.2. The reactor was divided into 150 sections and the equations 3.23 to 3.25 analogously used for the mass balance across each section in calculating the overall conversion at any given operating conditions.

The IBDH reaction parameters in rate expression were evaluated by varying the feed flow rates during the control experiments at 500-650 ^oC. Figure 3.23 gives the procedure used in determining the

constants k_0, E, A, and B in equations 3.30 and 3.31 with each temperature point being used. Equation 3.32 presents the final power law rate equation for the dehydrogenation reaction occurring in the Pt/Al_2O_3 catalyst. In these conditions, equation 3.32 was obtained as a combined rate equation only capable of being used to study the specific flow conditions and reactor structure of this study.

$$Rate = 8.85\times10^{-12}\exp\left(\frac{-28540}{RT}\right)\left(P_{isobutane} - \frac{P_{isobutylene}\times P_{hydrogen}}{1041.06\exp\left(\frac{-9256.2}{T+273}\right)}\right) \tag{3.32}$$

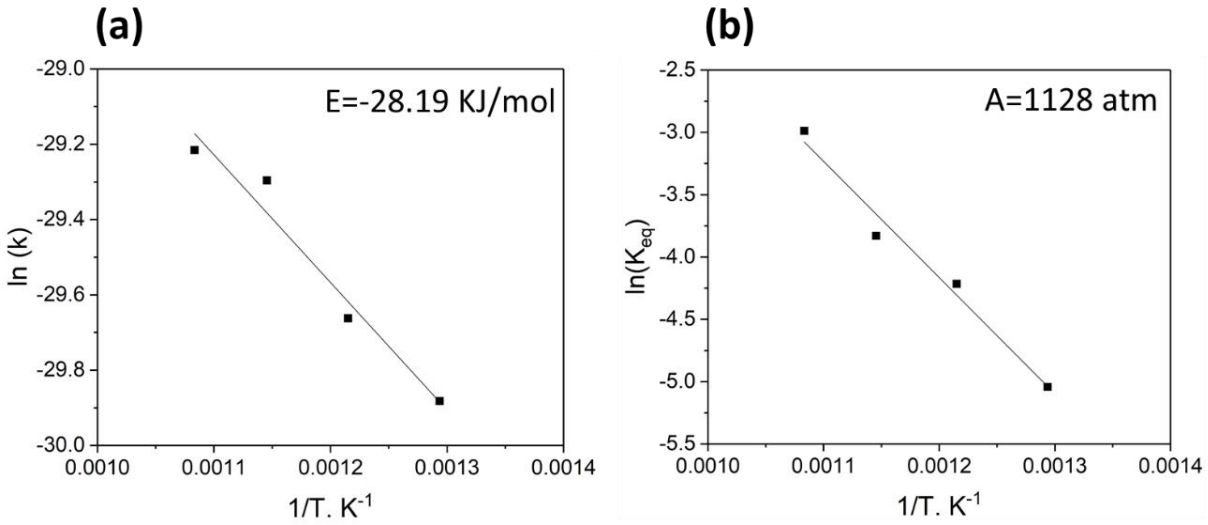

Figure 3.23. IBDH reaction rates in PBR mode showing (a) relationship between rate constant and temperature and (b) relationship between equilibrium constant and temperature

3.3.3 Results and discussion

SEM images revealed that the MFI-type zeolite membrane is ~12 μm thick as shown in Figure 3.24. Figure 3.25 shows the binary gas permeation characteristics for H_2/i-C_4H_{10} and H_2/i-C_4H_8 mixture from RT to 600 °C. At room temperature, membrane was more selective to i-C_4H_{10} and i-C_4H_8 as separation was adsorption dominant and H_2/i-C_4H_{10} separation factor was less than 1. On increasing the temperature,

separation becomes diffusion dominant and H_2 being smaller molecule diffuses faster and therefore H_2 permeance increases faster than i-C_4H_{10} and i-C_4H_8. Upon increasing to 600 °C, a H_2 permeance of 8.1 × 10^{-8} mol m^{-2} s^{-1} Pa^{-1} as well as a H_2/i-C_4H_{10} permselectivity of 8.3 was measured. This is higher than the Knudsen factor of 5.4, revealing that the membrane possessed only minor defects for nonselective viscous flow. Table 3.5 shows the gas permeation data which was evaluated for the MFI zeolite membrane right immediately ~215 h of operations at >500 °C. This involved ~65 h under dry gas permeation and ~150 h during IBDH reaction conditions. The permeation values were obtained from the data of H_2/i-C_4H_8 and H_2/i-C_4H_{10} binary mixtures, and analyzed with pressure of 1 atm (both feed and permeate side) at 23-600 °C.

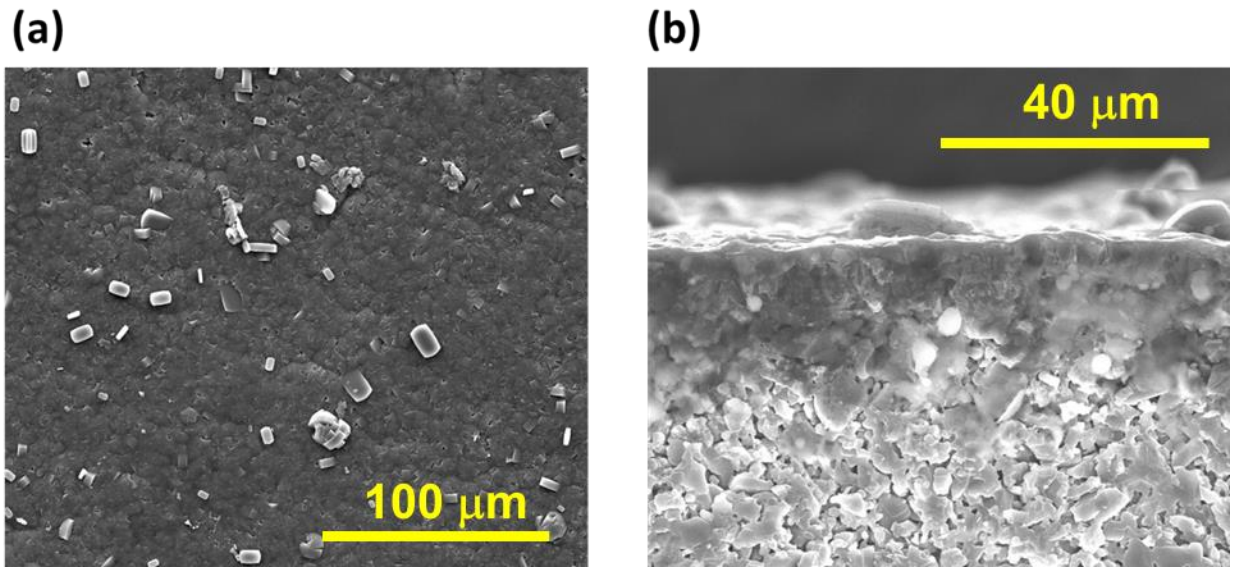

Figure 3.24. (a) Surface and (b) cross sectional SEM images of the secondary grown MFI zeolite membranes before the IBDH reaction

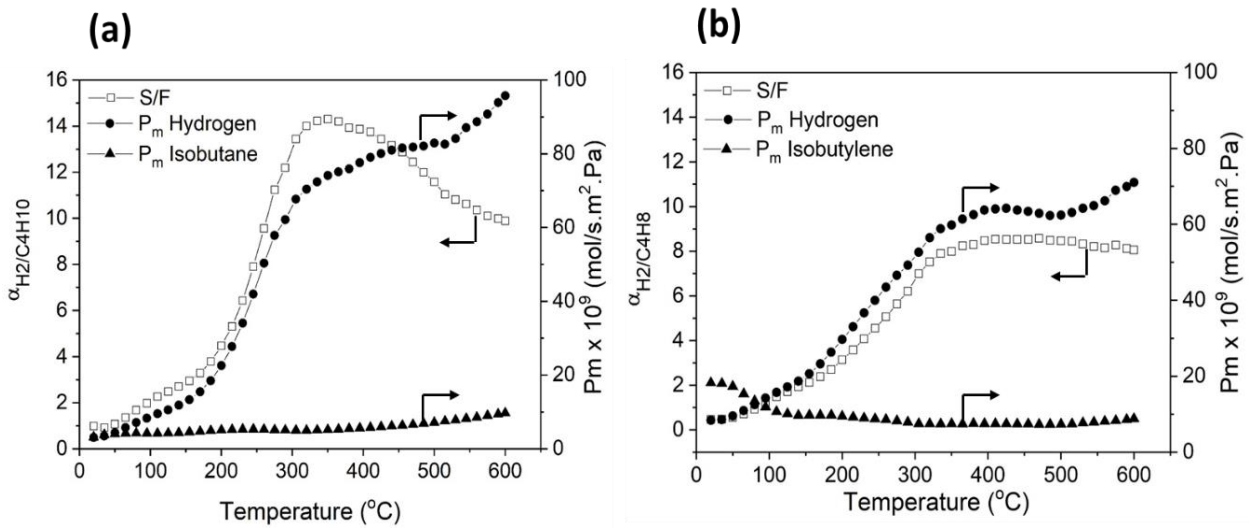

Figure 3.25. Separation performance of (a) H_2/i-C_4H_{10} (b) H_2/i-C_4H_8 equimolar mixtures in MFI zeolite membranes as a function of temperature

Table 3.5. $P_{m,i}$ and $\alpha_{H2/i}$ values for H_2, i-C_4H_{10} and i-C_4H_8 after ~215 h of operation

T (°C)	Property	H_2	i-C_4H_{10}	i-C_4H_8
550	$P_{m,i}$ 10^{-8}, mol m^{-2} s^{-1} Pa^{-1}	7.6	0.8	1
	$\alpha_{H2/i}$	-	9.6	7.8
600	$P_{m,i}$ 10^{-8}, mol m^{-2} s^{-1} Pa^{-1}	8.2	0.9	1.3
	$\alpha_{H2/i}$	-	9.8	6.7

For high temperature IBDH reactions, the MFI zeolite PBMR was tested at 500-650 °C with only pure i-C_4H_{10} in the feed, WHSV of 1.37 h^{-1}, and Ar was used as sweep gas with a flow rate (F_{Ar}) of 20 cm^3/min. As shown in Figure 3.26, i-C_4H_{10} conversion in the PBMR increased from 12% at 500 °C to 26% at 650 °C. This can be explained by the endothermic nature of the reaction, which causes more products to form at higher temperature. Because of timely H_2 removal, IBDH reaction in the PBMR moved towards

the product side, leading to a larger i-C_4H_{10} conversion than that obtained by the PBR and the equilibrium limit. Moreover, at higher temperature, the faster reaction rate caused the higher i-C_4H_8 selectivity and yield. As shown in Figure 3.26(a), the calculated values were very close to the experimental values. For PBR, experimental conversion values were little higher than the modelling results. This can be explained by the fact that there were many side reactions in the experiment which not only lead to the formation of many side products such as propylene, ethylene, ethane, methane, and propane but these side reactions also contributed to the conversion, while in the model only IBDH reaction is considered. For PBMR, the model predicted slightly higher values than experiment probably because permeance values of i-C_4H_{10}, i-C_4H_8 and H_2 were assumed constant for the model but permeance values for the experiment slightly decreased as reaction proceeded. The reduction in permeance values for i-C_4H_{10}, i-C_4H_8 and H_2 was due to accumulation of the coke in the membrane pores as the reaction proceeds. Highest isobutylene selectivity and isobutylene yield was 97% and 26% for PBMR, which is considerably higher than 90% and 10%, respectively, for PBR at 650 ^oC. As shown in Figure 3.26(c), $y_{H2,P}$ increased with temperature, which can be attributed to the higher H_2 permeance value at the elevated temperature. As H_2 permeation increased in the permeate side with temperature, H_2 flux across the membrane increased, which caused the increase in R_{H2}.

Figure 3.27 show the molar concentrations of species in the reactors. The permeate stream of the PBMR in Figure 3.27(b) has a larger H_2 molar concentration than both the PBMR retentate in Figure 3.27(a) stream and the single PBR exit stream in Figure 3.27(c). In the PBMR retentate stream, H_2 and i-C_4H_{10} molar concentration are lower than the single PBR exit stream. This indicates that H_2 permeation across the membrane improves i-C_4H_{10} conversion in PBMR higher than PBR and thus lower molar concentration of H_2 and i-C_4H_{10} for PBMR retentate than single PBR exit stream. The H_2 molar concentration in the PBMR permeate stream is considerably larger than that of the retentate stream. This is also because of H_2 removal across the membrane.

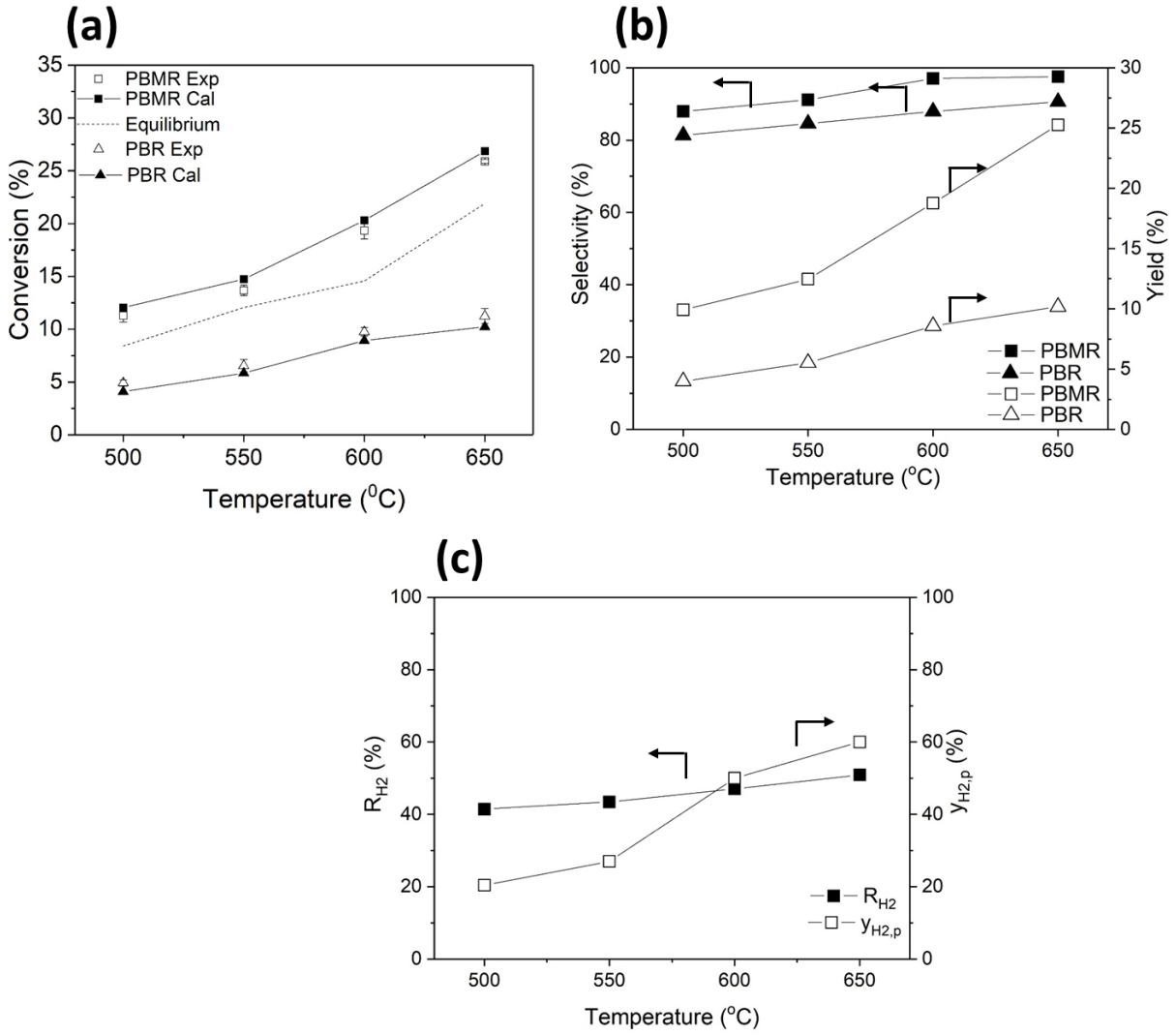

Figure 3.26. (a) i-C_4H_{10} conversion, (b) i-C_4H_8 selectivity and i-C_4H_8 yield, and (c) R_{H2} and $y_{H2,p}$ in PBMR versus reaction temperature (WHSV = 1.37 h^{-1}; p_{perm} = 1 atm; *and* F_{Ar} = 20 cm^3/min)

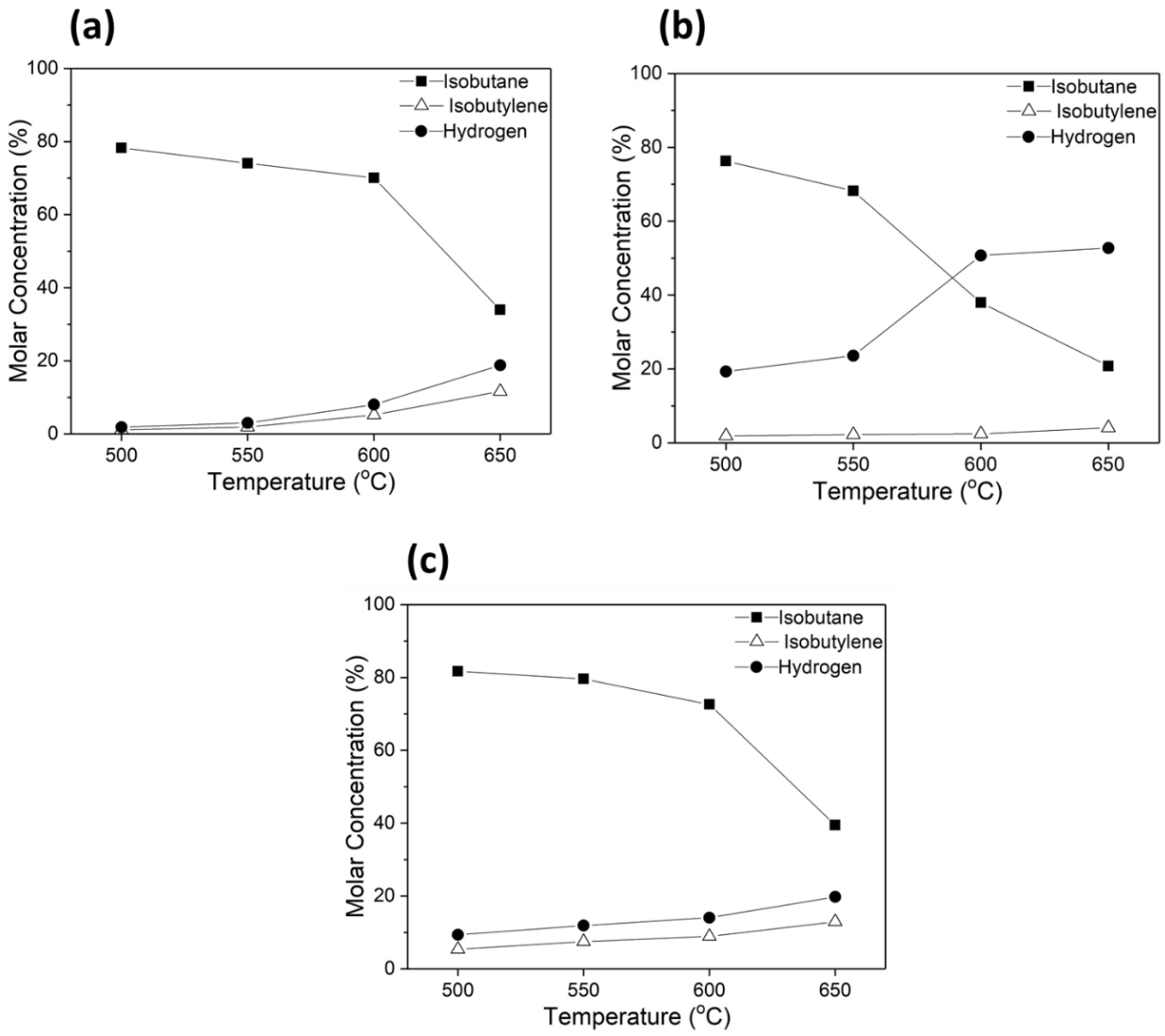

Figure 3.27. Molar concentration of i-C_4H_{10}, i-C_4H_{10} and H_2 for (a) PBMR retentate, (b) PBMR permeate, and (c) PBR versus reaction temperature (WHSV = 1.37 h^{-1}; p_{perm} = 1 atm; and F_{Ar} = 20 cm^3/min)

Figure 3.28 presents the IBDH reaction with the PBMR at WHSV of 0.82-2.74 h^{-1}, F_{Ar} of 20 cm^3/min, and 600 °C. The highest i-C_4H_{10} conversion of 22% was observed at lowest WHSV of 0.82 h^{-1} due to longer residence time of the reactant. In contrast, the reactant in the reactor spends less time at higher WHSV, which causes a decrease in both i-C_4H_8 selectivity, i-C_4H_8 yield, and H_2 production. With less H_2 forming in the reaction, the amount of H_2 permeated to the product side also decreases, which reduces the

flux of H_2 across the membrane. The reduced H_2 flux across the membranes causes $y_{H2,P}$ and R_{H2} to decrease with increase in WHSV as presented in Figure 3.28(c). In Figure 3.28(a), modeling results are shown along with experimental results for i-C_4H_{10} conversion values. The modeling values were in agreement with the experimental values. For increase in WHSV, the model correctly predicted the trend. As in the case of temperature enhancement, model slightly under predicted the i-C_4H_{10} conversion values for PBR and over predicted for PBMR for the reasons described in the previous section.

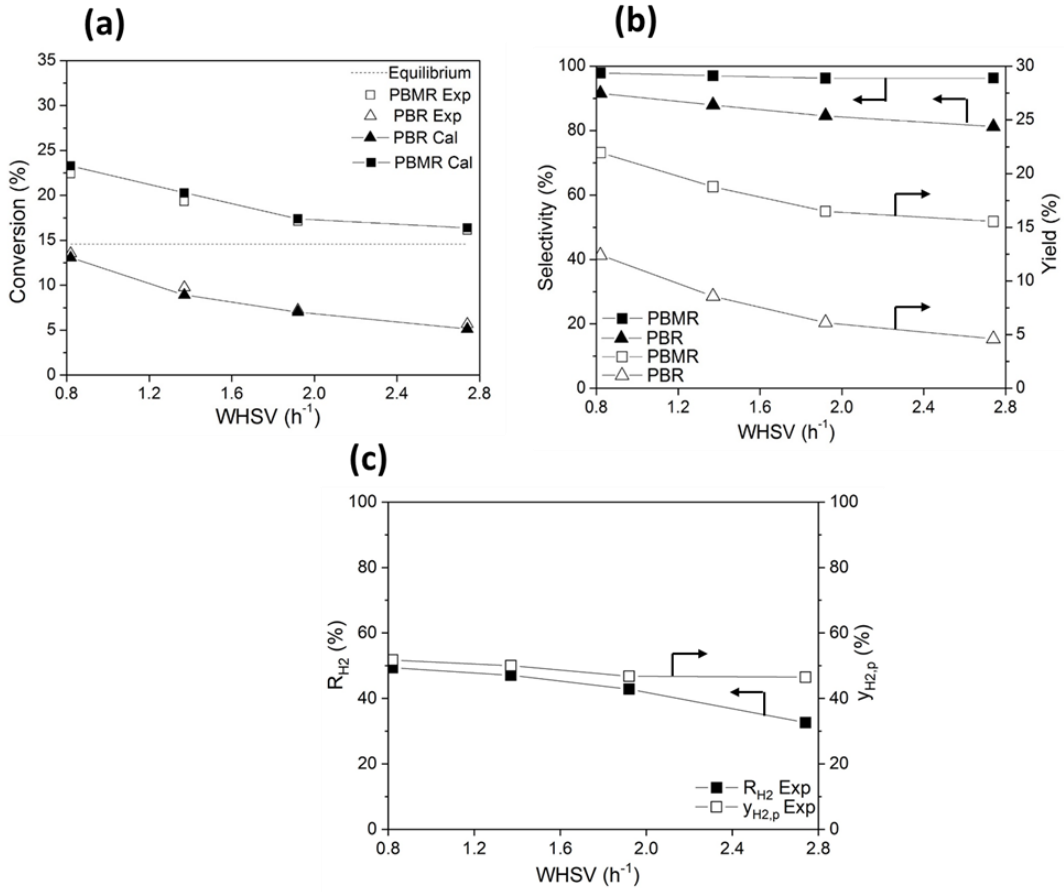

Figure 3.28. (a) i-C_4H_{10} conversion, (b) i-C_4H_8 selectivity and i-C_4H_8 yield, and (c) R_{H2} and $y_{H2,p}$ in PBMR versus WHSV (p_{perm} = 1 atm; temperature = 600 °C; and F_{Ar} of 20 cm^3/min)

In order to increase the driving force for H_2 removal from the feed side, the use of sweeping gas on the membrane permeate side is essential, which eventually assists in allowing reaction equilibrium to favor the product side. As shown in Figure 3.29, i-C_4H_{10} conversion, i-C_4H_8 selectivity, and i-C_4H_8 yield of the PBMRs strongly changes with F_{Ar}. The partial pressure of H_2 in the permeate was decreased with increasing F_{Ar}, which enhanced the H_2 permeation driving force across membrane, therefore strengthening the i-C_4H_{10} conversion. Moreover, the corresponding values of i-C_4H_8 selectivity and i-C_4H_8 yield were also increased with increasing F_{Ar}. Thus, at a large F_{Ar}, H_2 is removed more efficiently which in turn shifts the IBDH reaction toward the product side and a larger R_{H2} is achieved within the permeate stream as seen in Figure 3.29(c). However, due to H_2 depletion, the increased H_2 removal lead to a diminished value of $(y_{H2}/y_{i\text{-}C4H10})_{feed}$ in the reaction side. Therefore, based upon equation 3.3, minimizing $(y_{H2}/y_{i\text{-}C4H10})_{feed}$ reduces the value of $(y_{H2}/y_{i\text{-}C4H10})_{permeate}$ $(=\alpha_{H2/i\text{-}C4H10}(y_{H2}/y_{i\text{-}C4H10})_{feed})$, which provides understanding to the decreasing trend of $y_{H2,p}$ and increasing trend of R_{H2} under larger F_{Ar}.

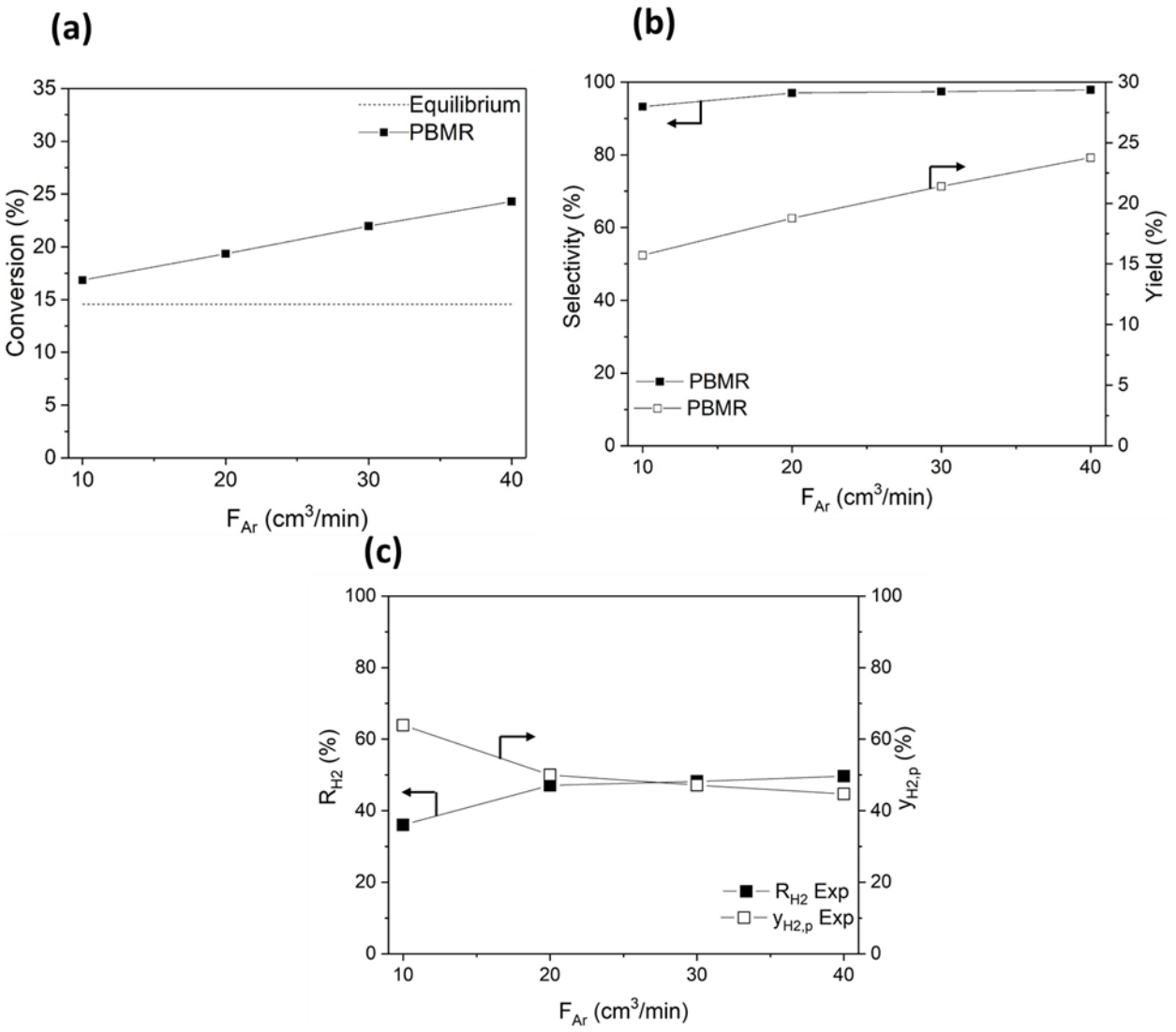

Figure 3.29. Effect of F_{Ar} on (a) i-C_4H_{10} conversion, (b) i-C_4H_8 selectivity and i-C_4H_8 yield, and (c) R_{H2} and $y_{H2,p}$ in PBMR (p_{perm} = 1 atm; WHSV = 1.37 h^{-1}; and temperature = 600 °C)

Moving further, the model was used to predict i-C_4H_{10} conversion beyond experimental conditions for two reasons: 1) to predict conversion values at reasonable experimental conditions without conducting experiments, and 2) to investigate the chances of achieving near complete conversion at experimentally available conditions. The PBMR performance was simulated by a 1D PFR model to study the reaction performance within and outside of the operating conditions utilized in this report. The effect of WHSV,

temperature, and F_{Ar} on i-C_4H_{10} conversion were studied. Reaction conditions were kept constant unless those were changed to study their effect: feed side pressure (p_{feed}) of 1 atm, WHSV of 0.45 h^{-1}, temperature of 600 °C, and F_{Ar} of 20 cm^3/min. Figure 3.30 shows simulated i-C_4H_{10} conversions for the MFI zeolite membrane reactors for different operating conditions. Figure 3.30(a) shows that both raising p_{feed} as well as temperature increase the PBMR i-C_4H_{10} conversion [155]. Above a certain pressure and temperature, i-C_4H_{10} conversion tended to plateau. The highest i-C_4H_{10} conversion in zeolite PBMR (91%) was achieved at p_{feed} > 6.5 atm and T > 750 °C, which are practically operational outside of a laboratory setup. The effect of WHSV and temperature on i-C_4H_{10} conversion is shown in Figure 3.30(b). Because reactant spend less time in the reactor with increasing WHSV, i-C_4H_{10} conversion decreases. The maximum i-C_4H_{10} conversion in the PBMR significantly varies with operating conditions. From these results, although zeolite membranes with only a moderate H_2 selectivity and permeance is used, it was found that i-C_4H_{10} conversion can be improved by the selection of proper operating conditions in the PBMR.

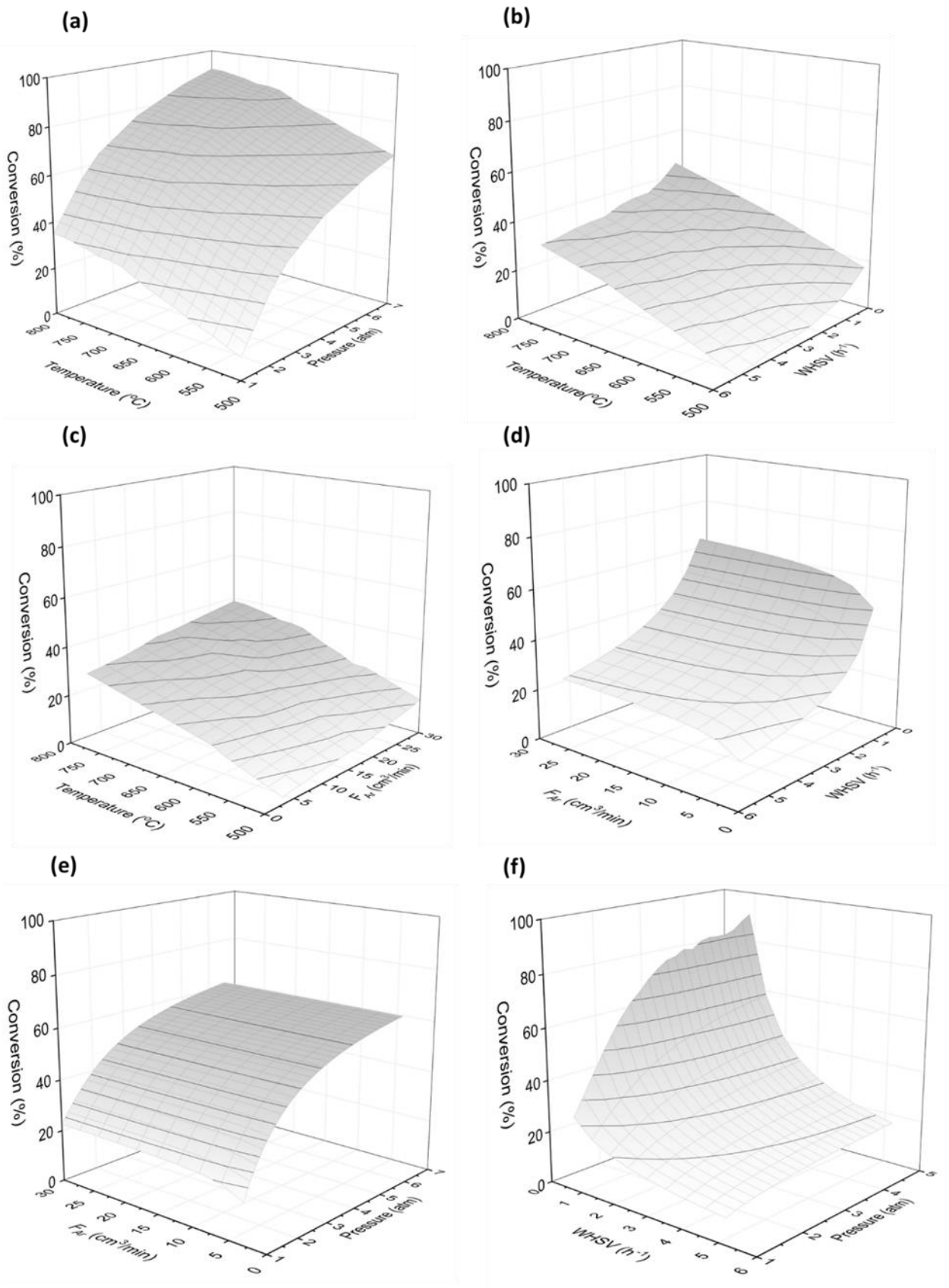
(a)
Conversion (%)
Temperature (°C)
Pressure (atm)
(b)
Conversion (%)
Temperature (°C)
WHSV (h-1)
(c)
Conversion (%)
Temperature (°C)
FAir (cm3/min)
(d)
Conversion (%)
FAir (cm3/min)
WHSV (h-1)
(e)
Conversion (%)
FAir (cm3/min)
Pressure (atm)
(f)
Conversion (%)
WHSV (h-1)
Pressure (atm)

Figure 3.30. i-C_4H_{10} conversion in the PBMR as a function of (a) pressure and temperature (F_{Ar} = 20 cm^3/min and WHSV = 1.37 h^{-1}), (b) WHSV and temperature (WHSV = 1.37 h^{-1} and p_{feed} = 1 atm), (c) F_{Ar} and temperature (p_{feed} = 1 atm and WHSV = 1.37 h^{-1}), (d) WHSV and F_{Ar} (temperature = 600 °C and P_{feed} = 1 atm), (e) WHSV and p_{feed} (F_{Ar} = 20 cm^3/min and temperature = 600 °C), and (f) p_{feed} and F_{Ar} (WHSV = 1.37 h^{-1} and temperature = 600 °C)

Figure 3.31 shows that i-C_4H_{10} conversion which has been measured by use of the 1D PFR model along the reactor length. Competition between H_2 permeation and the consumption of i-C_4H_{10} caused the maximum i-C_4H_{10} conversion to be found along the membrane length. For the PBR, gradual enhancement of i-C_4H_{10} conversion was observed along the reactor length due to a consecutive decrease in the i-C_4H_{10} partial pressure in the reaction side. For PBR in Figure 3.31(d), an increase in pressure reduces i-C_4H_{10} conversion slightly because the reaction tends to shift to the reactant side with increased pressure. For PBMR, i-C_4H_{10} conversion rapidly increased in beginning part of the reactor, which is due to combination effect of H_2 permeation and generation. The consumption of i-C_4H_{10}, H_2 generation, and H_2 permeation are increased at high temperatures and pressures, which further lead to the greater enhancement of i-C_4H_{10} conversion. With increasing the pressure to 2 atm, the i-C_4H_{10} conversion further increased for PBMR, as shown in Figure 3.31(c). This is due to enhanced H_2 transport through the membrane, which causes the equilibrium to shift towards the product side, and results in enhanced i-C_4H_{10} conversion.

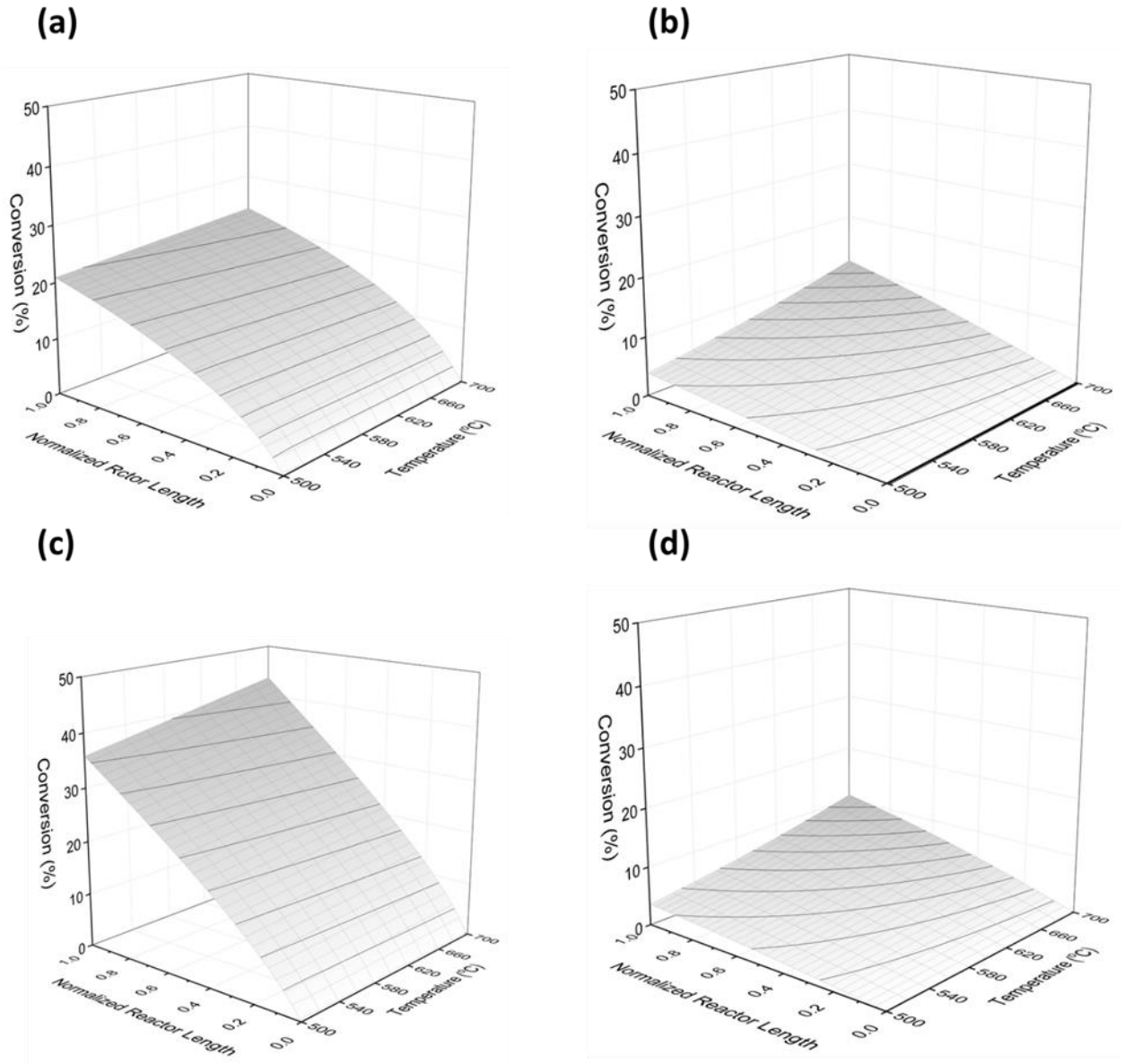

Figure 3.31. Calculated i-C_4H_{10} conversion along the reactor length as a function of temperature for (a) PBMR at 1 atm, (b) PBR at 1 atm, (c) PBMR at 2 atm, and (d) PBR at 2 atm (F_{Ar} = 20 cm^3/min and WHSV = 1.37 h^{-1})

CHAPTER IV

ZIF-8 MEMBRANES

Summary

ZIF-8 membranes were developed using the novel methods for propylene/propane gas separation. Impact of zinc source, seeding type and membrane synthesis duration on ZIF-8 membrane performance for propylene/propane gas separation was investigated. Silicalite seeding allowed for better attachment of ZIF-8 membrane layer on AAO support, due to hydrogen bonding which enhanced ZIF-8 membrane performance. ZnO atomic layer deposition (ALD) was used to cure the membrane defects, which led to a maximum of 91% enhancement in propylene/propane selectivity after only two ALD cycles.

ZIF-8 membrane was fabricated using novel the secondary growth method. Effect of seeding type, effect of zinc source, and effect of synthesis time on the ZIF-8 membrane performance was studied. Characterization techniques like SEM, EDS, XRD, XPS, and FT-IR were used to study the morphology, crystalline structure and bond structure in the ZIF-8 framework. ZIF-8 membrane separation performance for equimolar propylene/propane gas mixture was also discussed. Lastly, the impact of the ZnO atomic layer deposition (ALD) on healing the defects in ZIF-8 framework was studied.

4.1 ZIF-8 membrane preparation

Propylene and propane are industrially important gases. As discussed before propylene/propane separation is a difficult task. In this work, ZIF-8 membrane was designed to separate propylene/propane gas mixture. First AAO support was seeded and then by secondary growth, ZIF-8 membrane was fabricated. ZIF-8 membrane was fabricated with two types of seeding, namely, ZIF-8 seeding and silicalite seeding. Moreover, propylene/propane separation results were also evaluated for in situ ZIF-8 membrane. ZIF-8 and silicalite seed suspension are prepared by the following procedure.

ZIF-8 crystals were prepared following a procedure based on a previous study reported by Cravillon et al.[156]. $Zn(NO_3)_2.6H_2O$ (99.5%, Sigma-Aldrich) and 2-methylimidazole (mIm) (99.7%, Sigma-Aldrich) were dissolved in 50 ml methanol (MeOH) (99.5%, Sigma-Aldrich), separately. The molar ratio of Zn: mIm: MeOH was 1:4:1250. Then the mIm solution was added into the $Zn(NO_3)_2$ solution while stirring with a magnetic bar. The liquid mixture was stirred for 30 min, and then aged without stirring at 20 ^oC for 24 h. The white colloidal particles formed in the solution were collected by centrifugation, followed by washing with methanol for three times. The ZIF-8 powder was dried at room temperature overnight, and then re-dispersed into 100 ml methanol while sonicating for 30 min to prepare 0.05 wt.% ZIF-8 seed suspension.

Then silicalite seed nanoparticles were prepared by conventional heating method and the detailed synthesis procedure has been reported in previous publication [157]. To prepare silicalite seed suspension, NaOH (99.99%, Sigma-Aldrich) was dissolved in the mixture solution of H_2O and tetrapropylammonium hydroxide (TPAOH) solution (1 M, Sigma-Aldrich). SiO_2 (0.2-0.3 μm powder, Sigma-Aldrich) was added to the above solution gradually at 80 ^oC in water bath to clear solution with stirring. The molar ratio of each component was maintained as NaOH: H_2O: TPAOH: SiO_2 = 1: 131.5: 2.86: 9.42, respectively. After aging for 4 h, the solution was transferred into hydrothermal vessel and synthesized at 120 ^oC for 6 h. The synthesized powder was washed in deionized water in a centrifuge, followed by dilution to make 0.05 wt.% silicalite seed suspension.

Anodic alumina oxide (AAO) disks (diameter: 25 mm, thickness: 100 μm, pore size: 20 nm, porosity: 24%, Whatman) were used as the substrates. For seed layer coating, the AAO disks were immersed into the 0.05 wt.% seed suspensions, respectively, followed by sonicating for 5 min for the seeds to coat homogeneously on the support surface. The seeded AAO disks were dried at room temperature overnight. For membrane synthesis using secondary method, ZIF-8 layers on the seeded AAO supports were synthesized. The metal solution and the ligand solution were prepared separately. Specifically, 0.076 g of zinc chloride (99.99%, Sigma-Aldrich) or 0.165 g of zinc nitrate hexahydrate (98%, Sigma-Aldrich) was dissolved into 20 ml of DI water to prepare metal solution, and 3.165 g of mIm was dissolved into another 40 ml of DI water to prepare ligand solution. After mixing the metal and the ligand solution, the solution was stirred vigorously for 30 s, the dried AAO support was immersed vertically into the mixed solution and held with a Teflon vessel. The membrane synthesis time by secondary growth was varied for 5, 10, and 20 h, respectively, at room temperature. After membrane synthesis, the disk was taken out and immersed into 50 ml of fresh methanol for 12 h to remove any guest species like water from ZIF-8 framework and to prepare the evacuated form of ZIF-8 membrane for gas separation experiment. Water is less acidic than methanol and thus 2-methylimidazole can be deprotonated in water more easily than methanol. Thus, ZIF-8 membranes washed with methanol were denser and better intergrown. This process is known as the activation process [122, 158, 159]. Finally, the membrane was taken out from methanol and dried at room temperature for another 12 h. The process of the ZIF-8 membrane synthesis on AAO substrate is illustrated in Figure 4.1.

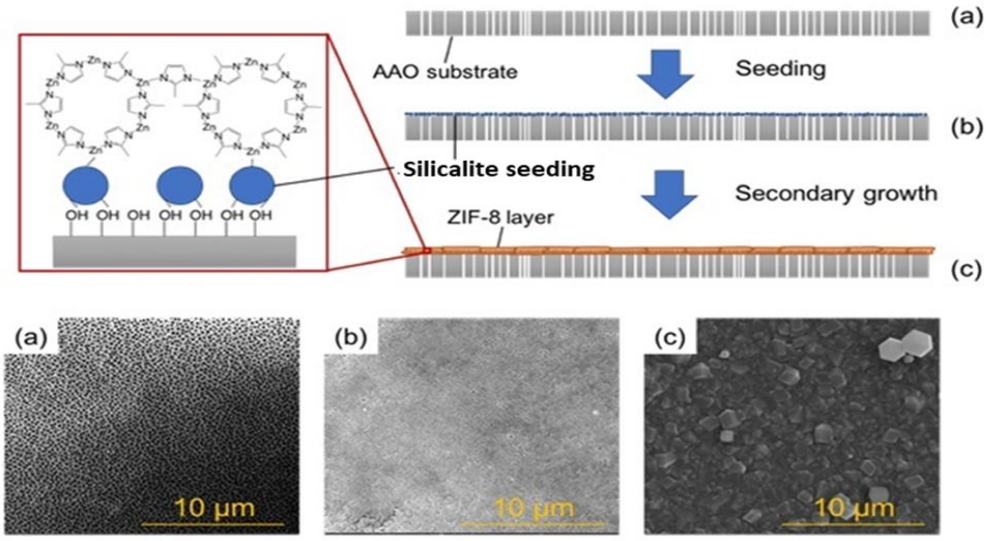

Figure 4.1. SEM images and schematics of (a) AAO substrate, (b) Silicalite seeding + AAO substrate, and (c) ZIF-8 membrane + silicalite seeding + AAO substrate

4.1.1 Experimental section

ZIF-8 membrane was used for the separation of propylene/propane gas mixtures. All ZIF-8 membranes were stored in a desiccator at room temperature before gas permeation measurements. Propylene/propane binary gas permeation measurements were performed at room temperature and atmospheric pressure. The membrane was mounted in a stainless steel cell with the membrane surface facing the feed side as shown in Figure 4.2. Feed was a mixture of propylene and propane each of 50 cm^3/min and the flowrate was controlled by mass flow controller (MFC). Argon was used as the sweeping gas at a flow rate of 100 cm^3/min and was supplied to the permeate side. Before recording data for each separation experiment, membrane separation was allowed to stabilize (concentration to become steady) and it took ~4 h for system to reach steady state. The composition of the permeate stream was analyzed by using an online gas chromatography (Shimadzu, GC-2014) equipped with a molecular sieve 13X column for the thermal conductivity detector (TCD).

The membrane permeance for gas component i is defined as:

$$P_{m,i} = \frac{Q_i}{A_m \times \Delta P_i} \tag{4.1}$$

where Q_i (mol/s) is the amount of the permeated gas through the membrane per second; A_m (m^2) is the active membrane area; ΔP_i (Pa) is the transmembrane partial pressure difference of component i between feed and permeate sides.

The propylene/propane separation factor for the binary mixture is defined as:

$$\alpha_{C_3H_6/C_3H_8} = \frac{(y_{C_3H_6}/y_{C_3H_8})_{permeate}}{(y_{C_3H_6}/y_{C_3H_8})_{feed}} \tag{4.2}$$

where $y_{C_3H_6}$ and $y_{C_3H_8}$ are mole fractions of propylene and propane, respectively.

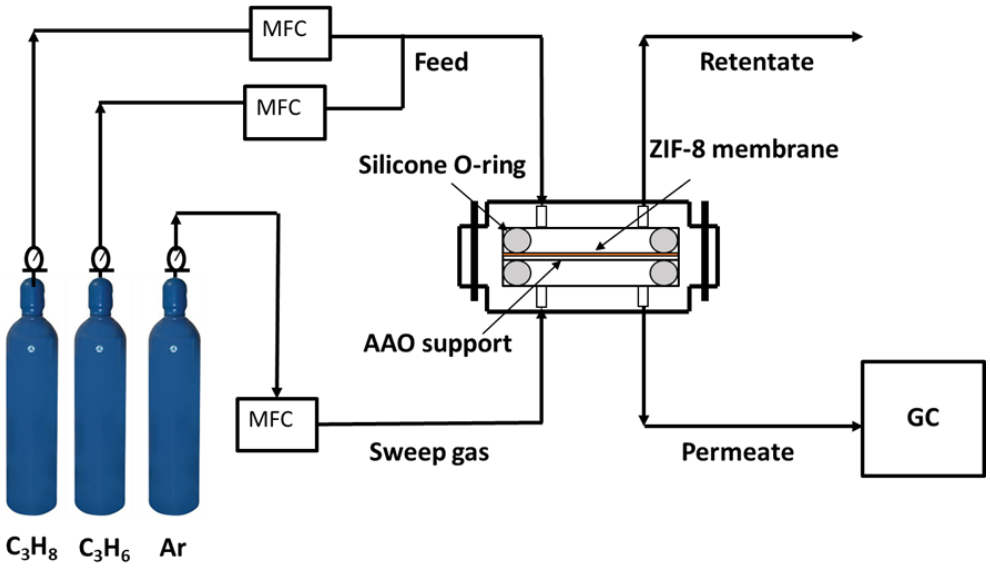

Figure 4.2. Schematic showing the experimental setup for the C_3H_6/C_3H_8 separation

4.1.2 Results and discussion

Effect of seeding

The crystalline structure of the ZIF-8 membrane was compared with the XRD patterns from the literature [128, 160]. The XRD patterns of the ZIF-8 membranes grown on ZIF-8 seed layers (Figure 4.3c) were sharper (peak intensity 110 was higher) than those without seed layers (Figure 4.3b), which suggests increased crystallinity of the ZIF-8 layers. This can be understood by the fact that an extra seeded ZIF-8 layer facilitates the formation of ZIF-8 crystals on AAO substrate in comparison to the ZIF-8 membrane without seeding layer. In addition, silicalite seeded ZIF-8 membranes (Figure 4.3d) also showed sharper peaks than ZIF-8 membrane directly grown on AAO substrate (Figure 4.3b) indicating the enhancement in crystallinity. Figure 4.3d represents ZIF-8 membrane successfully grown on the silicalite-seeded AAO substrate by matching the typical XRD peaks at the 2θ of 7^{o} and 12^{o} [161].

Figure 4.4 shows SEM images that were used to study the morphology of pristine AAO substrate and ZIF-8 membranes synthesized with and without seeding process. Uniformly distributed pore channels can be clearly seen for the AAO substrate (Figure 4.4a). In ZIF-8 membrane without seeding (Figure 4.4b1), the cracks are clearly visible on the ZIF-8 membrane layer, which can be explained by the fact that ZIF-8 layer is not very well grown on the AAO substrate without seeding. XRD patterns shown in Figure 4.3 also confirm the relatively insufficient ZIF-8 membrane growth without seeding process [118]. Lack of active sites on AAO substrate might be the reason for the poor ZIF-8 structure formation (Figure 4.4b1). However, introduction of seeding material (ZIF-8 or silicalite) on the AAO substrate improved the ZIF-8 membrane morphology (Figure 4.4c and Figure 4.4d). Seeding material helped in avoiding the adverse impact of AAO substrate on ZIF-8 crystal nucleation and improved ZIF-8 membrane morphology. In addition, silicalite seeding nanoparticles attach more firmly on AAO substrate due to hydrogen bonding and provide a more uniform surface for secondary ZIF-8 membrane layer growth (Figure 4.4d) in comparison to the ZIF-8 nanocrystal seeding (Figure 4.4c). Hydrogen bonding takes place by the direct bonding of silicalite crystals

with the substrate, which allows for a robust seeded silicalite layer [140, 162, 163]. However for ZIF-8 nanocrystal as the seeding layer, more disassociated ZIF-8 crystals attached on the top of the membrane surface, which further resulted in a less intergrown ZIF-8 layer than the layer grown on silicalite seeded AAO substrate. For silicalite seeded AAO substrate, the ZIF-8 layer was smoother, uniformly covered and more robust.

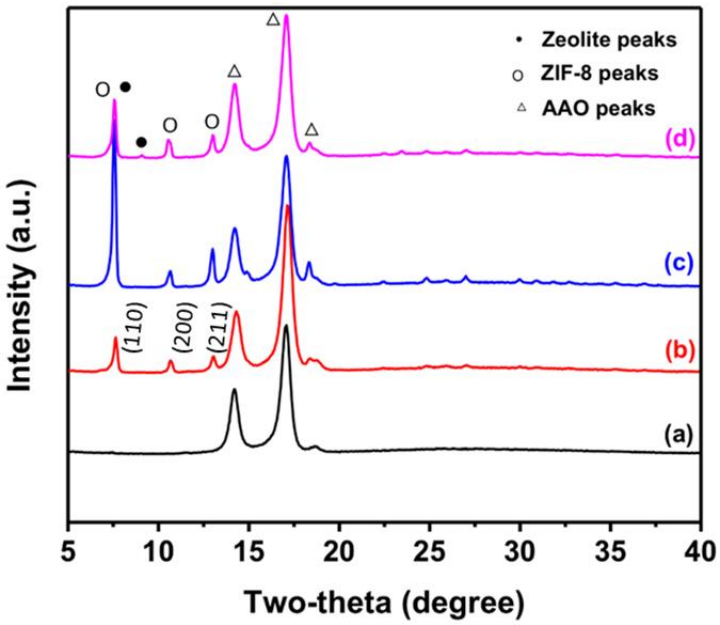

Figure 4.3. XRD patterns of (a) pristine AAO substrate, (b) ZIF-8 membrane without seeding layer, (c) ZIF-8 membrane with ZIF-8 nanocrystals as the seeding layer, and (d) ZIF-8 membrane with silicalite nanocrystals as the seeding layer

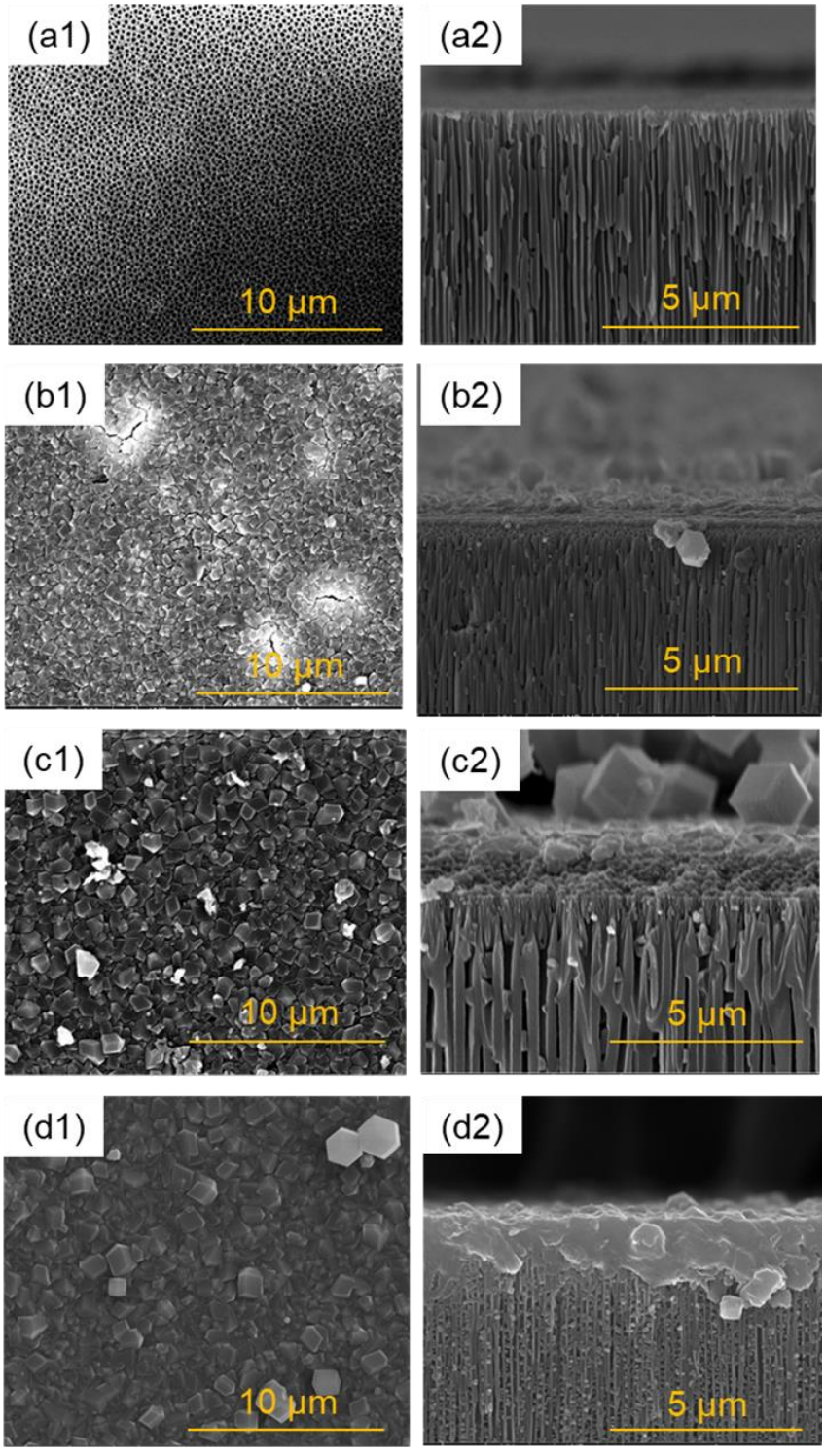
(a1)
10 μm
(a2)
5 μm
(b1)
10 μm
(b2)
5 μm
(c1)
10 μm
(c2)
5 μm
(d1)
10 μm
(d2)
5 μm

Figure 4.4. Surface SEM images and cross section SEM images of (a1, a2) pristine AAO support, ZIF-8 membranes synthesized at 10 h (b1, b2) without seeding process, (c1, c2) with ZIF-8 nanocrystals as the seeding layer, and (d1, d2) with silicalite nanocrystals as the seeding layer, respectively

Table 4.1 shows the elemental composition on the surface of different membranes obtained from EDX spectroscopy. Silicon concentration was dropped from 26.25 wt.% for silicalite seeded AAO substrate to 0.33 wt.% for silicalite seeded + ZIF-8 membrane. Silicalite seed has silica, which is responsible for silicon concentration. XPS beam can detect elements only up to ~2.5 nm depth, and after ZIF-8 growth, XPS could not detect the silica and hence there was a drop in the silicon concentration. There was an increase in the concentration of carbon, nitrogen and zinc after ZIF-8 membrane fabrication. During secondary synthesis, use of $ZnCl_2$ and mIm introduced more zinc, nitrogen, and carbon in the membrane framework and thus there was an increase in the concentration of these elements.

Figure 4.5 shows the XPS spectra for C 1s, N 1s, and Zn 2p. Particularly, Zn $2p_{3/2}$ and Zn $2p_{1/2}$ showed two intense peaks at 1022 eV and 1045 eV, respectively [123, 128]. Two distinct peaks for Zn implies that the majority of the Zn are in the tetrahedral coordination. For ZIF-8 membrane with silicalite seeding, the peak slightly shifted towards higher binding energy for Zn and N atoms, which indicates the decrease in number of unsaturated Zn-N bonds and thus reduction of defects in the ZIF-8 framework. The N 1s peak at 398.8 eV can be assigned to the imidazole group in ZIF-8 framework based on the literature [164-167]. C 1s showed peak at 286.3 eV, which depicts the carbon linked to N in the methyl imidazole group, and was found to be in good agreement with previously reported literature [165, 168]. The FT-IR results for ZIF-8 membrane are summarized in Figure 4.6. The band at 1580 cm^{-1} corresponds to the C=N stretch. In addition, the bands at 1146 cm^{-1} are for =C-H and C-N and 995 cm^{-1} is for the C=C-N, respectively. Moreover, the stretch 3134 cm^{-1} is for C-H bond [169-171].

Table 4.1. Elemental composition (wt.%) for MFI seeded AAO support, MFI seed+ ZIF-8 membrane, ZIF-8 seeded AAO support, ZIF-8 seed+ ZIF-8 membrane, and ZIF-8 in-situ membrane

Description	Silicon	Carbon	Nitrogen	Zinc
Silicalite seed	26.25	25.08	2.28	0.20
Silicalite seed+ ZIF-8 membrane	0.33	63.72	19.35	8.03
ZIF-8 seed	1.13	54.79	24.73	10.91
ZIF-8 seed + ZIF-8 membrane	-	56.55	25.96	11.01
ZIF-8 in-situ membrane	0.04	56.44	26.01	11.54

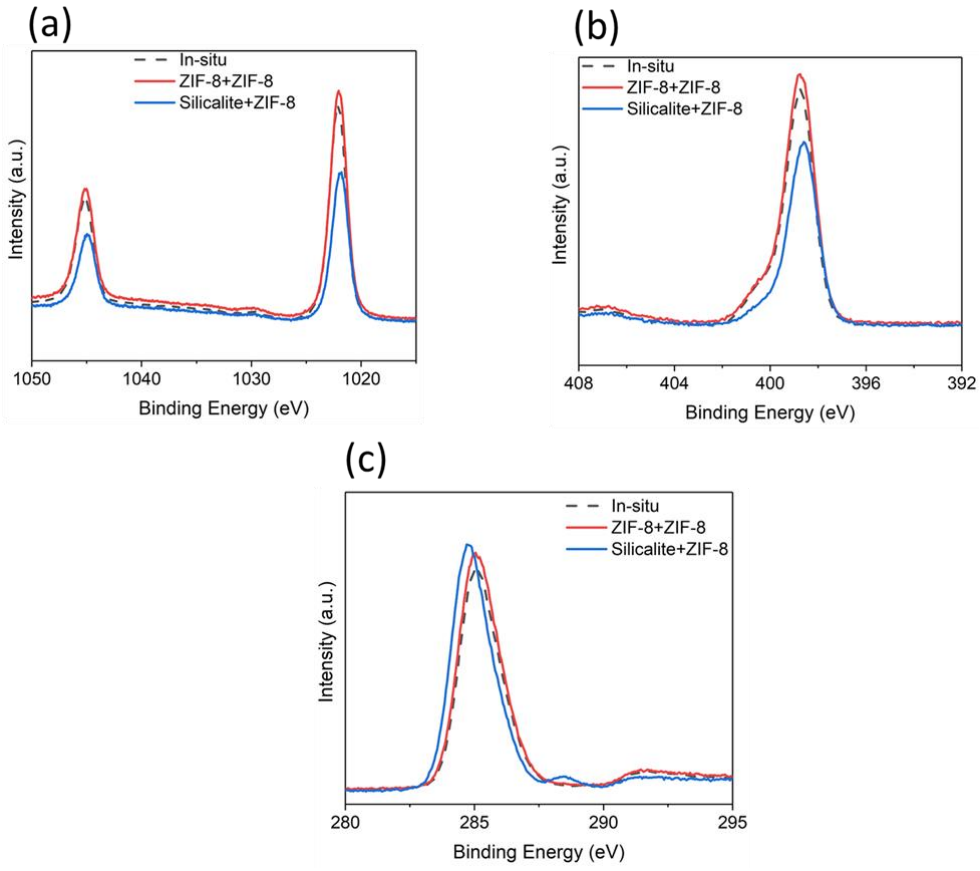

Figure 4.5. XPS spectra for (a) Zn 2p 1s, (b) N 1s, and (c) C 1s of ZIF-8 membrane for in-situ ZIF-8 membrane, ZIF-8 seeding + ZIF-8 membrane, and silicalite seeding + ZIF-8 membrane

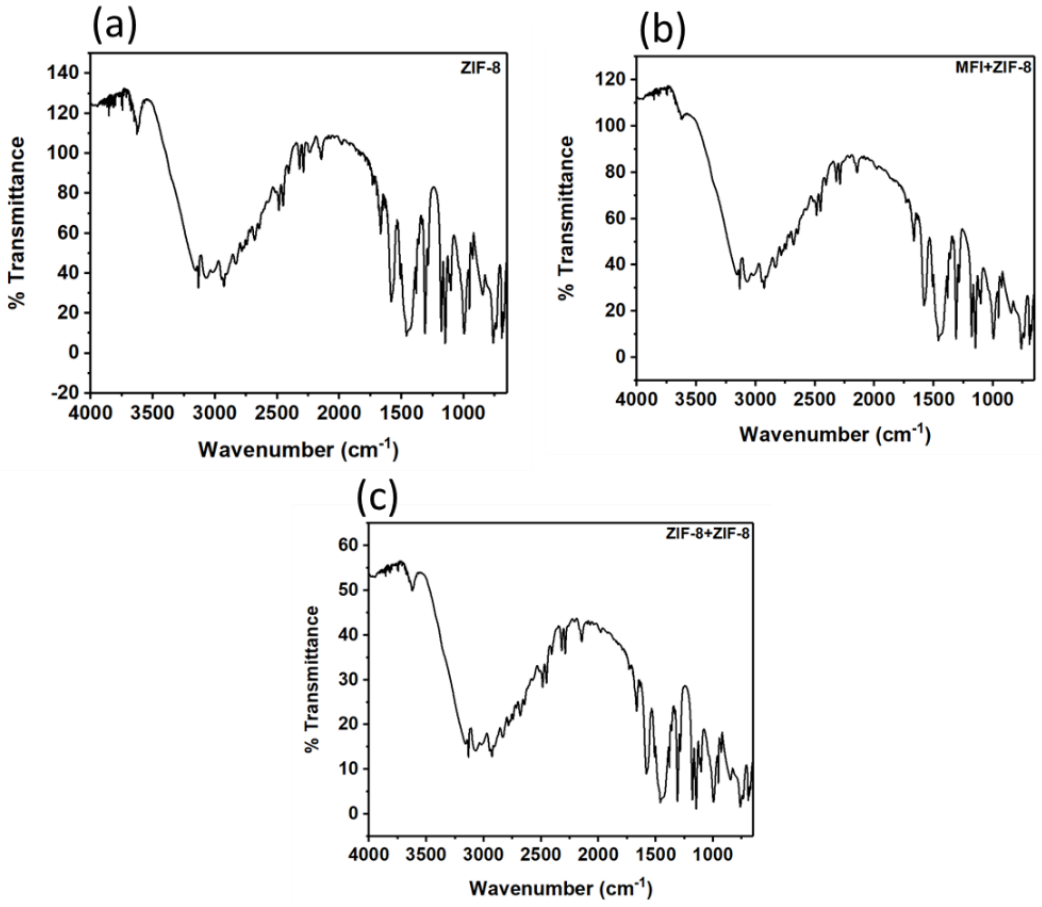

Figure 4.6. FT-IR spectra of (a) in-situ ZIF-8 membrane, (b) Silicalite seeding + ZIF-8 membrane, and (c) ZIF-8 seeding + ZIF-8 membrane

BET surface area and pore volume for ZIF-8 membrane with silicalite seeding are shown in Table 4.2. Specific surface area for ZIF-8 membranes lies in the range of 1000-1600 m^2/g [172], which indicates the ZIF-8 structure formation [169]. Figure 4.7 shows the N_2 adsorption/desorption isotherm to investigate the N_2 accessible porous characteristic. ZIF-8 membrane with silicalite seeding showed type-1 isotherm,

which is expected for microporous materials (pore size < 2 nm). In addition, there was a sudden increase in N_2 adsorption around a threshold pressure of 0.95 (P/P_0). This is known as the gate opening effect and is caused by the reorientation of flexible organic linker (mIm) [173-175].

Table 4.2. BET surface area and pore volume of ZIF-8 membrane as measured by N_2 adsorption at 77K

Membrane	BET surface area (m^2/g)	Pore volume (cm^3/g)
ZIF-8 membrane (this work)	1474	0.71
ZIF-8 membrane [169]	1046	0.51

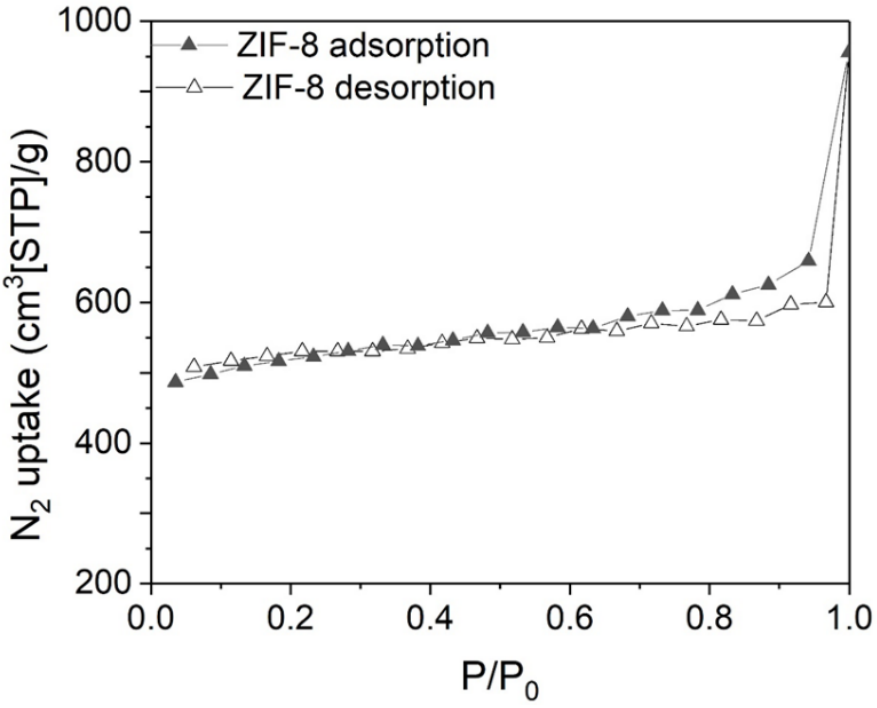

Figure 4.7. N_2 adsorption and desorption isotherms for ZIF-8 membranes

Effect of zinc sources

Effect of different zinc sources on ZIF-8 membrane growth was investigated. The morphology of ZIF-8 membranes synthesized with zinc nitrate ($ZnNO_3$) and zinc chloride ($ZnCl_2$) as zinc source, respectively, are shown in Figure 4.8. Under the same synthesis conditions in terms of reagent, molar amount and temperature, ZIF-8 membrane in which $ZnNO_3$ was used as the zinc source showed smaller ZIF-8 crystal size, less intergrown ZIF-8 surface, and thinner ZIF-8 film in comparison to the membrane where $ZnCl_2$ was used as the zinc source. The difference in morphology of ZIF-8 crystals is due to the high reactivity of $ZnNO_3$ in comparison to $ZnCl_2$, which probably led to the faster reaction during the membrane synthesis and thus generated smaller crystal size. Schejn et al. [137] also reported morphological differences of the ZIF-8 crystals from the two zinc sources. Moreover, when $ZnNO_3$ was used as the Zn source, ZIF-8 layer forms only on the substrate while $ZnCl_2$ also promotes ZIF-8 film formation inside AAO substrate. Thus, ZIF-8 membrane with $ZnCl_2$ enhanced membrane grain boundary structure. As a result, with $ZnCl_2$ as the zinc source, the appropriate ZIF-8 crystal size for the propylene/propane separations can be synthesized [128, 137].

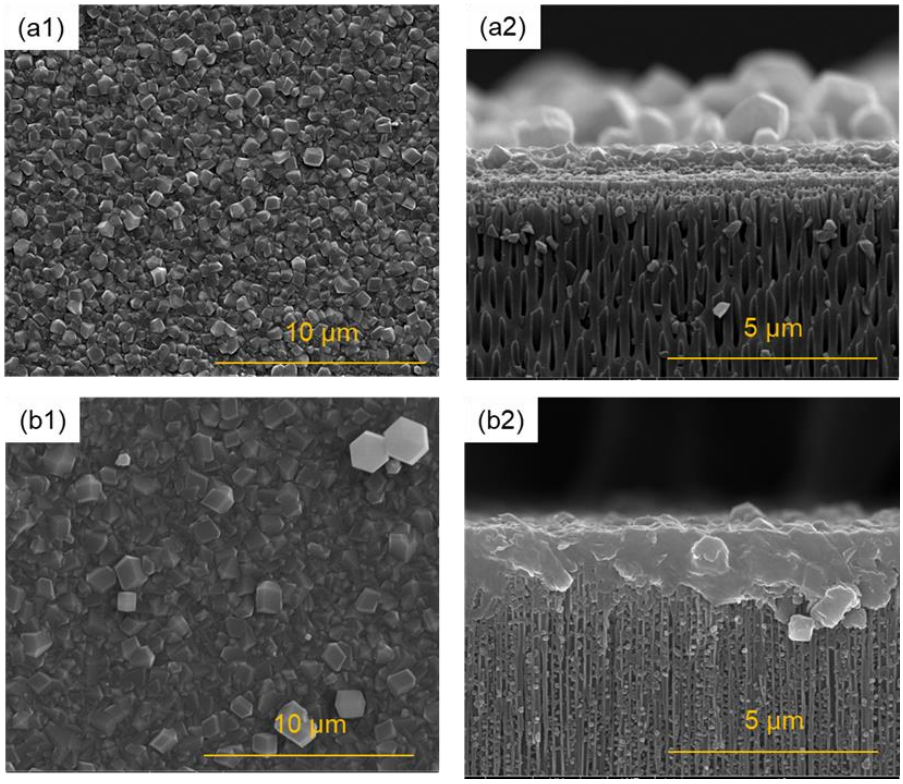

Figure 4.8. Surface SEM images and cross section SEM images of ZIF-8 membranes synthesized at 10 h (a1, a2) with zinc nitrate and (b1, b2) zinc chloride as the zinc source, respectively, with silicalite nano-crystals as the seeding layer

Effect of synthesis duration

The morphology of the ZIF-8 membranes synthesized with various durations of 5, 10, and 20 h, respectively, are shown in Figure 4.9. The ZIF-8 crystals started to be formed from synthesis duration of 5 h, with the limited number of ZIF-8 crystals randomly distributed on top of silicalite seeded AAO substrate (Figure 4.9a). After 10 h synthesis duration, a ZIF-8 layer was uniformly formed (Figure 4.9b). As shown in Figure 4.9a2 & 4.9b2, there was slight change in membrane thickness (650 nm for 5 h and 850 nm for 10 h). For synthesis duration of 20 h (Figure 4.9c), there was significant growth of ZIF-8 crystals on the surface. The number of accumulated ZIF-8 crystals significantly increased [137], which caused a slight

decline of propylene/propane gas selectivity and propylene gas permeance as can be seen in Table 4.5. For more than 20 h of synthesis time, the membrane got thicker, which led to further decline in ZIF-8 membrane separation performance. Based on SEM images and separation results as depicted in Figure 4.9b, it was found that for 10 h of synthesis, a well-intergrown continuous ZIF-8 layer was successfully formed with an average membrane thickness of ~850 nm.

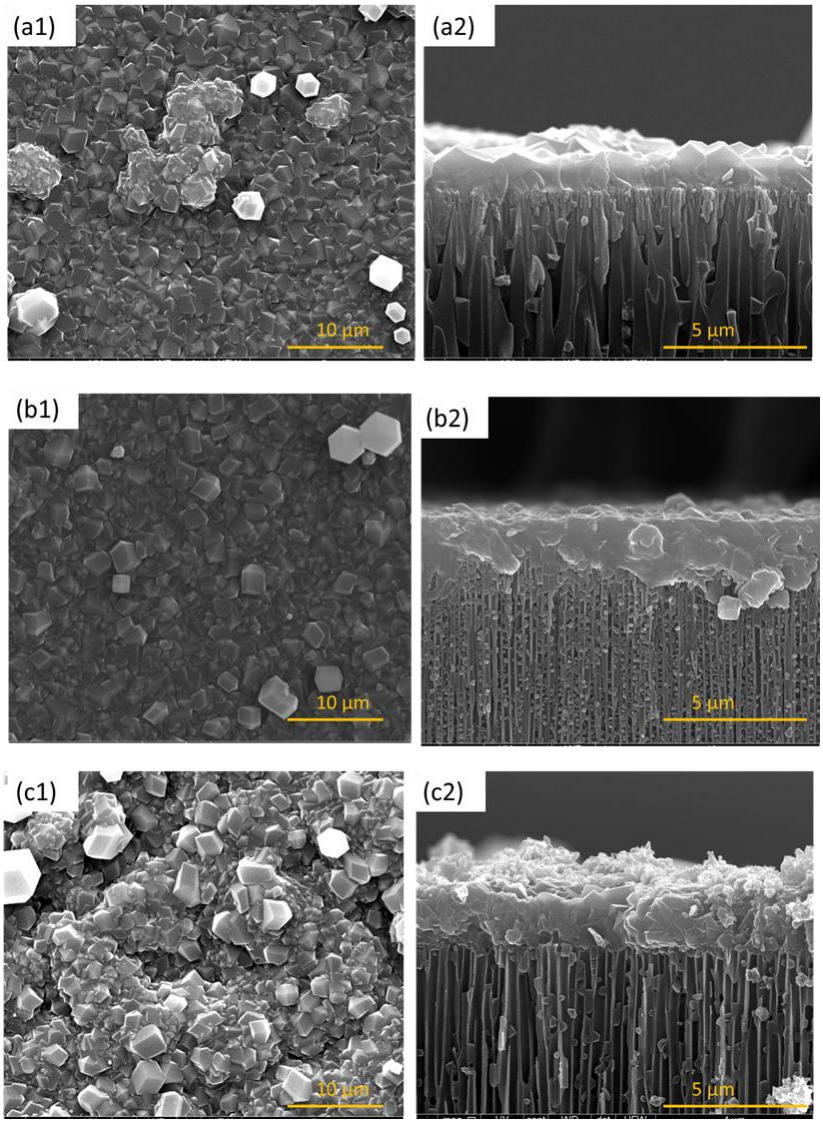

Figure 4.9. (a1, b1, c1) Surface SEM images and (a2, b2, c2) cross section SEM images of ZIF-8 membranes with silicalite nanocrystals as the seeding layer with the synthesis time of 5, 10, and 20 h, respectively

The membranes synthesized at various conditions were tested for the propylene/propane binary gas mixture separation at room temperature for performance evaluation. Table 4.3 presents the results for the

propylene/propane mixture gas separation factor and propylene permeance values at room temperature. In Table 4.3, ZIF-8 membrane synthesized without seeding process (in-situ) showed lower propylene/propane separation factor due to the cracks and defects formed on the ZIF-8 layer (Figure 4.4b). It was found that different seeding materials had different effects on the membrane performances. The ZIF-8 membranes grown on the silicalite seeded AAO substrate exhibited significantly higher performance than membranes using ZIF-8 nanoparticles as seeding material. This can be explained by the strong interactions between silicalite and AAO substrate through hydrogen bonding, which allows for a better grown secondary ZIF-8 layer. The interaction anchored silicalite seeds more firmly onto AAO substrate, which provided a more stable seeding layer and allowed better reproducibility and control of the membrane quality. In this case, a highly ordered ZIF-8-membrane structure was obtained under such environment.

Table 4.3. Propylene/propane binary gas separation results with ZIF-8 membrane synthesized without seeding process, with ZIF-8 nanocrystals as the seeding layer, and with silicalite nanocrystals as the seeding layer, respectively.

Seeding layer	$\alpha_{C_3H_6/C_3H_8}$	P_{m,C_3H_6} ($\times 10^{-8}$ mol.m^{-2}s^{-1}Pa^{-1})
None	84	0.86
ZIF-8 nanoparticle	112	1.27
Silicalite seeding	170	0.90

The results of propylene/propane binary gas separations by using ZIF-8 membranes with different zinc sources were shown in Table 4.4. ZIF-8 membrane prepared with $ZnNO_3$ as the zinc source showed relatively higher propylene permeance and lower propylene/propane separation factor compared with those prepared with $ZnCl_2$. As shown in Figure 4.8, ZIF-8 membrane prepared from $ZnNO_3$ were less intergrown and showed thinner ZIF-8 membrane layer than those with $ZnCl_2$. In addition, the different ZIF-8 crystal sizes affected membrane stability and gas adsorption [128, 137], indicating that appropriate ZIF-8 crystal

size for the propylene/propane separations can be achieved by using $ZnCl_2$. Therefore, $ZnCl_2$ was found to be a promising candidate for greatly improving the membrane synthesis efficiency.

Table 4.4. Propylene/propane binary gas separation results with ZIF-8 membrane synthesized with zinc nitrate and zinc chloride as the zinc source, respectively, on silicalite seeded AAO

Zinc Source	$\alpha_{C_3H_6/C_3H_8}$	P_{m,C_3H_6} ($\times 10^{-8}$ mol.m^{-2}s^{-1}Pa^{-1})
$Zn(NO_3)_2$	47	0.99
$ZnCl_2$	170	0.90

The ZIF-8 membranes synthesized at various synthesis duration were also tested for an equimolar propylene/propane gas mixture and the results are summarized in Table 4.5. Propylene/propane separation factor significantly increased for synthesis duration of 10 h from 5 h with a slight decline in propylene permeance. However, further increase in membrane synthesis time decreased propylene permeance and slightly reduced the propylene/propane separation factor. In this case, 10 h was found to be the optimized membrane synthesis time for membrane preparation.

Table 4.5. Propylene/propane binary gas separation results with ZIF-8 membrane synthesized at 5, 10, and 20 h, respectively

Synthesis time (h)	$\alpha_{C_3H_6/C_3H_8}$	P_{m,C_3H_6} ($\times 10^{-8}$ mol.m^{-2}s^{-1}Pa^{-1})
5	128	1.00
10	170	0.90
20	168	0.77

4.2 Atomic layer deposition (ALD) on ZIF-8 membrane

4.2.1 Experimental section

A thin layer of ZnO ALD was coated on the ZIF-8 membranes grown over AAO support to heal the defects in the ZIF-8 membrane. The ZnO film was formed through the following mechanism [176]:

$$Zn(C_2H_5)_2 + H_2O\ (g) \rightarrow ZnO + 2C_2H_6\ (g) \quad (4.3)$$

The procedure was carried out using the ALD unit (OkYay Tech, Turkey). During ALD process, the chamber was maintained at 70 ^oC with a baseline pressure of ~200 milliTorr. To achieve homogeneous coating, membranes were initially stabilized inside the chamber for 30 min prior to deposition. Using N_2 as the gas carrier, sequential dosing of DI water and diethylzinc, $Zn(C_2H_5)_2$, (Strem Chemicals Inc., >95%) was then conducted to coat a thin layer of ZnO with a film thickness of ~2 Å per cycle. In between dosing of precursor, the chamber was purged with N_2 to ensure that the precursors did not react in vapor phase but rather at the surface of the ZIF-8 membranes. Figure 4.10 shows the schematic diagram of the ALD process.

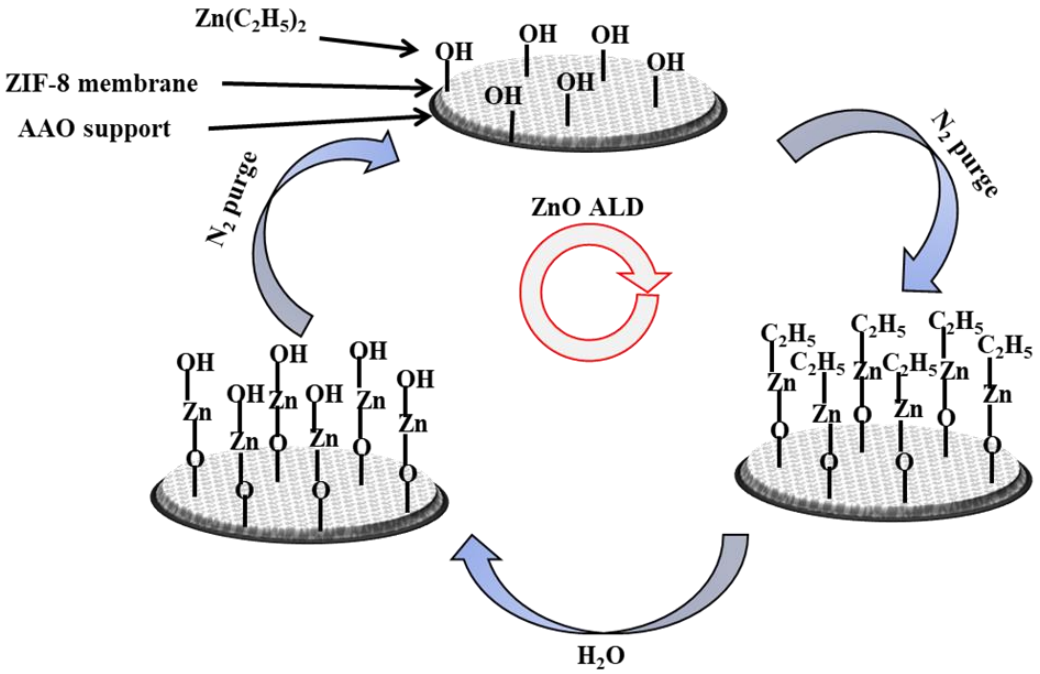

Figure 4.10. Schematic diagram of the ALD process for depositing ZnO on the surface of ZIF-8 membrane using diethylzinc and water precursors

4.2.2 Results and discussion

In this work, ZnO ALD was used to heal the defects in the ZIF-8 framework. Absence of Zn is the primary reason for the defects in the ZIF-8 framework. With the help of ZnO ALD the vacant Zn spaces in ZIF-8 framework was replaced with new Zn atoms and thus more robust ZIF-8 framework can be made as can be seen in Figure 4.11.

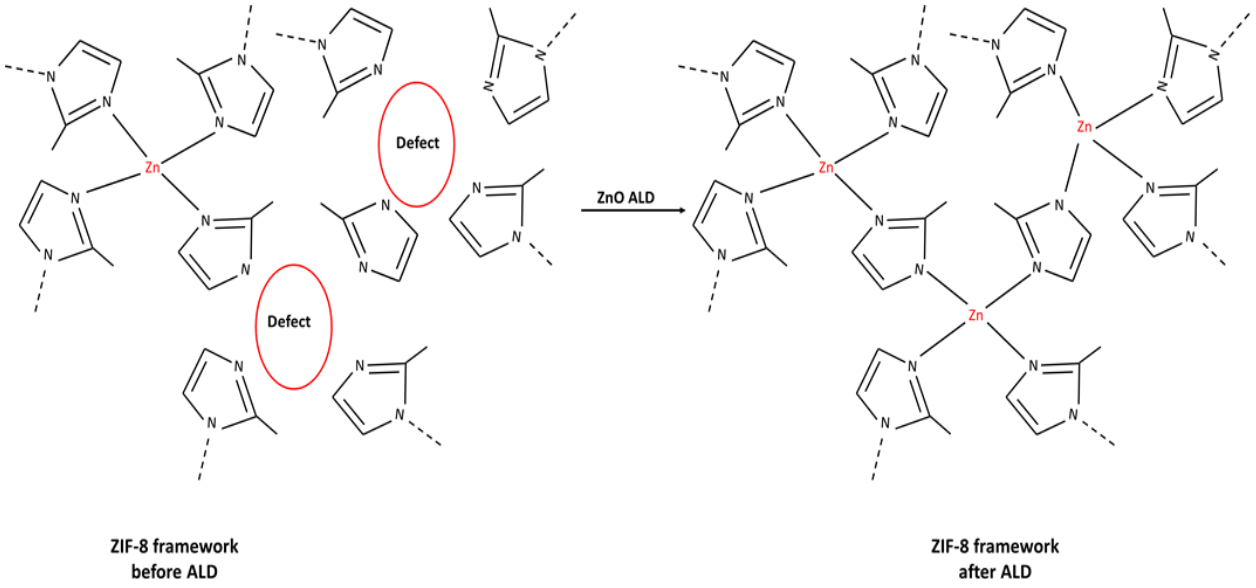

Figure 4.11. Defect healing using ZnO atomic layer deposition in ZIF-8 membrane

ALD ZIF-8 membrane were characterized with SEM, EDS, XPS, XRD, and FT-IR. Figure 4.12 shows the SEM images for the pristine AAO substrate, ZIF-8 membrane, and ZIF-8 membrane after ALD. The synthesis of ZIF-8 membranes on AAO support was carried out using a secondary growth method with water as a solvent. There was a visual difference between the AAO support (Figure 4.12a0) having a straight narrow pore channel and homogenously grown ZIF-8 membrane (Figure 4.12a1) on the AAO support. The membranes were successfully fabricated with a uniform structure and the membrane thickness was ~850 nm. Mostly defects in ZIF-8 framework are present due to metal (Zn)/ligand vacancy or dangling linker vacancy [177]. The probable reason for these effects was the solvation effect. It has been reported that when metal complexes come in contact with water as a solvent, the ions which are formed have a countering effect which results in salt formation in the eventual ZIF-8 framework [177]. This salt formation has effects on the pore structure of the membrane due to the lack of proper linkage between the atoms [112, 177]. Due to these defects there is a viscous flow of gases across membrane which comprises separation performance of the ZIF-8 membrane. ZnO was deposited using atomic layer deposition (ALD) technique to fill the Zn

vacancies in the ZIF-8 framework in order to reduce viscous flow across ZIF-8 membrane by eliminating defects which further enhanced the C_3H_6/C_3H_8 separation performance for the ZIF-8 membranes [178].

Further EDX elemental mapping was done on AAO support, ZIF-8 membrane and ALD ZIF-8 membrane. Figure 4.13 shows the EDX elemental mapping for pristine AAO substrate, ZIF-8 membrane, and ALD ZIF-8 membrane. It can be seen that the concentration of Zn atom was higher for ALD ZIF-8 membrane than ZIF-8 membrane. In Table 4.6 we can see the increase in Zn concentration between pristine AAO substrate (0.098 wt.%) and ZIF-8 membrane (2.42 wt.%). Table 4.6 also summarizes the elemental concentration for the AAO support, ZIF-8 membrane, and ALD ZIF-8 membrane. During the membrane fabrication, $ZnCl_2$ was used as a precursor, which is responsible for the increase in Zn concentration after ZIF-8 fabrication. There was a marginal increase in Zn concentration for the ALD ZIF-8 membrane (3.49 wt.%) from the ZIF-8 membrane (2.42 wt.%). The increase in Zn concentration can be explained with the Zn being deposited during ALD. Moreover, carbon and nitrogen content in the ZIF-8 membrane was higher than in pristine support. Ligand mIm used in the membrane fabrication step, which is responsible for the increase in carbon and nitrogen content in the ZIF-8 membrane. ZIF-8 membrane before and after ALD showed smaller Al content than pristine support. This was because the thickness of the ZIF-8 membrane did not allow the beam to penetrate and detect AAO support, which was the primary source of Al content.

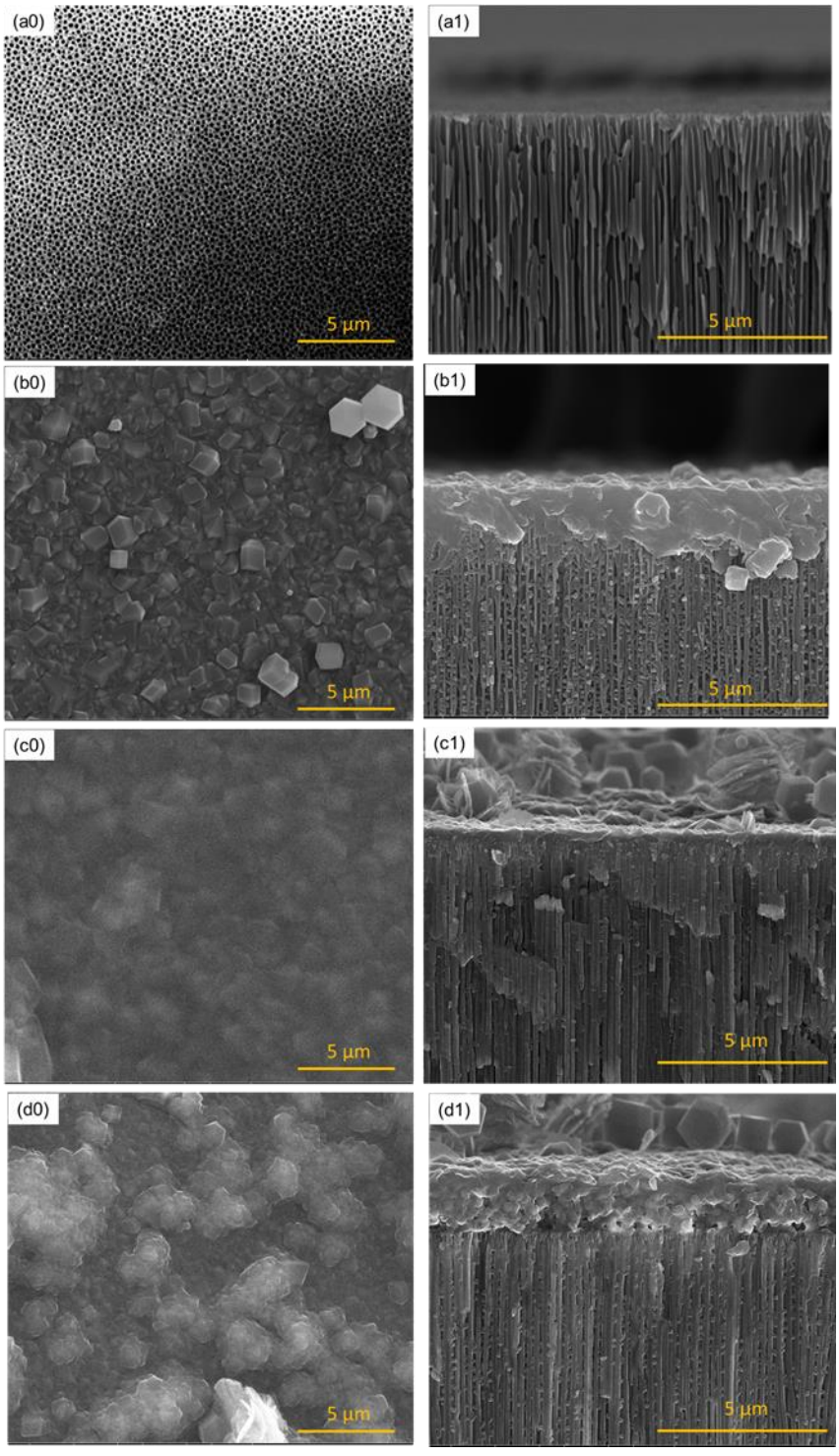
(a0)
5 µm
(a1)
5 µm
(b0)
5 µm
(b1)
5 µm
(c0)
5 µm
(c1)
5 µm
(d0)
5 µm
(d1)
5 µm

Figure 4.12. SEM images of (a0) pristine AAO substrate, (a1) ZIF-8 membrane (b0) ZIF-8 surface, (b1) ZIF-8 cross-section, (c0, c1) ZIF-8 surface and cross-section after two cycles of ZnO ALD, and (d0, d1) ZIF-8 surface and cross-section after four cycles of ZnO ALD

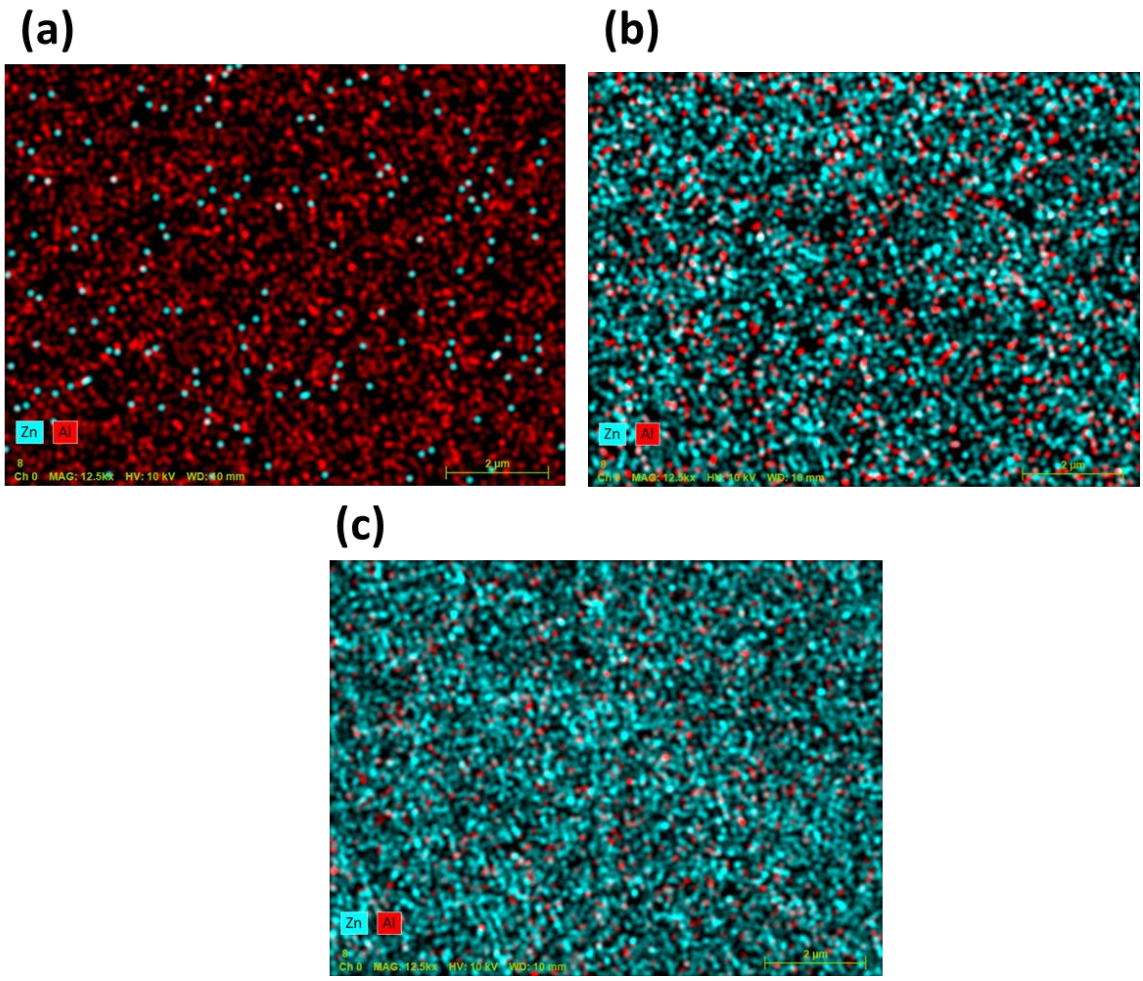

Figure 4.13. EDX colored images of (a) pristine AAO substrate, (b) ZIF-8 membrane, and (c) ALD ZIF-8 membrane

Table 4.6. Weight (%) for pristine AAO substrate, ZIF-8 membrane and ALD ZIF-8 membrane

Membrane	Carbon	Nitrogen	Zinc	Aluminium
AAO Substrate	23.32	12.22	0.098	64.36
ZIF-8 on AAO substrate	53.54	43.82	2.42	0.20
ALD ZIF-8 membrane on AAO substrate	53.23	44.52	3.49	0.15

The crystal pattern of the ZIF-8 membrane was characterized by using X-ray diffraction represented in Figure 3. The XRD analysis showed a clear confirmation that the synthesized membranes have a high crystallinity as demonstrated by XRD. Moreover, the XRD patterns confirmed that these studies were in consistent with previously reported XRD data [128, 160]. Both ZIF-8 and ALD ZIF-8 showed that crystal growth and peaks were observed at 2θ of 7 and 11° [161] which means there was no noticeable difference between their reflections before and after ZnO ALD.

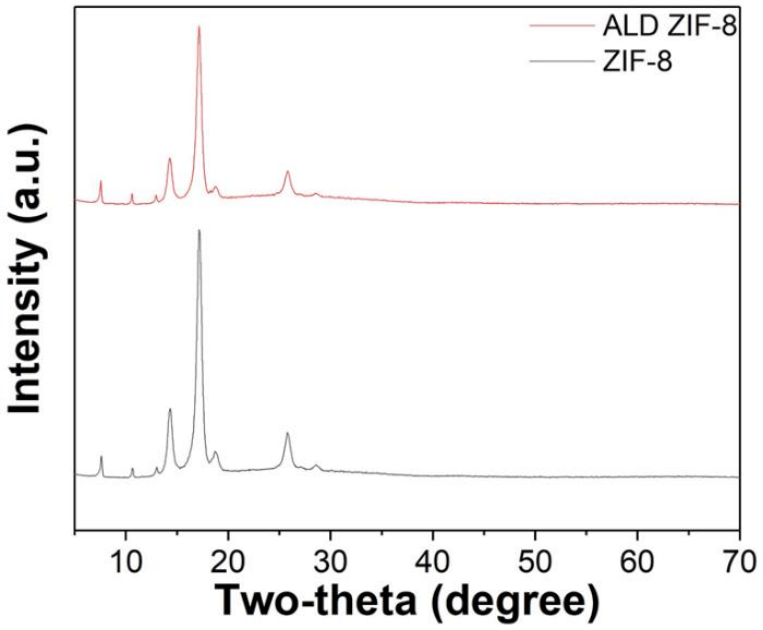

Figure 4.14. XRD patterns of pristine ZIF-8 membrane and ZIF-8 membrane after two cycles of ZnO ALD

In this work, effect of ZnO atomic layer deposition (ALD) on ZIF-8 membrane performance for propylene/propane separation was studied. ZIF-8 membrane showed enhanced performance for propylene/ propane separation after ZnO ALD. To understand the enhanced performance of ZIF-8 membrane for the propylene/propane binary mixture separation, XPS was performed. Figure 4.15 depicts the Zn 2p, N 1s, and C 1s spectra of the ZIF-8 membrane before and after ALD. As demonstrated in Figure 4.15, the Zn 2p spectra showed two distinct peaks at 1022 and 1045 eV, which are characteristic of Zn 2p 3/2 and Zn 2p ½, respectively and also shows that the majority of the zinc atoms are in the tetrahedral coordination state [123]. The observed peak intensities were higher for the ALD ZIF-8 membranes compared to the ZIF-8 membranes. Also from Table 4.6 we observed, the concentration of Zn and N enhanced post ZnO ALD treatment. This is an indication that via the ALD approach, the number of Zn atoms in the oxidation state corresponding ZIF-8 framework (bonded to N atom) increased [179]. In additional Zn 2p 3/2 and Zn 2p ½ peak shifted to higher binding energy post-ZnO ALD treatment, which further indicates the reduction in the number of the unsaturated Zn atoms in the ZIF-8 framework [180, 181]. Similar enhancement in peak

intensity and shift in the binding energy was also observed for C 1s and N 1s (corresponding to Zn-N bond) in Figure 4.15 [177, 180-182]. The increased peak intensity and the shift in binding energy for Zn and N indicate that the ZnO ALD helped in healing the defects of the ZIF-8 framework [123, 164]. The enhanced Zn-N bonding in the ZIF-8 framework post-ALD treatment helped in reducing the defects, which further enhanced propylene/propane separation performance for the ZIF-8 membrane [164, 168]. Moreover, C 1s peak (at 285 eV) showed similar results in terms of peak intensity and binding energy before and after ZnO ALD (Figure 4.15) [183]. This peak corresponds to the carbon from the imidazole group, and it was in a good agreement with the previously reported literature for ZIF-8 membranes [164, 165]. XPS results, along with the data represented in Table 4.6, indicate that there was no significant increase in the carbon atomic percentage after ALD.

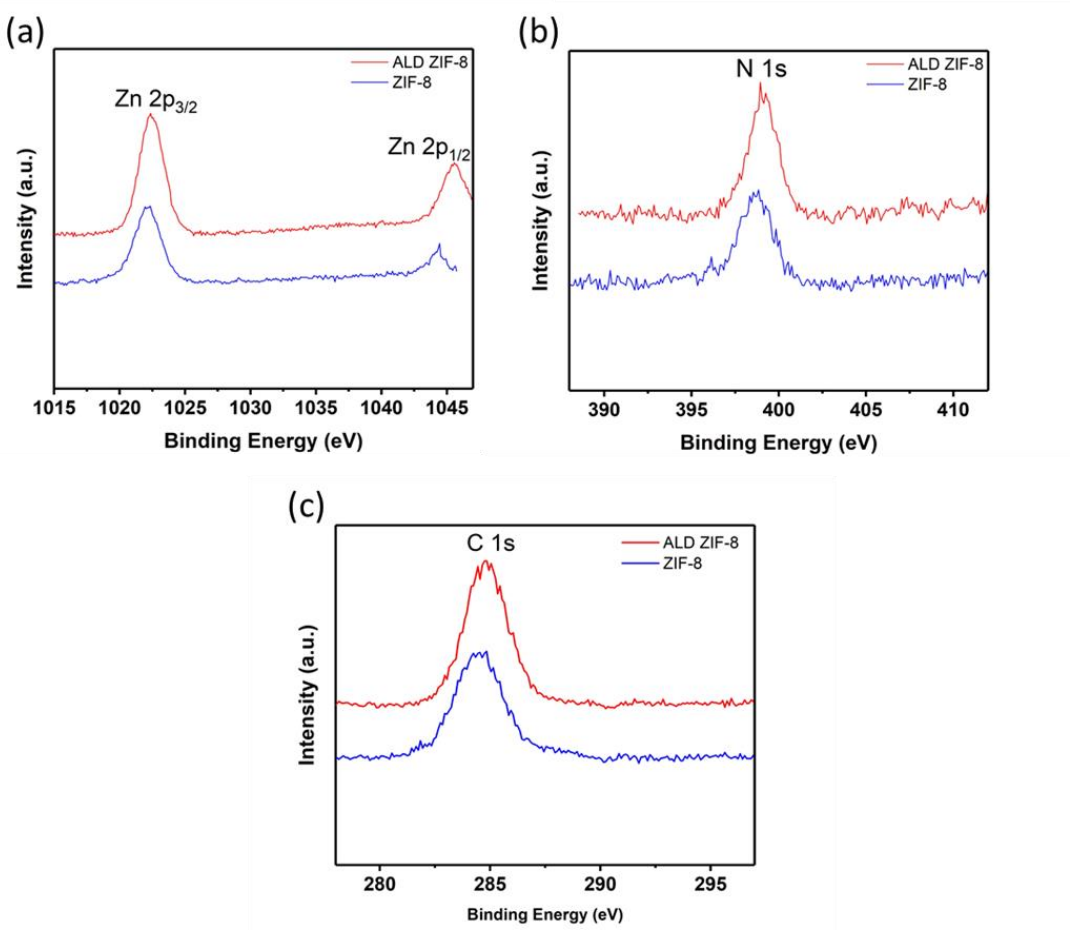

Figure 4.15. XPS spectra of ZIF-8 nonporous thin film: (a) Zn 2p, (b) N 1s, and (c) C 1s

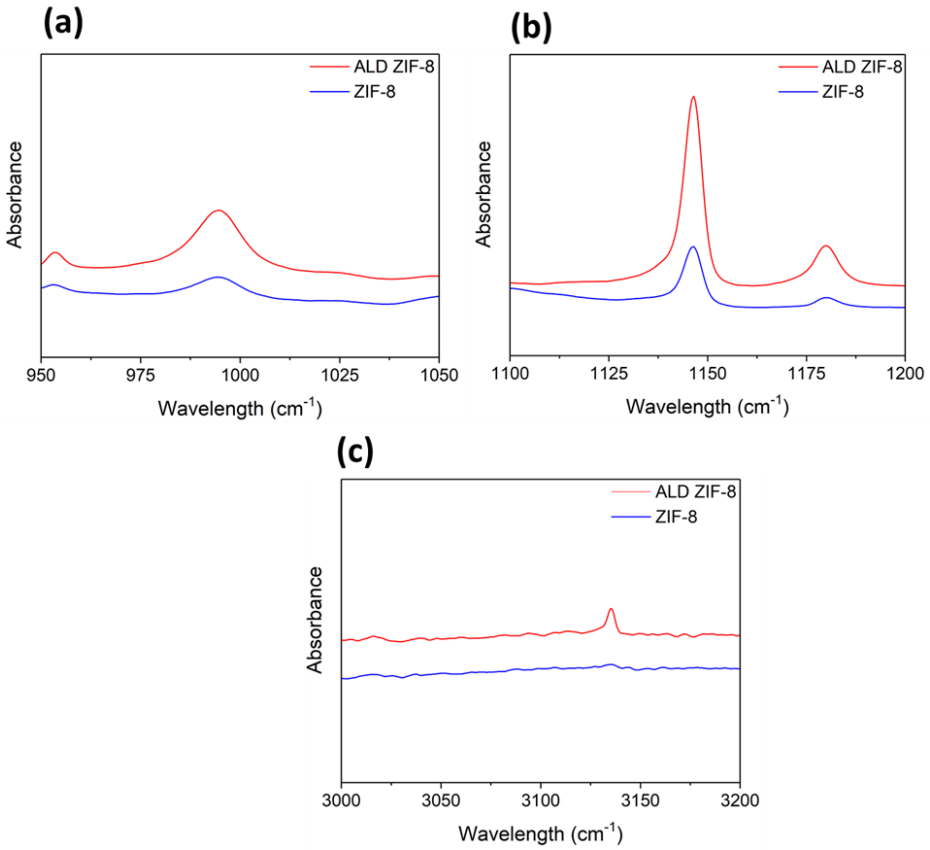

Figure 4.16. FT-IR spectra of ZIF-8 nonporous thin film: (a) Zn 2p, (b) N 1s, and (c) C 1s

The FT-IR spectra for ZIF-8 and ALD ZIF-8 membrane are shown in Figure 4.16. The band at 995 cm^{-1} is for the C=C-N twisting, 1146 cm^{-1} is for =C-H and C-N bending, and 3134 cm^{-1} is for the =C-H asymmetric stretching [171]. Figure 4.16 shows the enhancement of FT-IR peak (at 995 cm^{-1}, 1146 cm^{-1}, and 3134 cm^{-1}) intensities after ZnO ALD on ZIF-8 membranes. It is in agreement with the XPS results and indicates the increase in robustness of the ZIF-8 framework after ZnO ALD, and this further confirms the reduction of defects in the ZIF-8 framework after ZnO ALD [169, 171].

The N_2 adsorption test was performed on ZIF-8 and ZnO ALD ZIF-8 membranes, to investigate the N_2 accessible porous characteristics showed in Figure 4.17. Type-1 isotherm was exhibited in membranes, which is common for microporous materials (pore size <2 nm) [170]. Desorption hysteresis was visible for $P/P_0 > 0.8$ for both ZIF-8 and ALD ZIF-8 membrane, which indicates the presence of capillaries

in the structure and thus the presence of mesopores. However, the membranes maintained the majority of its pores mostly in the micropore and some in the mesopore domain [172]. The specific surface area and pore volume of ZIF-8 and ALD ZIF-8 membranes are as shown in Table 4.7. Typically ZIF-8 has a specific surface area ranges from 1000 to 1600 $m^2 g^{-1}$ [184], and the range varies depending on the concentration of the unreacted residues [185]. The ZIF-8 membrane and the ALD ZIF-8 membrane showed a similar specific surface area and pore volume. It was shown that there is no substantial change in pore structure of the ZIF-8 membrane. The ALD process probably helps to reduce the surface defects in the ZIF-8 framework, and it has little effect on pore structures, thus reducing the viscous flow across the ZIF-8 membrane and enhancing the propylene/propane separation performance.

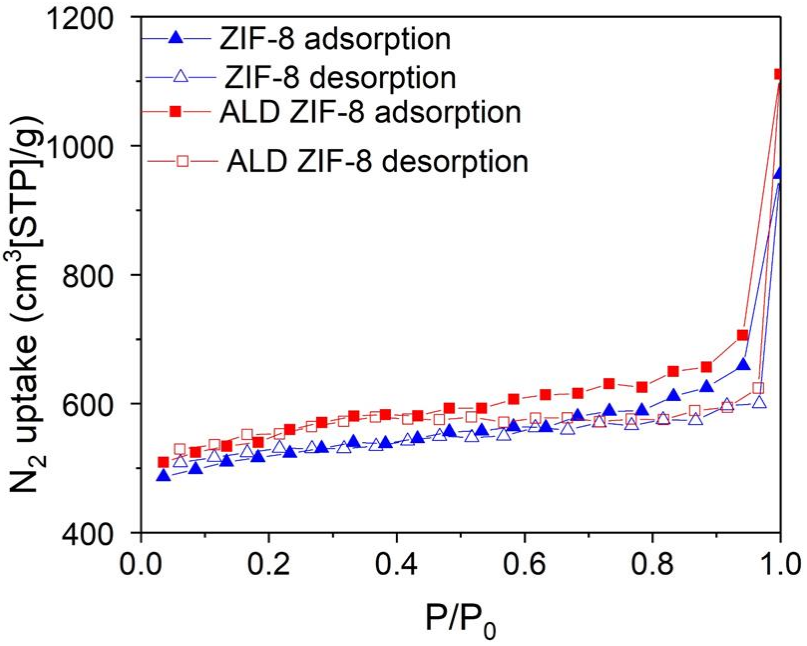

Figure 4.17. N_2 adsorption and desorption isotherms for ZIF-8 and ZIF-8 ALD membranes

Table 4.7. BET surface area and pore volume of ZIF-8 and two cycles of the ZnO ALD ZIF-8 membrane as measured by N_2 adsorption at 77K.

Description	BET ($m^2\ g^{-1}$)	Pore volume ($cm^3\ g^{-1}$)
ZIF-8 membrane (this work)	1474	0.71
ALD ZIF-8 membrane (this work)	1424	0.70
ZIF-8 membrane [169, 186]	1046	0.51

The synthesized membranes were tested on propylene/propane gas separation. With the increase in the number of ALD cycles on ZIF-8 membranes, the C_3H_6/C_3H_8 separation factor increases first (141 to 270) and then starts to decrease (270 to 238). ZnO ALD cycles, as described in the previous section, helps in reducing defects in ZIF-8 membranes. It fixes the Zn vacancies in the top layer of ZIF-8 membranes, thus the viscous flow across the membrane gets reduced and the C_3H_6/C_3H_8 separation factor increases. However, further ALD reduces the pore size in the ZIF-8 membranes possibly below the size of both the propylene and propane, which causes the reduction in the C_3H_6/C_3H_8 separation factor as can be seen in Figure 4.18. C_3H_6 and C_3H_8 permeance values monotonically decrease (1×10^{-8} to 0.59×10^{-8} mol $m^{-2}\ s^{-1}\ Pa^{-1}$) with the number of ZnO ALD cycles. Initially it is because of reduction in viscous flow and then due to reduction in pore size. However, membranes showed similar trend for C_3H_6/C_3H_8 separation performance with the number of the ZnO ALD cycles but there were some variation in the values for the C_3H_6/C_3H_8 separation factors and permeance values. Overall ~80% of ZIF-8 membrane showed similar trend for C_3H_6/C_3H_8 separation performance with the number of ZnO ALD cycles.

However, membranes showed similar behavior for the C_3H_6/C_3H_8 separation but there were some variation in the values for C_3H_6/C_3H_8 separation factors and permeance values as depicted in the Table 4.8.

Table 4.8 shows the variation of the C_3H_6/C_3H_8 separation factor with the number of ALD cycles. It can be seen for ZIF-8 membranes percentage enhancement in the C_3H_6/C_3H_8 separation factor was as high as 91%.

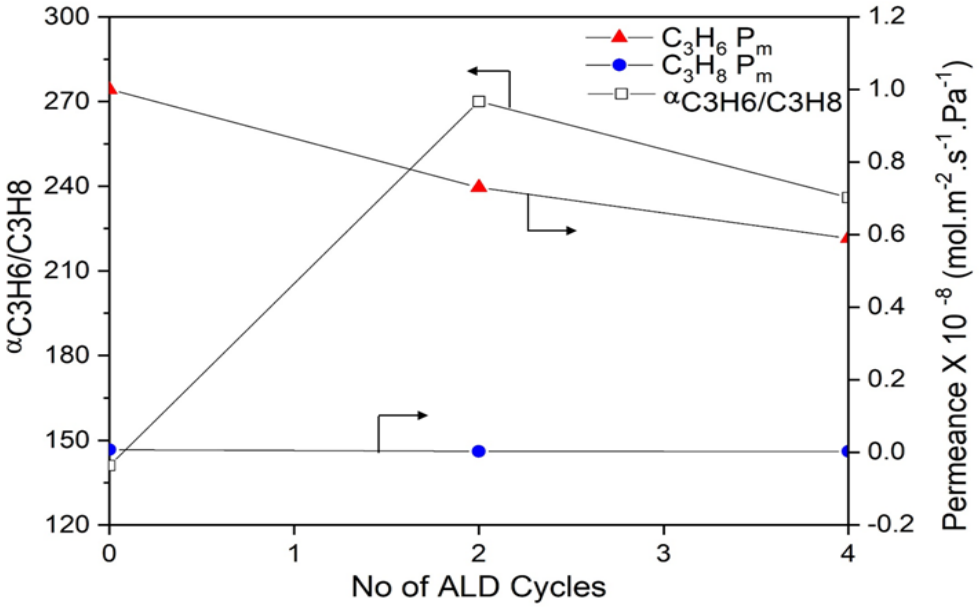

Figure 4.18. Effect of number of ZnO ALD cycles on C_3H_6/C_3H_8 separation performance

Table 4.8. Gas permeation results for equimolar C_3H_6/C_3H_8 mixtures through methanol exchanged ZIF-8 membranes with number of ZnO ALD cycles

	C_3H_6/C_3H_8 separation factor			C_3H_6 Permeance			C_3H_8 Permeance		
	No of ALD Cycles								
Membrane	0	2	4	0	2	4	0	2	4
M1	178	243	237	0.76	0.48	0.43	0.0042	0.0019	0.0018
M2	206	250	187	0.79	0.71	0.51	0.0038	0.0028	0.0027
M3	141	270	238	1.00	0.73	0.59	0.0071	0.0027	0.0025
M4	129	264	232	0.92	0.9	0.77	0.0071	0.0034	0.0033

Moreover, the obtained results were compared with previously reported literature for secondary growth of ZIF-8 membrane [112, 118, 123, 187-194] as shown in Figure 4.19. In Figure 4.19 we can see the comparison of our results with the previously published data. It is clear that C_3H_6/C_3H_8 separation factor from this work are one of the best among the available literature. However, propylene permeance values still need to be enhanced in order to compete with the best ZIF-8 membranes. We are already working on designing the thinner ZIF-8 membrane which can help in obtaining high permeance without compromising C_3H_6/C_3H_8 separation factor. Typically, the industrial requirements for propylene/propane membrane gas separation need separation factor ~35 and ~1 barrer minimum permeability [195]. This makes our ZIF-8 membrane, if can be scaled up, an ideal candidate for industrial purposes in terms of performance.

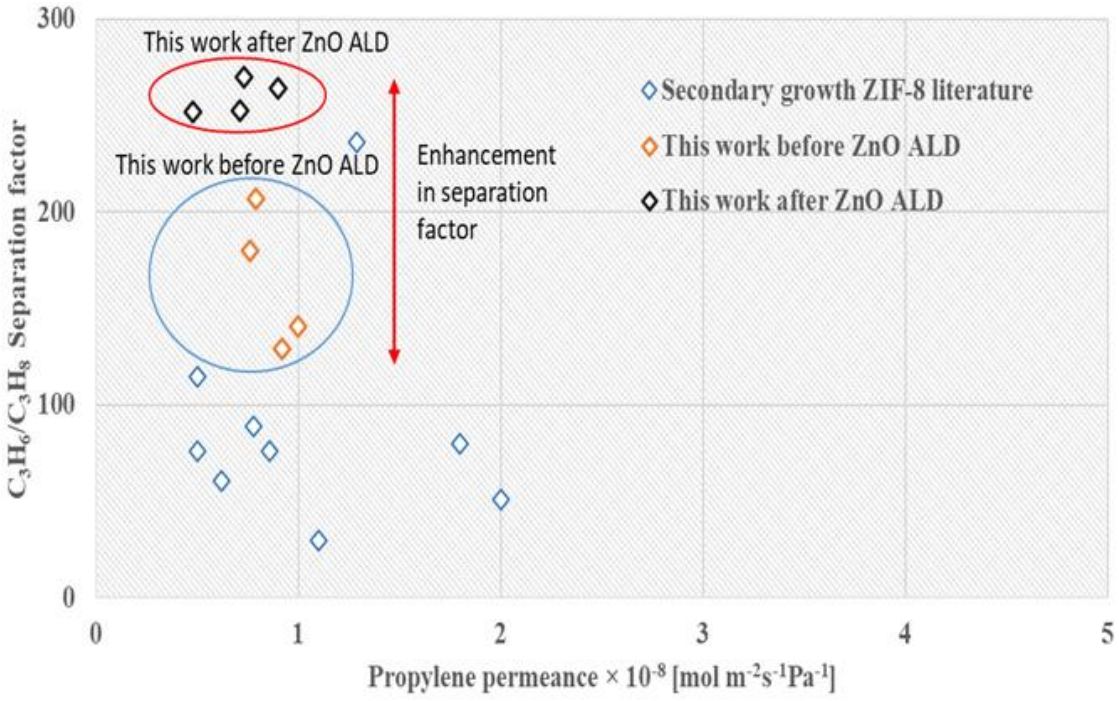

Figure 4.19. Effect of number of ZnO ALD cycles on C_3H_6/C_3H_8 separation performance

CHAPTER V

SUMMARY AND FUTURE WORK

The purpose of this work was to develop novel ways to produce industrially important chemicals such as ethylene, propylene, and isobutylene, efficiently. Membrane reactor were used to overcome the thermodynamic limitations, which exists in the dehydrogenation reactions. With experimental results, a comparative study was conducted between packed bed reactor (PBR) and packed bed membrane reactor (PBMR). A 1D PFR model was also developed for dehydrogenation reactions. Model results were validated with the experimental values. Model was also used to predict the corresponding alkane conversion values beyond experimental conditions. Detailed conclusions are explained in the following sections.

5.1. Ethane dehydrogenation reaction

The MFI zeolite membrane with moderate H_2 selectivity and H_2 permeance was successfully used to investigate the impact of pressure on the packed bed membrane reactors (PBMR) for ethane dehydrogenation (EDH) reaction. In this work not only the thermodynamic limitation was successfully surpassed but also the 1D PFR model was developed which was used to predict the impact of operating conditions beyond experimental conditions. The maximum ethane conversion, ethylene selectivity and ethylene yield obtained were 29%, 97%, and 28%, respectively. The impact of reaction pressure on H_2 recovery (R_{H2}) and permeate side H_2 concentration ($y_{H2,p}$) was also studied. R_{H2} increased with increasing pressure as more H_2

was transferred to permeate side but $y_{H2,p}$ decreased with increase in pressure because ethane diffusion across the membrane also increased significantly with an increase in pressure. Increasing pressure adversely affected the methanation as less H_2 was available in the reaction side for methanation reaction to proceed. H_2 was also used in the feed to enhance the catalyst stability. Increasing H_2 amount in the feed enhanced the stability of the catalyst. However, there was a slight decrease in reaction performance parameters with increase in the H_2 concentration in the feed. The simulation results accurately predicted ethane conversion for both PBMR and packed bed reactor (PBR). The model predicted ethane conversion of 93% at WHSV of 0.45 h^{-1}, pressure of 3.0 atm and A/A_0 of 1.5. Overall, EDH PBMR showed increase in ethane conversion and significantly reduced the undesirable side reactions with the enhancement of reaction pressure.

5.2 Propane dehydrogenation reaction

Effect of different operating parameters such as temperature, pressure, space velocity and sweep gas flow rate on propane dehydrogenation (PDH) reaction was studied using MFI zeolite membrane. However, the separation performance was moderate for MFI zeolite membrane for H_2/propane but it helped in enhancing PDH reaction performance considerably for PBMR. A 1D PFR model was used not only to validate experimental results but also to predict reaction performance beyond experimental conditions. The maximum propane conversion, propylene selectivity and propylene yield obtained were 49%, 97%, and 47%, respectively. H_2 recovery (R_{H2}) increased with increasing pressure as more H_2 was transferred to permeate side but permeate side H_2 concentration ($y_{H2,p}$) decreased with increase in pressure because propane and unreacted propylene also diffuses across the membrane which reduced the concentration of H_2 in the permeate side. Increasing the pressure reduced the methane selectivity for both PBMR and PBR. Model predicted the propane conversion results very well for both the PBMR and PBR. Highest propane conversion predicted was 99% at WHSV of 1.1 h^{-1}, pressure of 3.0 atm, and A/A_0 of 1.5. MFI zeolite membrane significantly enhanced the propane conversion for PDH reaction.

5.3 Isobutane dehydrogenation reaction

Isobutane dehydrogenation (IBDH) reaction was performed by experiments and by modeling for microporous MFI-type zeolite membranes. It was found that PBMR successfully exceeded the equilibrium limit and enhanced the i-C_4H_{10} conversion due to H_2 permeation across the membrane. The IBDH PBMR exhibited higher conversion, selectivity, and yield than the PBR. The impact of operating specifications upon H_2 recovery (R_{H2}) was studied and R_{H2} as high as 52 % was obtained in PBMR. For the lab scale PBMR, the one dimensional PFR model was satisfactorily predicted the conversion values for the IBDH reaction. The zeolite PBMR predicted i-C_4H_{10} conversion of > 90% at F_{Ar} of ~ 20 cm^3/min, temperature > 600 °C, pressure ~ 6.5 atm while the membrane had moderate H_2 selectivity ($\alpha_{H2/i\text{-}C4H10}$ ~ 9.9, and $\alpha_{H2/i\text{-}C4H8}$ ~ 8.1) and permeance ($P_{m,H2} < 10^{-7}$ mol m^{-2} s^{-1} Pa^{-1}). With an exceptional chemical resistance and hydro-thermal stability, the MFI-type zeolite membranes are highly likely to be useful for creating PBMRs for high-temperature IBDH reaction.

5.4 ZIF-8 membrane for propylene/propane gas separation

Propylene/propane gas separation is one of the most difficult problem in industry. Propylene and propane have similar molecular sizes and almost same physical properties, which makes separation even more difficult. ZIF-8 membrane was developed using novel fabrication techniques for propylene/propane gas separation. Effect of seeding, effect of zinc salts and membrane synthesis time on ZIF-8 membrane performance for propylene/propane gas separation was studied. Among in situ ZIF-8 membrane, silicalite seeded and ZIF-8 seeded ZIF-8 membranes, silicalite seeded ZIF-8 membranes exhibited highest separation performance for propylene/propane gas mixture with a separation factor of 170 and propylene permeance of 0.9×10^{-8} mol m^{-2} s^{-1} Pa^{-1}. Silicalite seeding helped in proper growth of ZIF-8 membrane over AAO support. Moreover, impact of different zinc source such as $ZnCl_2$ and $ZnNO_3$ was also investigated. $ZnCl_2$ as precursor showed higher separation performance because $ZnNO_3$ as precursor reacted faster, and the

eventual ZIF-8 membrane were less intergrown, and showed thinner ZIF-8 membrane layer than those with zinc chloride. ZIF-8 crystal size affected membrane stabilities and gas adsorptions indicating that the appropriate ZIF-8 crystal size for the propylene/propane separations can be achieved by using zinc chloride as zinc source. ZIF-8 membrane with zinc chloride as precursor showed propylene/propane separation factor of 170 and propylene permeance of 0.9×10^{-8} mol m^{-2} s^{-1} Pa^{-1}. The appropriate time for ZIF-8, membrane fabrication was evaluated as 10 h. With increase in the membrane synthesis time from 10 h to 20 h, propylene/propane separation factor was reduced from 170 to 168 and propylene permeance from 0.9×10^{-8} to 0.7×10^{-8} mol m^{-2} s^{-1} Pa^{-1}. To summarize, the optimized conditions for ZIF-8 membrane fabrication were: silicalite seeding, $ZnCl_2$ as precursor for zinc source, and 10 h of synthesis time.

Though ZIF-8 membrane exhibited exceptional separation performance for the propylene/propane gas mixture. However, there were still some inherent defects and pinholes in the ZIF-8 framework. Healing those defects can further improve the performance of these membranes. Mostly defects in ZIF-8 membrane were because of Zn vacancies in the ZIF-8 framework. In this work, ZnO atomic layer deposition (ALD) was used to heal those Zn vacancies. With XPS and FT-IR results, it was confirmed that there were more Zn-N bonds in the ZIF-8 framework post ALD, which indicated the decrease in number of defects in the ZIF-8 framework. ALD only helped in healing the top layer of the ZIF-8 membrane. Doing more ALD cycles on ZIF-8 membranes only made more deposition of ZnO on the ZIF-8 pores. This resulted in the enhancement of ZIF-8 membrane separation performance initially and then the separation performance goes down. ZIF-8 membranes showed enhancement in propylene/propane separation factor only with first 2 cycles of ALD and further ALD cycles reduced the separation factor. On an average ZIF-8 membrane separation factor for propylene/propane gas separation increased from 141 to 270 (91% enhancement) for first 2 ALD cycles. However, propylene and propane gas permeance reduced monotonously with number of ALD cycles.

5.5 Future work

In this work, impressive results have been presented. We believe there is still scope for further improvement in the performance of dehydrogenation reaction and propylene/propane gas mixture separation performance. Here we present the tentative ideas, which can be used in future.

5.5.1 Dehydrogenation reactions

During my Ph.D., I focused on dehydrogenation of ethane, propane and isobutane using MFI zeolite membrane. MFI zeolite membrane has moderate separation performance for the H_2/Alkane gas separation. Alternatives membranes with better separation performance can enhance performance of dehydrogenation reactions. Silica membranes based of tetraethoxysilane (TEOS), bis(triethoxysilyl)ethane (BTESE), and bis(triethoxysilyl)methane (BTESM) have exhibited better H_2/alkane separation performance at the room temperature than MFI zeolite membranes [27, 196]. Average pore size for silica membranes derived from different silica sources have been in the following order: BTESE derived silica membrane >BTESM derived silica membrane > TEOS derived silica membrane [27, 197, 198]. However, silica membranes are not stable at high temperature, which limits their applicability for the dehydrogenation reaction, which are feasible only at high temperature (> 500 ^oC). If the thermal stability of silica membrane can be improved and their H_2/Alkane separation performance can be sustained at high temperature, silica membrane can yield excellent performance for alkane dehydrogenation reaction.

There have been some works for the use of silica membrane for low temperature operation (< 250 ^oC). Oda et. al used silica membrane reactor for the dehydrogenation of methyl cyclohexane (MCH). Silica membrane showed excellent hydrogen permeance at 573 K in the order of 10^{-6} mol m^{-2} s^{-1} Pa^{-1}. Membrane reactor showed equilibrium shifts as expected for reaction temperature between 473 to 553 K and reaction pressure ranging from 0.1 to 0.25 MPa. Hydrogen purity as high as 99.95% was achieved in the membrane

reactor. A simulation model was also developed which successfully predicted reaction performance [199]. Li et. al also used silica membrane for the MCH dehydrogenation reaction. Membrane exhibited high H_2 permeance of 1.29×10^{-6} mol m^{-2} s^{-1} Pa^{-1} and very high H_2/C_3H_8 and H_2/SF_6 selectivity of 6680 and 48,900. Extraction of H_2 from membrane helped in achieving the MCH conversion higher than thermodynamic limitation and with almost pure H_2 in the permeate stream [200]. Battersby et. al used cobalt based silica membrane for water gas shift membrane reaction. During single gas dry testing He/N_2 and the H_2/CO_2 selectivity increased from 75-400 and 45-160 as the temperature was increased from 100 to 250 ^oC. H_2 permeation purity of 89-95% and high water ratio conversion was obtained. Doping the membrane with cobalt helped in enhancing its hydrothermal stability over a period of 200 h of operation [201].

Though BTESM and BTESE derived silica membranes also showed the impressive separation performance for H_2/Alkane gas mixture, TEOS based silica membrane were chosen as potential candidates for enhancing the performance of dehydrogenation reaction at higher temperature. TEOS based membrane was chosen because it does not have any carbon in its structure unlike the BTESM and BTESE derived silica membrane. To improve the thermal study of TEOS based silica membrane, aluminum was introduced into silica membrane structure. At room temperature, TEOS based silica membrane showed H_2/C_3H_8 selectivity of 10 against 6.1 from MFI zeolite membrane at 500 ^oC. This indicates that TEOS based silica membrane would help in enhancing dehydrogenation reaction performance better than MFI zeolite membrane because of its better separation ability. Exposure of silica membrane, to high temperature causes rapid densification in the membrane which causes the change in membrane pore structure [202]. Octahedral Al atoms replaced tetrahedral Si atoms in the framework and thus made the structure more compact. This modified structure showed resistance for high temperature degradation. TEOS based silica membrane was showing slight back permeation at high temperature which indicates defects in their framework. However, after inclusion of Al in the framework no back permeation was observed even at 600 ^oC. Further studies for investigating the stability of TEOS based silica membrane will be needed to ensure their applicability in high temperature alkane dehydrogenation reaction.

5.5.2 Propylene/propane gas separations

The propylene/propane separation results depicted in this thesis are at room temperature. However, in industry propylene/propane separation are performed at ~ 150 ^{o}C. This shows the need of hydrothermal stability of ZIF-8 membrane so that these membranes can be used in industry. ZIF membranes have been known to be sensitive to temperature and moisture which limits their use for many practical applications [203].

In this work, AAO support was used for the fabrication of ZIF-8 membrane. Chemical property of the support plays a key role in the hydrothermal stability of the ZIF membranes. ZIF crystals are thermally stable even at 500 ^{o}C. However, when ZIF membranes are grown on a different support, intercrystalline defects occur during high temperature operation. This is because of the heterogeneous nucleation of the ZIF crystals on support and different thermal expansion coefficient of the ZIF-8 and the support. Improving hydrothermal stability of ZIF-8 membrane has been a challenge. AAO support is acidic in nature. As stated before, metal oxide support substantially affects the hydrothermal stability of the ZIF membranes. ZIF membranes fabricated on alumina support showed fatal degradation even at relatively moderate temperature of 200 ^{o}C due to its acidic nature. Kim et. al exhibited that the ZIF membranes fabricated on neutral support like SiO_2 and basic supports like MgO have their structures intact even at adverse hydrothermal conditions. With characterization techniques such as SEM and XRD, enhanced hydrothermal stability of the ZIF-7 membrane was confirmed [203-206]. Methods like the use ZnO ALD on AAO support might change the acidic nature of the support. The ZnO ALD modified support will be used for the fabrication of ZIF-8 membrane. ZnO ALD modified AAO support might enhance the thermal stability of the ZIF-8 membranes and will facilitate ZIF-8 membrane use for high temperature operation.

REFERENCES

[1] E. McLeary, J. Jansen, F. Kapteijn, Zeolite based films, membranes and membrane reactors: Progress and prospects, Microporous and Mesoporous Materials 90 (2006) 198-220.

[2] https://www.esi-africa.com/industry-sectors/business-and-markets/global-ethylene-capacity-to-see-considerable-growth-of-27/.

[3] E. Gobina, R. Hughes, Ethane dehydrogenation using a high-temperature catalytic membrane reactor, Journal of membrane science 90 (1994) 11-19.

[4] https://www.statista.com/statistics/1065879/global-propylene-production-capacity/.

[5] https://www.grandviewresearch.com/press-release/global-isobutene-market.

[6] J. Armor, Applications of catalytic inorganic membrane reactors to refinery products, Journal of Membrane Science 147 (1998) 217-233.

[7] J. Armor, Catalysis with permselective inorganic membranes, Applied catalysis 49 (1989) 1-25.

[8] J. Armor, Challenges in membrane catalysis, ChemInform 24 (1993) no-no.

[9] G. Saracco, V. Specchia, Catalytic inorganic-membrane reactors: present experience and future opportunities, Catalysis Reviews—Science and Engineering 36 (1994) 305-384.

[10] J. Shu, B. Grandjean, A.V. Neste, S. Kaliaguine1, Catalytic palladium-based membrane reactors: A review, The Canadian Journal of Chemical Engineering 69 (1991) 1036-1060.

[11] H. Itoh, T. Ono, S. Nagano, E. Kikuchi, Sekiyu Grakkaishi, submitted for publication (1990).

[12] J. Zaman, A. Chakma, Inorganic membrane reactors, Journal of Membrane Science 92 (1994) 1-28.

[13] G. Saracco, G. Vesteeg, W.P.M. van Swaaij, Current hurdles to the success of high-temperature membrane reactors, Journal of membrane science 95 (1994) 105-123

[14] A. Paul, C.B. Musgrave, Catalyzed dehydrogenation of ammonia–borane by iridium dihydrogen pincer complex differs from ethane dehydrogenation, Angewandte Chemie 119 (2007) 8301-8304.

[15] V. Galvita, G. Siddiqi, P. Sun, A.T. Bell, Ethane dehydrogenation on Pt/Mg (Al) O and PtSn/Mg (Al) O catalysts, Journal of Catalysis 271 (2010) 209-219.

[16] S. Dangwal, R. Liu, S.-J. Kim, High-temperature ethane dehydrogenation in microporous zeolite membrane reactor: Effect of operating conditions, Chemical Engineering Journal 328 (2017) 862-872.

[17] T. Matsuda, I. Koike, N. Kubo, E. Kikuchi, Dehydrogenation of isobutane to isobutene in a palladium membrane reactor, Applied Catalysis A: General 96 (1993) 3-13.

[18] T. Ioannides, G. Gavalas, Catalytic isobutane dehydrogenation in a dense silica membrane reactor, Journal of membrane science 77 (1993) 207-220.

[19] D. Casanave, P. Ciavarella, K. Fiaty, J.-A. Dalmon, Zeolite membrane reactor for isobutane dehydrogenation: Experimental results and theoretical modelling, Chemical Engineering Science 54 (1999) 2807-2815.

[20] P. Ciavarella, D. Casanave, H. Moueddeb, S. Miachon, K. Fiaty, J.-A. Dalmon, Isobutane dehydrogenation in a membrane reactor: influence of the operating conditions on the performance, Catalysis Today 67 (2001) 177-184.

[21] M. Gimeno, Z. Wu, J. Soler, J. Herguido, K. Li, M. Menéndez, Combination of a Two-Zone Fluidized Bed Reactor with a Pd hollow fibre membrane for catalytic alkane dehydrogenation, Chemical Engineering Journal 155 (2009) 298-303.

[22] D.E. Resasco, Dehydrogenation by heterogeneous catalysts, Encyclopedia of Catalysis (2000).

[23] D.B. Kang, A.B. Anderson, Theoretical interpretation of the cyclohexane. fwdarw. benzene reaction on the platinum (III) surface, Journal of the American Chemical Society 107 (1985) 7858-7861.

[24] D. Sanfilippo, I. Miracca, Dehydrogenation of paraffins: synergies between catalyst design and reactor engineering, Catalysis Today 111 (2006) 133-139.

[25] T. Masuda, N. Fukumoto, M. Kitamura, S.R. Mukai, K. Hashimoto, T. Tanaka, T. Funabiki, Modification of pore size of MFI-type zeolite by catalytic cracking of silane and application to preparation of H2-separating zeolite membrane, Microporous and mesoporous materials 48 (2001) 239-245.

[26] J. Dong, Y. Lin, M.Z.-C. Hu, R.A. Peascoe, E.A. Payzant, Template-removal-associated microstructural development of porous-ceramic-supported MFI zeolite membranes, Microporous and mesoporous materials 34 (2000) 241-253.

[27] M. Kanezashi, M. Kawano, T. Yoshioka, T. Tsuru, Organic–inorganic hybrid silica membranes with controlled silica network size for propylene/propane separation, Industrial & Engineering Chemistry Research 51 (2011) 944-953.

[28] S. Kallus, P. Langlois, G. Romanos, T. Steriotis, E. Kikkinides, N. Kanellopoulos, J. Ramsay, " NCSR DEMOKRITOS, Institute of Physical Chemistry, 15310 Ag, Paraskevi Attikis, Greece, Characterisation of Porous Solids V 128 (2000) 467.

[29] J. Dong, Y. Lin, W. Liu, Multicomponent hydrogen/hydrocarbon separation by MFI-type zeolite membranes, AIChE Journal 46 (2000) 1957-1966.

[30] J.H. Moon, C.H. Lee, Hydrogen separation of methyltriethoxysilane templating silica membrane, AIChE journal 53 (2007) 3125-3136.

[31] K.S. Rothenberger, A.V. Cugini, B.H. Howard, R.P. Killmeyer, M.V. Ciocco, B.D. Morreale, R.M. Enick, F. Bustamante, I.P. Mardilovich, Y.H. Ma, High pressure hydrogen permeance of porous stainless steel coated with a thin palladium film via electroless plating, Journal of membrane science 244 (2004) 55-68.

[32] M.B. Shiflett, H.C. Foley, Ultrasonic deposition of high-selectivity nanoporous carbon membranes, Science 285 (1999) 1902-1905.

[33] Z. Tang, J. Dong, T.M. Nenoff, Internal surface modification of MFI-type zeolite membranes for high selectivity and high flux for hydrogen, Langmuir 25 (2009) 4848-4852.

[34] M. Tsapatsis, G. Xomeritakis, H. Hillhouse, S. Nair, V. Nikolakis, G. Bonilla, Z. Lai, Zeolite membranes, Cattech 3 (1999) 148-163.

[35] Z. Zheng, Synthesis and characterization of ultramicroporous zeolitic membranes for hydrogen separation, University of Cincinnati, 2008.

[36] D. Lewis, C. Freeman, C. Catlow, Predicting the templating ability of organic additives for the synthesis of microporous materials, The Journal of Physical Chemistry 99 (1995) 11194-11202.

[37] J. Dong, Y. Lin, M. Kanezashi, Z. Tang, Microporous inorganic membranes for high temperature hydrogen purification, Journal of Applied Physics 104 (2008) 13.

[38] B.M. Weckhuysen, R.A. Schoonheydt, Alkane dehydrogenation over supported chromium oxide catalysts, Catalysis Today 51 (1999) 223-232.

[39] M.C. Haibach, S. Kundu, M. Brookhart, A.S. Goldman, Alkane metathesis by tandem alkane-dehydrogenation–olefin-metathesis catalysis and related chemistry, Accounts of chemical research 45 (2012) 947-958.

[40] J. Caro, M. Noack, P. Kölsch, R. Schäfer, Zeolite membranes–state of their development and perspective, Microporous and mesoporous materials 38 (2000) 3-24.

[41] M. Kanezashi, J. O'Brien, Y. Lin, Template-free synthesis of MFI-type zeolite membranes: Permeation characteristics and thermal stability improvement of membrane structure, Journal of membrane science 286 (2006) 213-222.

[42] A. Huang, F. Liang, F. Steinbach, T.M. Gesing, J.r. Caro, Neutral and cation-free LTA-type aluminophosphate (AlPO4) molecular sieve membrane with high hydrogen permselectivity, Journal of the American Chemical Society 132 (2010) 2140-2141.

[43] J.M. van de Graaf, E. van der Bijl, A. Stol, F. Kapteijn, J.A. Moulijn, Effect of operating conditions and membrane quality on the separation performance of composite silicalite-1 membranes, Industrial & engineering chemistry research 37 (1998) 4071-4083.

[44] J. Coronas, J. Santamaría, Separations using zeolite membranes, Separation and Purification methods 28 (1999) 127-177.

[45] A. Moparthi, R. Uppaluri, B. Gill, Economic feasibility of silica and palladium composite membranes for industrial dehydrogenation reactions, Chem Eng Res Des 88 (2010) 1088-1101.

[46] A. Avila, Z. Yu, S. Fazli, J. Sawada, S. Kuznicki, Hydrogen-selective natural mordenite in a membrane reactor for ethane dehydrogenation, Microporous Mesoporous Mater. 190 (2014) 301-308.

[47] V. Galvita, G. Siddiqi, P. Sun, A.T. Bell, Ethane dehydrogenation on Pt/Mg(Al)O and PtSn/Mg(Al)O catalysts, J. Catal. 271 (2010) 209-219.

[48] O.O. James, S. Mandal, N. Alele, B. Chowdhury, S. Maity, Lower alkanes dehydrogenation: Strategies and reaction routes to corresponding alkenes, Fuel Process. Technol 149 (2016) 239-255.

[49] M.P. Lobera, S. Escolástico, J.M. Serra, High ethylene production through oxidative dehydrogenation of ethane membrane reactors based on fast oxygen-ion conductors, ChemCatChem 3 (2011) 1503-1508.

[50] E. Gobina, K. Hou, R. Hughes, Ethane dehydrogenation in a catalytic membrane reactor coupled with a reactive sweep gas, Chem. Eng. Sci. 50 (1995) 2311-2319.

[51] E. Gobina, R. Hughes, Reaction assisted hydrogen transport during catalytic dehydrogenation in a membrane reactor, Appl. Catal., A 137 (1996) 119-127.

[52] A. Champagnie, T. Tsotsis, R. Minet, E. Wagner, Ethane dehydrogenation in a catalytic membrane reactor, ChemInform 23 (1992).

[53] J. Szegner, K.L. Yeung, A. Varma, Effect of catalyst distribution in a membrane reactor: experiments and model, AlChE J. 43 (1997) 2059-2072.

[54] A. Brunetti, G. Barbieri, E. Drioli, T. Granato, K.-H. Lee, A porous stainless steel supported silica membrane for WGS reaction in a catalytic membrane reactor, Chemical Engineering Science 62 (2007) 5621-5626.

[55] A. Brunetti, G. Barbieri, E. Drioli, K.-H. Lee, B. Sea, D.-W. Lee, WGS reaction in a membrane reactor using a porous stainless steel supported silica membrane, Chemical Engineering and Processing: Process Intensification 46 (2007) 119-126.

[56] D. Lee, P. Hacarlioglu, S.T. Oyama, The effect of pressure in membrane reactors: trade-off in permeability and equilibrium conversion in the catalytic reforming of CH 4 with CO 2 at high pressure, Topics in catalysis 29 (2004) 45-57.

[57] G. Barbieri, A. Brunetti, T. Granato, P. Bernardo, E. Drioli, Engineering evaluations of a catalytic membrane reactor for the water gas shift reaction, Industrial & engineering chemistry research 44 (2005) 7676-7683.

[58] A.S. Augustine, Y.H. Ma, N.K. Kazantzis, High pressure palladium membrane reactor for the high temperature water–gas shift reaction, International Journal of Hydrogen Energy 36 (2011) 5350-5360.

[59] A. Ricca, V. Palma, G. Iaquaniello, E. Palo, A. Salladini, Highly selective propylene production in a membrane assisted catalytic propane dehydrogenation, Chemical Engineering Journal 330 (2017) 1119-1127.

[60] G. Karagiannakis, S. Zisekas, C. Kokkofitis, M. Stoukides, Effect of H2O presence on the propane decomposition reaction over Pd in a proton conducting membrane reactor, Applied Catalysis A: General 301 (2006) 265-271.

[61] B. Xu, T. Li, B. Zheng, W. Hua, Y. Yue, Z. Gao, Enhanced stability of HZSM-5 supported Ga 2 O 3 catalyst in propane dehydrogenation by dealumination, Catalysis letters 119 (2007) 283-288.

[62] Y. Ren, W. Hua, Y. Yue, Z. Gao, Dehydrogenation of propane to propene over phosphorus-modified HZSM-5 supported Ga 2 O 3, Reaction Kinetics and Catalysis Letters 95 (2008) 113-122.

[63] M. Chen, J. Xu, Y.-M. Liu, Y. Cao, H.-Y. He, J.-H. Zhuang, K.-N. Fan, Enhanced Activity of Spinel-type Ga 2 O 3–Al 2 O 3 Mixed Oxide for the Dehydrogenation of Propane in the Presence of CO 2, Catalysis letters 124 (2008) 369-375.

[64] Y. Liu, Z.H. Li, J. Lu, K.-N. Fan, Periodic density functional theory study of propane dehydrogenation over perfect Ga2O3 (100) surface, The Journal of Physical Chemistry C 112 (2008) 20382-20392.

[65] F. Zhang, R. Wu, Y. Yue, W. Yang, S. Gu, C. Miao, W. Hua, Z. Gao, Chromium oxide supported on ZSM-5 as a novel efficient catalyst for dehydrogenation of propane with CO2, Microporous and mesoporous materials 145 (2011) 194-199.

[66] A. Corma, J. Mengual, P.J. Miguel, IM-5 zeolite for steam catalytic cracking of naphtha to produce propene and ethene. An alternative to ZSM-5 zeolite, Applied Catalysis A: General 460 (2013) 106-115.

[67] X. Gao, Z. Tang, H. Zhang, D. Ji, G. Lu, Z. Wang, Z. Tan, Influence of particle size of ZSM-5 on the yield of propylene in fluid catalytic cracking reaction, Journal of Molecular Catalysis A: Chemical 325 (2010) 36-39.

[68] B.Y. Jibril, A. Atta, K. Melghit, Z. El-Hadi, H. Ala'a, Performance of supported Mg 0.15 V 2 O 5.15 2.4 H 2 O nanowires in dehydrogenation of propane, Chemical Engineering Journal 193 (2012) 391-395.

[69] M. Lobera, C. Téllez, J. Herguido, Y. Schuurman, M. Menéndez, TAP studies of Pt–Sn–K/γ-Al 2 O 3 catalyst for propane dehydrogenation, Chemical engineering journal 171 (2011) 1317-1323.

[70] E. Shelepova, A. Vedyagin, I. Mishakov, A. Noskov, Mathematical modeling of the propane dehydrogenation process in the catalytic membrane reactor, Chemical engineering journal 176 (2011) 151-157.

[71] Y. Cheng, M. Pena, K. Yeung, Hydrogen production from partial oxidation of methane in a membrane reactor, Journal of the Taiwan Institute of Chemical Engineers 40 (2009) 281-288.

[72] J. Szegner, K.L. Yeung, A. Varma, Effect of catalyst distribution in a membrane reactor: experiments and model, AIChE journal 43 (1997) 2059-2072.

[73] A. Iglesias-Juez, A.M. Beale, K. Maaijen, T.C. Weng, P. Glatzel, B.M. Weckhuysen, A combined in situ time-resolved UV–Vis, Raman and high-energy resolution X-ray absorption spectroscopy study on the deactivation behavior of Pt and Pt Sn propane dehydrogenation catalysts under industrial reaction conditions, Journal of Catalysis 276 (2010) 268-279.

[74] S. Sokolov, M. Stoyanova, U. Rodemerck, D. Linke, E.V. Kondratenko, Comparative study of propane dehydrogenation over V-, Cr-, and Pt-based catalysts: Time on-stream behavior and origins of deactivation, Journal of catalysis 293 (2012) 67-75.

[75] Q. Hassanusi, Thermodynamic Study of Propane Dehydrogenation Into Propylene, UMP, 2013.

[76] J.-S. Chang, H.-S. Roh, M.S. Park, S.-E. Park, Propane dehydrogenation over a hydrogen permselective membrane reactor, BULLETIN-KOREAN CHEMICAL SOCIETY 23 (2002) 674-678.

[77] T. Peters, O. Liron, R. Tschentscher, M. Sheintuch, R. Bredesen, Investigation of Pd-based membranes in propane dehydrogenation (PDH) processes, Chemical Engineering Journal 305 (2016) 191-200.

[78] Z. Wu, I. Hatim, B.F. Kingsbury, E. Gbenedio, K. Li, A novel inorganic hollow fiber membrane reactor for catalytic dehydrogenation of propane, AIChE journal 55 (2009) 2389-2398.

[79] Y. Yildirim, E. Gobina, R. Hughes, An experimental evaluation of high-temperature composite membrane systems for propane dehydrogenation, Journal of membrane science 135 (1997) 107-115.

[80] M. Sheintuch, O. Liron, A. Ricca, V. Palma, Propane dehydrogenation kinetics on supported Pt catalyst, Applied Catalysis A: General 516 (2016) 17-29.

[81] L. Didenko, V. Savchenko, L. Sementsova, P. Chizov, Some peculiarities of dehydrogenation of propane and n, Petroleum Chemistry 56 (2016) 459-464.

[82] R. Schäfer, M. Noack, P. Kölsch, M. Stöhr, J. Caro, Comparison of different catalysts in the membrane-supported dehydrogenation of propane, Catalysis Today 82 (2003) 15-23.

[83] Z. Ziaka, R. Minet, T. Tsotsis, A high temperature catalytic membrane reactor for propane dehydrogenation, Journal of membrane science 77 (1993) 221-232.

[84] J.P. Collins, R.W. Schwartz, R. Sehgal, T.L. Ward, C. Brinker, G.P. Hagen, C.A. Udovich, Catalytic dehydrogenation of propane in hydrogen permselective membrane reactors, Industrial & engineering chemistry research 35 (1996) 4398-4405.

[85] X. Liu, W.-Z. Lang, L.-L. Long, C.-L. Hu, L.-F. Chu, Y.-J. Guo, Improved catalytic performance in propane dehydrogenation of PtSn/γ-Al 2 O 3 catalysts by doping indium, Chemical Engineering Journal 247 (2014) 183-192.

[86] S. Kobayashi, S. Kaneko, M.-a. Ohshima, H. Kurokawa, H. Miura, Effect of iron oxide on isobutane dehydrogenation over Pt/Fe_2O_3-Al_2O_3 catalyst, Applied Catalysis A: General 417 (2012) 306-312.

[87] M. Farsi, A. Jahanmiri, M. Rahimpour, Optimal operating conditions of radial flow moving-bed reactors for isobutane dehydrogenation, Journal of Energy Chemistry 22 (2013) 633-638.

[88] Y. Zhang, Y. Zhou, L. Wan, M. Xue, Y. Duan, X. Liu, Effect of magnesium addition on catalytic performance of PtSnK/γ-Al_2O_3 catalyst for isobutane dehydrogenation, Fuel processing technology 92 (2011) 1632-1638.

[89] Y.-P. Tian, X.-M. Liu, M.J. Rood, Z.-F. Yan, Study of coke deposited on a VO_x-K_2O/γ-Al_2O_3 catalyst in the non-oxidative dehydrogenation of isobutane, Applied Catalysis A: General 545 (2017) 1-9.

[90] H. Zhao, H. Song, L. Chou, J. Zhao, J. Yang, L. Yan, Insight into the structure and molybdenum species in mesoporous molybdena–alumina catalysts for isobutane dehydrogenation, Catalysis Science & Technology 7 (2017) 3258-3267.

[91] C. Wei, F. Xue, C. Miao, Y. Yue, W. Yang, W. Hua, Z. Gao, Dehydrogenation of Isobutane with Carbon Dioxide over SBA-15-supported vanadium oxide catalysts, Catalysts 6 (2016) 171.

[92] G. Wang, H. Wang, H. Zhang, Q. Zhu, C. Li, H. Shan, Highly selective and stable NiSn/SiO_2 catalyst for isobutane dehydrogenation: Effects of Sn addition, ChemCatChem 8 (2016) 3137-3145.

[93] Y.-P. Tian, P. Bai, S.-M. Liu, X.-M. Liu, Z.-F. Yan, VO_x–K_2O/γ-Al_2O_3 catalyst for nonoxidative dehydrogenation of isobutane, Fuel Processing Technology 151 (2016) 31-39.

[94] J. Serrano-Ruiz, A. Sepúlveda-Escribano, F. Rodríguez-Reinoso, Bimetallic PtSn/C catalysts promoted by ceria: Application in the nonoxidative dehydrogenation of isobutane, Journal of Catalysis 246 (2007) 158-165.

[95] G.J. Siri, J.M. Ramallo-López, M.L. Casella, J.L. Fierro, F.G. Requejo, O.A. Ferretti, XPS and EXAFS study of supported PtSn catalysts obtained by surface organometallic chemistry on metals: Application to the isobutane dehydrogenation, Applied Catalysis A: General 278 (2005) 239-249.

[96] U. Rodemerck, M. Stoyanova, E.V. Kondratenko, D. Linke, Influence of the kind of VO_x structures in VO_x/MCM-41 on activity, selectivity and stability in dehydrogenation of propane and isobutane, Journal of Catalysis 352 (2017) 256-263.

[97] A.-h. Dong, K. Wang, S.-z. Zhu, G.-b. Yang, X.-t. Wang, Facile preparation of PtSn-La/Al_2O_3 catalyst with large pore size and its improved catalytic performance for isobutane dehydrogenation, Fuel Processing Technology 158 (2017) 218-225.

[98] T. Ehiro, H. Misu, S. Nitta, Y. Baba, M. Katoh, Y. Katou, W. Ninomiya, S. Sugiyama, Effects of acidic-basic properties on catalytic activity for the oxidative dehydrogenation of isobutane on calcium phosphates, doped and undoped with chromium, Journal of Chemical Engineering of Japan 50 (2017) 122-131.

[99] J. Van den Bergh, C. Gücüyener, J. Gascon, F. Kapteijn, Isobutane dehydrogenation in a DD3R zeolite membrane reactor, Chemical engineering journal 166 (2011) 368-377.

[100] L. Wang, C. Zhang, X. Gao, L. Peng, J. Jiang, X. Gu, Preparation of defect-free DDR zeolite membranes by eliminating template with ozone at low temperature, Journal of Membrane Science 539 (2017) 152-160.

[101] C. Feng, K. Khulbe, T. Matsuura, R. Farnood, A. Ismail, Recent progress in zeolite/zeotype membranes, Journal of Membrane Science and Research 1 (2015) 49-72.

[102] P. Ye, Zeolite Membrane Separation at Low Temperature, Luleå tekniska universitet, 2016.

[103] W. Liang, R. Hughes, The catalytic dehydrogenation of isobutane to isobutene in a palladium/silver composite membrane reactor, Catalysis Today 104 (2005) 238-243.

[104] L. Van Dyk, S. Miachon, L. Lorenzen, M. Torres, K. Fiaty, J.-A. Dalmon, Comparison of microporous MFI and dense Pd membrane performances in an extractor-type CMR, Catalysis today 82 (2003) 167-177.

[105] R.W. Baker, Future directions of membrane gas separation technology, Ind. Eng. Chem. Res. 41 (2002) 1393-1411.

[106] R.B. Eldridge, Olefin/paraffin separation technology: a review, Ind. Eng. Chem. Res. 32 (1993) 2208-2212.

[107] R.L. Burns, W.J. Koros, Defining the challenges for C_3H_6/C_3H_8 separation using polymeric membranes, J. Membr. Sci. 211 (2003) 299-309.

[108] S.M. Mauhar, B. Barjaktarovic, M. Sovilj, Optimization of propylene–propane distillation process, Chem. Pap. 58 (2004) 386-390.

[109] T. Merkel, R. Blanc, J. Zeid, A. Suwarlim, B. Firat, H. Wijmans, M. Asaro, M.L. Greene, Separation of Olefin/Paraffin Mixtures with Carrier Facilitated Membrane Final Report, Membrane Technology and Research, Inc., Menlo Park, CA, 2007.

[110] S. Zhou, Y. Wei, L. Li, Y. Duan, Q. Hou, L. Zhang, L.-X. Ding, J. Xue, H. Wang, J. Caro, Paralyzed membrane: Current-driven synthesis of a metal-organic framework with sharpened propene/propane separation, Science advances 4 (2018) eaau1393.

[111] S. Majumdar, Novel Membranes for Olefin/Paraffin Separation Final Report, Compact Membrane Systems, Inc., Newport, DE (United States), 2016.

[112] M.J. Lee, H.T. Kwon, H.-K. Jeong, Defect-dependent stability of highly propylene-selective zeolitic-imidazolate framework ZIF-8 membranes, J. Membr. Sci. 529 (2017) 105-113.

[113] C. Staudt-Bickel, W.J. Koros, Olefin/paraffin gas separations with 6FDA-based polyimide membranes, J. Membr. Sci. 170 (2000) 205-214.

[114] X. Ma, S. Williams, X. Wei, J. Kniep, Y. Lin, Propylene/propane mixture separation characteristics and stability of carbon molecular sieve membranes, Ind. Eng. Chem. Res. 54 (2015) 9824-9831.

[115] J.-i. Hayashi, H. Mizuta, M. Yamamoto, K. Kusakabe, S. Morooka, S.-H. Suh, Separation of ethane/ethylene and propane/propylene systems with a carbonized BPDA− pp ‘ODA polyimide membrane, Ind. Eng. Chem. Res. 35 (1996) 4176-4181.

[116] J.-i. Hayashi, H. Mizuta, M. Yamamoto, K. Kusakabe, S. Morooka, S.-H. Suh, Separation of ethane/ethylene and propane/propylene systems with a carbonized BPDA− pp ‘ODA polyimide membrane, Industrial & engineering chemistry research 35 (1996) 4176-4181.

[117] I.G. Giannakopoulos, V. Nikolakis, Separation of propylene/propane mixtures using faujasite-type zeolite membranes, Ind. Eng. Chem. Res. 44 (2005) 226-230.

[118] Y. Pan, T. Li, G. Lestari, Z. Lai, Effective separation of propylene/propane binary mixtures by ZIF-8 membranes, J. Membr. Sci. 390 (2012) 93-98.

[119] N. Hara, M. Yoshimune, H. Negishi, K. Haraya, S. Hara, T. Yamaguchi, Diffusive separation of propylene/propane with ZIF-8 membranes, J. Membr. Sci. 450 (2014) 215-223.

[120] Y. Pan, Y. Liu, G. Zeng, L. Zhao, Z. Lai, Rapid synthesis of zeolitic imidazolate framework-8 (ZIF-8) nanocrystals in an aqueous system, Chemical communications 47 (2011) 2071-2073.

[121] H.T. Kwon, H.-K. Jeong, In situ synthesis of thin zeolitic–imidazolate framework ZIF-8 membranes exhibiting exceptionally high propylene/propane separation, J. Am. Chem. Soc. 135 (2013) 10763-10768.

[122] M. Shah, H.T. Kwon, V. Tran, S. Sachdeva, H.-K. Jeong, One step in situ synthesis of supported zeolitic imidazolate framework ZIF-8 membranes: role of sodium formate, MICROPOR MESOPOR MAT 165 (2013) 63-69.

[123] Y. Pan, W. Liu, Y. Zhao, C. Wang, Z. Lai, Improved ZIF-8 membrane: effect of activation procedure and determination of diffusivities of light hydrocarbons, J. Membr. Sci. 493 (2015) 88-96.

[124] K.S. Park, Z. Ni, A.P. Côté, J.Y. Choi, R. Huang, F.J. Uribe-Romo, H.K. Chae, M. O’Keeffe, O.M. Yaghi, Exceptional chemical and thermal stability of zeolitic imidazolate frameworks, Proc. Natl. Acad. Sci. 103 (2006) 10186-10191.

[125] K. Li, D.H. Olson, J. Seidel, T.J. Emge, H. Gong, H. Zeng, J. Li, Zeolitic imidazolate frameworks for kinetic separation of propane and propene, JACS 131 (2009) 10368-10369.

[126] V.M.A. Melgar, J. Kim, M.R. Othman, Zeolitic imidazolate framework membranes for gas separation: a review of synthesis methods and gas separation performance, J IND ENG CHEM 28 (2015) 1-15.

[127] B.R. Pimentel, A. Parulkar, E.k. Zhou, N.A. Brunelli, R.P. Lively, Zeolitic Imidazolate Frameworks: Next-Generation Materials for Energy-Efficient Gas Separations, ChemSusChem 7 (2014) 3202-3240.

[128] H.T. Kwon, H.-K. Jeong, Improving propylene/propane separation performance of Zeolitic-Imidazolate framework ZIF-8 Membranes, Chem. Eng. Sci. 124 (2015) 20-26.

[129] C. Zhang, R.P. Lively, K. Zhang, J.R. Johnson, O. Karvan, W.J. Koros, Unexpected molecular sieving properties of zeolitic imidazolate framework-8, J. Phys. Chem. Lett 3 (2012) 2130-2134.

[130] Y. Pan, Y. Liu, G. Zeng, L. Zhao, Z. Lai, Rapid synthesis of zeolitic imidazolate framework-8 (ZIF-8) nanocrystals in an aqueous system, Chem comm 47 (2011) 2071-2073.

[131] S. Tanaka, K. Okubo, K. Kida, M. Sugita, T. Takewaki, Grain size control of ZIF-8 membranes by seeding-free aqueous synthesis and their performances in propylene/propane separation, J. Membr. Sci. 544 (2017) 306-311.

[132] M. He, J. Yao, Z.-X. Low, D. Yu, Y. Feng, H. Wang, A fast in situ seeding route to the growth of a zeolitic imidazolate framework-8/AAO composite membrane at room temperature, RSC Adv 4 (2014) 7634-7639.

[133] Y. Yoo, H.-K. Jeong, Rapid fabrication of metal organic framework thin films using microwave-induced thermal deposition, Chem Commun (2008) 2441-2443.

[134] M. Maksoud, N. Roques, S. Brandès, L. Arurault, J.-P. Sutter, Efficient growth of sub-micrometric MOF crystals inside the channels of AAO membranes, J. Mater. Chem A 1 (2013) 3688-3693.

[135] L.V. Meyer, J. Vogt, F.A. Brede, H. Schäfer, M. Steinhart, K. Müller-Buschbaum, In situ growth of luminescent MOF thin films of Sr/Eu (II)-imidazolate on functionalized nanostructured alumina, CrystEngComm 15 (2013) 9382-9386.

[136] C. Yim, M. Lee, M. Yun, G.-H. Kim, K.T. Kim, S. Jeon, CO_2-selective nanoporous metal-organic framework microcantilevers, Sci. Rep. 5 (2015) 10674.

[137] A. Schejn, L. Balan, V. Falk, L. Aranda, G. Medjahdi, R. Schneider, Controlling ZIF-8 nano-and microcrystal formation and reactivity through zinc salt variations, CrystEngComm 16 (2014) 4493-4500.

[138] L. Li, J. Yao, R. Chen, L. He, K. Wang, H. Wang, Infiltration of precursors into a porous alumina support for ZIF-8 membrane synthesis, Microporous Mesoporous Mater. 168 (2013) 15-18.

[139] J. Caro, Are MOF membranes better in gas separation than those made of zeolites?, Curr Opin Chem Eng 1 (2011) 77-83.

[140] N. Rangnekar, N. Mittal, B. Elyassi, J. Caro, M. Tsapatsis, Zeolite membranes–a review and comparison with MOFs, Chem. Soc. Rev. 44 (2015) 7128-7154.

[141] Z. Tang, S.-J. Kim, X. Gu, J. Dong, Microwave synthesis of MFI-type zeolite membranes by seeded secondary growth without the use of organic structure directing agents, Microporous Mesoporous Mater. 118 (2009) 224-231.

[142] S.-J. Kim, Z. Xu, G.K. Reddy, P. Smirniotis, J. Dong, Effect of pressure on high-temperature water gas shift reaction in microporous zeolite membrane reactor, Ind. Eng. Chem. Res. 51 (2012) 1364-1375.

[143] S.-J. Kim, S. Yang, G.K. Reddy, P. Smirniotis, J. Dong, Zeolite membrane reactor for high-temperature water-gas shift reaction: effects of membrane properties and operating conditions, Energy Fuels 27 (2013) 4471-4480.

[144] J. Szegner, K.L. Yeung, A. Varma, Effect of catalyst distribution in a membrane reactor: experiments and model, AlChE J. 43 (1997) 2059-2072.

[145] A.C. Bose, Inorganic membranes for energy and environmental applications, Springer 2009, p. 307-308.

[146] M. Hasany, M. Malakootikhah, V. Rahmanian, S. Yaghmaei, Effect of hydrogen combustion reaction on the dehydrogenation of ethane in a fixed-bed catalytic membrane reactor, Chin. J. Chem. Eng. 23 (2015) 1316-1325.

[147] M.L. Rodriguez, D.E. Ardissone, E. Heracleous, A.A. Lemonidou, E. López, M.N. Pedernera, D.O. Borio, Oxidative dehydrogenation of ethane to ethylene in a membrane reactor: A theoretical study, Catal. Today 157 (2010) 303-309.

[148] N. Hansen, R. Krishna, J. van Baten, A. Bell, F. Keil, Reactor simulation of benzene ethylation and ethane dehydrogenation catalyzed by ZSM-5: A multiscale approach, Chem. Eng. Sci. 65 (2010) 2472-2480.

[149] A. Manasilp, E. Gulari, Selective CO oxidation over Pt/alumina catalysts for fuel cell applications, Applied Catalysis B: Environmental 37 (2002) 17-25.

[150] A. Avila, Z. Yu, S. Fazli, J. Sawada, S. Kuznicki, Hydrogen-selective natural mordenite in a membrane reactor for ethane dehydrogenation, Microporous and Mesoporous Materials 190 (2014) 301-308.

[151] E. Gbenedio, Z. Wu, I. Hatim, B.F. Kingsbury, K. Li, A multifunctional Pd/alumina hollow fibre membrane reactor for propane dehydrogenation, Catalysis Today 156 (2010) 93-99.

[152] E. Simón, J.M. Rosas, A. Santos, A. Romero, Coke formation in copper catalyst during cyclohexanol dehydrogenation: Kinetic deactivation model and catalyst characterization, Chemical engineering journal 214 (2013) 119-128.

[153] P.L. Benito, A.G. Gayubo, A.T. Aguayo, M. Castilla, J. Bilbao, Concentration-dependent kinetic model for catalyst deactivation in the MTG process, Industrial & engineering chemistry research 35 (1996) 81-89.

[154] J. Szegner, K.L. Yeung, A. Varma, Effect of catalyst distribution in a membrane reactor: experiments and model, AIChE Journal-American Institute of Chemical Engineers 43 (1997) 2059-2072.

[155] S. Dangwal, R. Liu, S.V. Kirk, S.-J. Kim, Effect of Pressure on Ethane Dehydrogenation in MFI Zeolite Membrane Reactor, Energy Fuels 32 (2018) 4628-4637.

[156] J. Cravillon, R. Nayuk, S. Springer, A. Feldhoff, K. Huber, M. Wiebcke, Controlling zeolitic imidazolate framework nano-and microcrystal formation: insight into crystal growth by time-resolved in situ static light scattering, Chem. Mater. 23 (2011) 2130-2141.

[157] S.-J. Kim, C.W. Jones, S. Nair, Y. Liu, J.S. Moore, R.S. Dixit, J.G. Pendergast, S. Sarsani, Ion exchange of zeolite membranes by a vacuum 'flow-through'technique, Microporous Mesoporous Mater. 203 (2015) 170-177.

[158] K.S. Park, Z. Ni, A.P. Côté, J.Y. Choi, R. Huang, F.J. Uribe-Romo, H.K. Chae, M. O'Keeffe, O.M. Yaghi, Exceptional chemical and thermal stability of zeolitic imidazolate frameworks, PNAS 103 (2006) 10186-10191.

[159] Y. Pan, Z. Lai, Sharp separation of C2/C3 hydrocarbon mixtures by zeolitic imidazolate framework-8 (ZIF-8) membranes synthesized in aqueous solutions, Chem comm 47 (2011) 10275-10277.

[160] S.S. Ray, M. Okamoto, Polymer/layered silicate nanocomposites: a review from preparation to processing, Prog. Polym. Sci. 28 (2003) 1539-1641.

[161] S. Nishihama, Y. Tsutsumi, K. Yoshizuka, Separation of tetramethyl ammonium hydroxide using an MFI-type zeolite-coated membrane, Sep. Purif. Technol. 120 (2013) 129-133.

[162] L. Li, J. Yao, R. Chen, L. He, K. Wang, H. Wang, Infiltration of precursors into a porous alumina support for ZIF-8 membrane synthesis, MICROPOR MESOPOR MAT 168 (2013) 15-18.

[163] A. Jentys, G. Warecka, M. Derewinski, J.A. Lercher, Adsorption of water on ZSM 5 zeolites, J. Phys. Chem. 93 (1989) 4837-4843.

[164] N. Liédana, A. Galve, C.s. Rubio, C. Téllez, J. Coronas, CAF@ ZIF-8: one-step encapsulation of caffeine in MOF, ACS Appl. Mater. Interfaces 4 (2012) 5016-5021.

[165] G. Xue, Q. Dai, S. Jiang, Chemical reactions of imidazole with metallic silver studied by the use of SERS and XPS techniques, JACS 110 (1988) 2393-2395.

[166] F. Tian, D.F. Taber, A.V. Teplyakov, –NH–Termination of the Si (111) Surface by Wet Chemistry, JACS 133 (2011) 20769-20777.

[167] M.H. Matloob, M.W. Roberts, Electron spectroscopic study of nitrogen species adsorbed on copper, J. Chem. Soc., Faraday Trans.2 1: Phys. Chem. Condens. Phases 73 (1977) 1393-1405.

[168] R. Dedryvère, L. Gireaud, S. Grugeon, S. Laruelle, J.-M. Tarascon, D. Gonbeau, Characterization of lithium alkyl carbonates by X-ray photoelectron spectroscopy: experimental and theoretical study, J. Phys. Chem. B 109 (2005) 15868-15875.

[169] F. Cacho-Bailo, B. Seoane, C. Téllez, J. Coronas, ZIF-8 continuous membrane on porous polysulfone for hydrogen separation, J. Membr. Sci. 464 (2014) 119-126.

[170] M.J.C. Ordoñez, K.J. Balkus Jr, J.P. Ferraris, I.H. Musselman, Molecular sieving realized with ZIF-8/Matrimid® mixed-matrix membranes, J. Membr. Sci. 361 (2010) 28-37.

[171] P. Cheng, Y.H. Hu, H_2O-functionalized zeolitic Zn(2-methylimidazole)$_2$ framework (ZIF-8) for H_2 storage, J. Phys. Chem. 118 (2014) 21866-21872.

[172] M.C. Duke, B. Zhu, C.M. Doherty, M.R. Hill, A.J. Hill, M.A. Carreon, Structural effects on SAPO-34 and ZIF-8 materials exposed to seawater solutions, and their potential as desalination membranes, Desalination 377 (2016) 128-137.

[173] S. Park, H.-K. Jeong, In-situ linker doping as an effective means to tune zeolitic-imidazolate framework-8 (ZIF-8) fillers in mixed-matrix membranes for propylene/propane separation, J. Membr. Sci. 596 (2020) 117689.

[174] P. Krokidas, S. Moncho, E.N. Brothers, M. Castier, H.-K. Jeong, I.G. Economou, On the efficient separation of gas mixtures with the mixed-linker zeolitic-imidazolate framework-7-8, ACS Appl. Mater. Interfaces 10 (2018) 39631-39644.

[175] D. Fairen-Jimenez, S. Moggach, M. Wharmby, P. Wright, S. Parsons, T. Duren, Opening the gate: framework flexibility in ZIF-8 explored by experiments and simulations, J. Am. Chem. Soc. 133 (2011) 8900-8902.

[176] T. Tynell, M. Karppinen, Atomic layer deposition of ZnO: a review, SEMICOND SCI TECH. 29 (2014) 043001-043009.

[177] C. Zhang, C. Han, D.S. Sholl, J. Schmidt, Computational characterization of defects in metal–organic frameworks: Spontaneous and water-induced point defects in ZIF-8, J. Phys. Chem. Lett. 7 (2016) 459-464.

[178] X. Ma, P. Kumar, N. Mittal, A. Khlyustova, P. Daoutidis, K.A. Mkhoyan, M. Tsapatsis, Zeolitic imidazolate framework membranes made by ligand-induced permselectivation, Science 361 (2018) 1008-1011.

[179] Z. Xiao, Y. Liu, J. Zhang, D. Zhao, Y. Lu, D. Shen, X. Fan, Electrical and structural properties of p-type ZnO: N thin films prepared by plasma enhanced chemical vapour deposition, Semicond Sci Technol 20 (2005) 796.

[180] R. Wei, H.Y. Chi, X. Li, D. Lu, Y. Wan, C.W. Yang, Z. Lai, Aqueously Cathodic Deposition of ZIF-8 Membranes for Superior Propylene/Propane Separation, Adv. Funct. Mater. 30 (2020) 1907089.

[181] H. Chen, L. Wang, J. Yang, R.T. Yang, Investigation on hydrogenation of metal–organic frameworks HKUST-1, MIL-53, and ZIF-8 by hydrogen spillover, J. Phys. Chem. 117 (2013) 7565-7576.

[182] D.S. Sholl, R.P. Lively, Defects in metal–organic frameworks: challenge or opportunity?, J. Phys. Chem. Lett. 6 (2015) 3437-3444.

[183] M. Futsuhara, K. Yoshioka, O. Takai, Optical properties of zinc oxynitride thin films, Thin Solid Films 317 (1998) 322-325.

[184] S.R. Venna, J.B. Jasinski, M.A. Carreon, Structural evolution of zeolitic imidazolate framework-8, J. Am. Chem. Soc. 132 (2010) 18030-18033.

[185] S.R. Venna, M.A. Carreon, Highly permeable zeolite imidazolate framework-8 membranes for CO2/CH4 separation, J. Am. Chem. Soc. 132 (2010) 76-78.

[186] J. Cravillon, S. Münzer, S.-J. Lohmeier, A. Feldhoff, K. Huber, M. Wiebcke, Rapid room-temperature synthesis and characterization of nanocrystals of a prototypical zeolitic imidazolate framework, Chem. Mater. 21 (2009) 1410-1412.

[187] M.J. Lee, M.R.A. Hamid, J. Lee, J.S. Kim, Y.M. Lee, H.-K. Jeong, Ultrathin zeolitic-imidazolate framework ZIF-8 membranes on polymeric hollow fibers for propylene/propane separation, J. Membr. Sci. 559 (2018) 28-34.

[188] G. Ramu, M. Lee, H.-K. Jeong, Effects of zinc salts on the microstructure and performance of zeolitic-imidazolate framework ZIF-8 membranes for propylene/propane separation, MICROPOR MESOPOR MAT 259 (2018) 155-162.

[189] D. Liu, X. Ma, H. Xi, Y. Lin, Gas transport properties and propylene/propane separation characteristics of ZIF-8 membranes, J. Membr. Sci. 451 (2014) 85-93.

[190] N.T. Tran, J. Kim, M.R. Othman, Microporous ZIF-8 membrane prepared from secondary growth for improved propylene permeance and selectivity, MICROPOR MESOPOR MAT 285 (2019) 178-184.

[191] J. Yu, Y. Pan, C. Wang, Z. Lai, ZIF-8 membranes with improved reproducibility fabricated from sputter-coated ZnO/alumina supports, Chem. Eng. Sci. 141 (2016) 119-124.

[192] N.T. Tran, J. Kim, M.R. Othman, Microporous ZIF-8 and ZIF-67 membranes grown on mesoporous alumina substrate for selective propylene transport, Sep. Purif. Technol. 233 (2020) 116026.

[193] H.T. Kwon, H.-K. Jeong, Highly propylene-selective supported zeolite-imidazolate framework (ZIF-8) membranes synthesized by rapid microwave-assisted seeding and secondary growth, ChemComm 49 (2013) 3854-3856.

[194] J. Sun, C. Yu, H.-K. Jeong, Propylene-selective thin zeolitic imidazolate framework membranes on ceramic tubes by microwave seeding and solvothermal secondary growth, Crystals 8 (2018) 373.

[195] C.W. Colling, G.A. Huff Jr, J.V. Bartels, Processes using solid perm-selective membranes in multiple groups for simultaneous recovery of specified products from a fluid mixture, Google Patents, 2004.

[196] M. Kanezashi, W. Shazwani, T. Yoshioka, T. Tsuru, Separation of propylene/propane binary mixtures by bis (triethoxysilyl) methane (BTESM)-derived silica membranes fabricated at different calcination temperatures, Journal of membrane science 415 (2012) 478-485.

[197] R. Kreiter, M.D. Rietkerk, H.L. Castricum, H.M. van Veen, J.E. ten Elshof, J.F. Vente, Stable hybrid silica nanosieve membranes for the dehydration of lower alcohols, ChemSusChem: Chemistry & Sustainability Energy & Materials 2 (2009) 158-160.

[198] G. Lu, J.D. Da Costa, M. Duke, S. Giessler, R. Socolow, R. Williams, T. Kreutz, Inorganic membranes for hydrogen production and purification: a critical review and perspective, Journal of colloid and interface science 314 (2007) 589-603.

[199] K. Oda, K. Akamatsu, T. Sugawara, R. Kikuchi, A. Segawa, S.-i. Nakao, Dehydrogenation of methylcyclohexane to produce high-purity hydrogen using membrane reactors with amorphous silica membranes, Industrial & Engineering Chemistry Research 49 (2010) 11287-11293.

[200] G. Li, T. Niimi, M. Kanezashi, T. Yoshioka, T. Tsuru, Equilibrium shift of methylcyclohexane dehydrogenation in a thermally stable organosilica membrane reactor for high-purity hydrogen production, International Journal of Hydrogen Energy 38 (2013) 15302-15306.

[201] S. Battersby, S. Smart, B. Ladewig, S. Liu, M.C. Duke, V. Rudolph, J.C.D. da Costa, Hydrothermal stability of cobalt silica membranes in a water gas shift membrane reactor, Separation and Purification Technology 66 (2009) 299-305.

[202] G. Fotou, Y. Lin, S.E. Pratsinis, Hydrothermal stability of pure and modified microporous silica membranes, Journal of materials science 30 (1995) 2803-2808.

[203] J. Kim, D. Lee, Marked inducing effects of metal oxide supports on the hydrothermal stability of zeolitic imidazolate framework (ZIF) membranes, Journal of Materials Chemistry A 4 (2016) 5205-5215.

[204] S. Lee, J. Kim, J. Kim, D. Lee, Zeolitic Imidazolate Framework Membrane with Marked Thermochemical Stability for High-Temperature Catalytic Processes, Chemistry of Materials 30 (2018) 447-455.

[205] X. Liu, Y. Li, Y. Ban, Y. Peng, H. Jin, H. Bux, L. Xu, J. Caro, W. Yang, Improvement of hydrothermal stability of zeolitic imidazolate frameworks, Chemical Communications 49 (2013) 9140-9142.

[206] D. Farrusseng, S. Aguado, C. Pinel, Metal–organic frameworks: opportunities for catalysis, Angewandte Chemie International Edition 48 (2009) 7502-7513.

APPENDICES

The following figure shows the schematic diagram depicting the algorithm used for building 1D PFR model in MATLAB for ethane, propane and isobutane dehydrogenation reaction.

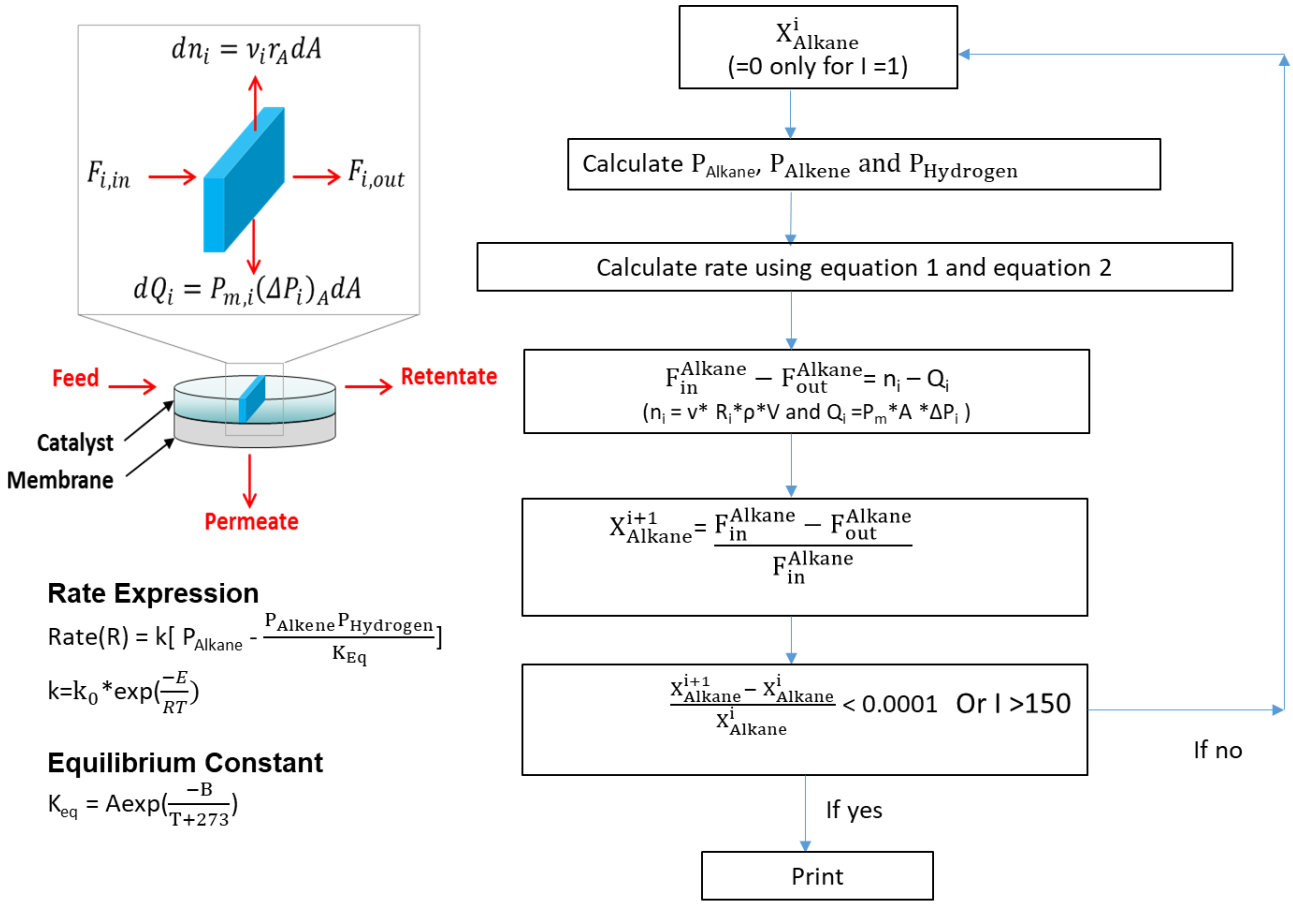

Figure A.1. Schematic of the algorithm used for developing model for ethane, propane, and isobutane de-hydrogenation reaction in MATLAB

The following table shows the value of reaction rate constant (k_0), activation energy (E), equilibrium constant parameter A, and equilibrium constant parameter B used for the model development in MATLAB

Table A1. Model parameters for ethane, propane and isobutane dehydrogenation reaction

	k_0 (mol s^{-1} $gcatalyst^{-1}$ Pa^{-1})	E (J/Mol)	A (atm)	B (K)
Ethane dehydrogenation reaction*	4.01×10^{-3}	20.6	7.28×10^{-6}	-17000
Propane dehydrogenation reaction	4.01×10^{-10}	-34.8	723.49	-8813.7
Isobutane dehydrogenation reaction	8.85×10^{-12}	-28.5	1041.06	-9256.2

*For ethane dehydrogenation reaction unit of k_0 is mol m^{-2} s^{-1} Pa^{-1} , E is kcal mol^{-1}, A is pascal and B is K

Table A.2: Properties of different gases used in developing the MATLAB model for ethane, propane and isobutane dehydrogenation reactions

	Molecular weight (g)	Density (g/cc)
Hydrogen	2	0.00008988
Argon	40	0.001784
Ethane	30	0.00135
Ethylene	28	0.0018
Propane	44	0.002
Propylene	42	0.00174
Isobutane	58	0.00251
Isobutylene	56	0.588

The detailed code for the Alkane dehydrogenation reaction for Packed Bed Membrane Reactor (PBMR) is as follows

```
% Alkane dehydrogenation reaction

% Membrane Parameters

Mc=0.55;              % Mass of catalyst in g

A=1.34E-06;           % Area of membrane in m^2

A1=3.14*A;

S= 0.45;              % Space velocity in h^-1

K0=k0;                % Constant is mentioned in Table A.1 of this appendix

E0= E;                % Constant is mentioned in Table A.1 of this appendix

MAl=40;               % Molecular weight are mentioned in Table A.1 in g

Mh2=2;                % Molecular weight of hydrogen are mentioned in Table A.1 in g

MAlk=28;              % Molecular weight of ethylene in g

VAl=1.5;              % Flow rate of alkane in ccm

VAlk=0;               % Flow rate of alkene in ccm

Vh2=0;                % Flow rate of hydrogen in ccm

VAr=20;               % Flow rate of argon in ccm

s=P;                  % Pressure of feed side in atm

P_r=101325*s;         % Pressure in retentate side in pascal

P_p=101325;           % Pressure in permeate side in pascal

R=8.314;              % Universal gas constant J/mol-K

%DAl=4.08E-4;         % Density of alkane in mol/cc

%DAlk=4.08E-4;        % Density of alkene in mol/cc

%Dh2= 4.08E-4;        % Density of hydrogen in mol/cc

%DAr=4.08E-4;         % Density of argon in mol/cc

%DAl=0.0000453;       % Density of alkane in mol/cc

%DAlk=0.00004214;     % Density of alkene in mol/cc
```

```
%Dh2= 0.00004494;          % Density of hydrogen in mol/cc
%DAr=0.0000446;            % Density of argon in mol/cc
% Mole Fractions in Feed
yAl=1;                 % Mole fraction for alkane in feed
yAlk=0.0000001;        % Mole fraction for alkene in feed
yh2=0.0000001;         % Mole fraction for hydrogen in feed
yAr=0;                   % Mole fraction for argon in feed

% Mole Fractions in permeate side
yAlp=0;                          % Mole fraction for alkane in permeate
yAlkp=0;                         % Mole fraction for alkene in permeate
yh2p=0;                          % Mole fraction for hydrogen in permeate
yArp=1;                          % Mole fraction for argon in permeate
T=873;                           % Temperature in kelvin
% Molar flow rates of components in feed
FAl=(VAl*P_r*0.000001)/(R*T*60);       % Molar flow rate of alkane in mol/min
FAli=FAl;                                % Storing initial value for final conversion calculation
FAly=(VAlk*P_r*0.000001)/(R*T*60);     % Molar flow rate of alkene in mol/min
Fh2=(Vh2*P_r*0.000001)/(R*T*60);       % Molar flow rate of hydrogen in mol/min
FAr=0;
% Partial pressures of components in feed
PAl=P_r*yAl;         % Partial pressure for alkane in pascal
PAlk=P_r*yEty;       % Partial pressure for alkene in pascal
Ph2=yh2*P_r;         % Partial pressure for hydrogen in pascal
PAr=yAr*P_r;
```

```
% Molar flow rates of components in sweep gas
FArp=(VAr*P_r*0.000001)/(R*T*60);
FAlp=0;          % Molar flow rate of alkane in mol/min in permeate
FAlkp=0;         % Molar flow rate of alkene in mol/min in permeate
Fh2p=0;          % Molar flow rate of hydrogen in mol/min in permeate
%Equilibrium constant
keq=101325*7280000*exp((-17000)/T);          % Equilibrium constant in pascal
k=K0*exp((-E0)/(T*R));                       % rate constant  in mol/s.m2.pascal

    % Calculaton of permeance
    Pmh2=6.2E-08;                    % Permeance of hydrogen (mol/s.m2.pascal)
    PmAlk=1.62E-08;          % Permeance of alkene (mol/s.m2.pascal)
    PmAl=1.3E-08;                    % Permeance of alkane (mol/s.m2.pascal)
    PmAr=9.44E-08;                   % Permeance of argon (mol/s.m2.pascal)
    %PmAl=0.0000000198*exp(0.0002*(T-273));       % Permeance of alkane (mol/s.m2.pascal)
    %PmAlk=0.0000000259*exp(0.0001*(T-273));      % Permeance of alkene (mol/s.m2.pascal)
    %Pmh2=0.0000000245*exp(0.0034*(T-273));       % Permeance of hydrogen (mol/s.m2.pascal)
    Results=zeros(150,3);
  for i=1:150                                    % No of sections
    i;
    Rate=k*(PAl-((PAlk*Ph2)/(keq)));             % Mol/s.m2
    % Differential pressure for each component across membrane
    dpAl=P_r*yAl-P_p*yAlp;           % Differential pressure for alkane in pascal
    dpAlk=P_r*yAlk-P_p*yAlkp;        % Differential pressure for alkene in pascal
    dph2=P_r*yh2-P_p*yh2p;           % Differential pressure for hydrogen in pascal
```

```
dpAr=P_r*yAr-P_p*yArp;              % Differential pressure for argon in pascal
% Molar flow rate of each component in permeate
%FAlp=FAlp+PmAl*A*dpAl*60;          % Molar flow rate of alkane in mol/min in permeate
%FAlkp=FAlkp+PmAlk*A*dpAlk*60;      % Molar flow rate of alkene in mol/min in permeate
%Fh2p=Fh2p+Pmh2*A*dph2*60;          % Molar flow rate of hydrogen in mol/min in permeate
%Ftp=FAlkp+Fh2p+FAr;                % Total molar flow rate in permeate in mol/min
FAlp=FAlp+PmAl*A*dpAl;              % Molar flow rate of alkane in mol/min in permeate
FAlkp=FAlkp+PmAlk*A*dpAlk;          % Molar flow rate of alkene in mol/min in permeate
Fh2p=Fh2p+Pmh2*A*dph2;              % Molar flow rate of hydrogen in mol/min in permeate
FArp=FArp+PmAr*A*dpAr;              % Molar flow rate of argon in mol/min in permeate
Ftp=FAltp+FAlkp+Fh2p+FArp;          % Total molar flow rate in permeate in mol/min

% Calculation of flux through the membranes
FluxAlp=FAlp/(A);                   % Flux of alkane across the membrane in mol/s.m^2
FluxAlkp=FAlkp/(A);                 % Flux of alkene across the membrane in mol/s.m^2
Fluxh2p=Fh2p/(A);                   % Flux of hydrogen across the membrane in mol/s.m^2

% Molar flow rate of each component in retentate
FAl=FAl-Rate*A-PmAl*A1*dpAl;        % Molar flow rate of alkane in mol/min
FAlk=FAlk+Rate*A-PmAlk*2*A1*dpAlk;  % Molar flow rate of alkene in mol/min
Fh2=Fh2+Rate*A-Pmh2*A1*2*dph2;      % Molar flow rate of hydrogen in mol/min
FAr=FAr+Rate*A-PmAr*2*A1*dpAr;      % Molar flow rate of argon in mol/min
Ft=FAl+FAlk+Fh2+FAr;                % Total molar flow rate in retentate in mol/min
Results(i,1) = yAl;                 % Saving alkane mole fraction
Results(i,2) = yAlk;                % Saving alkene mole fraction
```

```
  Results(i,3) = yh2;                    % Saving hydrogen mole fraction

  % Mole fraction of each component in permeate
  yAlp=FAlp/Ftp;              % Mole fraction of alkane in permeate
  yAlkp=FAlkp/Ftp;             % Mole fraction of alkene in permeate
  yh2p=Fh2p/Ftp;              % Mole fraction of eydrogen in permeate
  yArp= FArp/Ftp;             % Mole fraction of argon in permeate

  % Mole fraction of each component in retentate
  yAl=FAl/Ft;             % Mole Fraction for alkane in retentate
  yAlk=FAlk/Ft;            % Mole fraction for alkene in retentate
  yh2=Fh2/Ft;             % Mole fraction for hydrogen in retentate
  yAr=FAr/Ft;                 % Mole fraction for argon in retentate
  % Caluculation of revised partial pressures in retentate side
  PAl=P_r*yAl;                % Revised partial pressure of alkane in retentate in pascal
  PAlk=P_r*yAlk;              % Revised partial pressure of alkene in retentate in pascal
  Ph2=P_r*yh2;                % Revised partial pressure of argon in retentate in pascal
  X=(FAli-FAl-FAlp)/(FAli); % Conversion after section i

  Results(i,4) = X;           % Storing conversion after section i
end
FAl                   % Printing alkane exit flow rate from retentate in mol/min
FAlp                  % Printing alkane exit flow rate from retentate in mol/min
FAli                  % Printing alkane inlet flow rate in mol/min
X=(FAli-FAl-FAlp)/(FAli)    % Printing overall alkane conversion
```

VITA

Shailesh Singh Dangwal

Candidate for the Degree of

Doctor of Philosophy

Dissertation: MICROPOROUS INORGANIC MEMBRANES FOR HIGH TEMPERATURE ALKANE DEHDROGENATION AND PRODUCTS SEPARATION

Major Field: Chemical Engineering

Biographical:

Education:

Completed the requirements for the Doctor of Philosophy in Chemical Engineering at Oklahoma State University, Stillwater, Oklahoma in December, 2020.

Completed the requirements for the Master of Science in Chemical Engineering at Oklahoma State University, Stillwater, Oklahoma in 2017.

Completed the requirements for the Bachelor of Technology in Chemical Engineering at Indian Institute of Technology, Guwahati, India in 2012.

Experience:
Jan. 2016- Dec. 2020: Research Assistant, Oklahoma State University, OK

Jul. 2013- Dec. 2015: Senior Engineer at Orient Cement Limited, Hyderabad, India

Jul. 2012- Jul. 2013: Engineer at Orient Cement Limited, Hyderabad, India

Honors and Awards:
Received Dennis Hussey Scholarship for the year 2018-19 at Oklahoma State University

Received Robberson Summer Dissertation Fellowship for the 2018-2019 academic year